Synthesis, organization and dynamic behaviour in poly(*p*-octylstyrene)-*b*-poly(butyl methacrylate) block copolymer systems

Ph.D. Thesis

Peter Černoch

Charles University in Prague, Faculty of Science
Department of Physical and Macromolecular Chemistry

Prague, 2007

The thesis has been prepared under supervision of RNDr. Petr Štěpánek, Dr.Sc., in the Department of Supramolecular Polymer Systems of the Institute of Macromolecular Chemistry, the Academy of Sciences of the Czech Republic.
For anionic polymerization of used polymers we have appreciated the wide experience and help of Ing. Lubomír Lochmann, Dr.Sc., who participated as consultant of the thesis.

I hereby declare that this submission is my own work and that, to the best of my knowledge and belief, it contains no material previously published or written by another person nor material which to a substantial extent has been accepted for the award of any other degree or diploma of the university or other institute of higher learning, except where due acknowledgment has been made in the text.

In Prague .....

Peter Černoch

Abstract

This work is part of a global project of our department, where we focus on synthesis and studies of derivatives of block copolymers made of styrenes and methacrylates.

Here we investigate the combination poly(*p*-octylstyrene) and poly(*n*-butyl methacrylate) which, according to our opinion, has great potential in being usable in various applications. Because of high incompatibility of the components, which makes easier the (micro)phase separation, such system can be used especially in the field of nanotechnology or also as a model in fundamental research.

The work started by anionic polymerization of a series of homopolymers and nearly-symmetric diblock copolymers. The products were isolated and characterized by GPC and DSC methods. We also tried to obtain temperatures of order-disorder transition (ODT) characteristic of symmetric copolymers, however, because of the unsuitable grain structure combined with strong incompatibility of the blocks, it was found that the ODT temperature was out of the measurement range.

After that we focused on a study of bulk properties of diblock copolymers using small-angle X-ray scattering and transmission electron microscopy. In these experiments we confirmed regular lamellar organization in all samples, which corresponds to the theoretical predictions resulting from the general phase diagram of diblock copolymers.

In the next part of the work we used atomic force microscopy to study systematically the modification of thin layers of the synthesized copolymers by vapor-treatment using simple organic solvents. The vapor-treatment is a useful method to change actual topographical and/or microphase arrangement of thin films. Here we tried to find a relation between the solvent quality for diblock copolymer components and the resulting structure. According to our results, in order to get a structured surface, it is suitable that the solvent has at least a weak interaction (solubility or swelling) for both homopolymer chains. Using thermodynamically "good" solvents had no effect in our cases, to the contrary with results in some other publications dealing with different systems. We also confirmed that using suitable solvents it is possible to obtain parallel or perpendicular arrangement of final structures, with respect to the supporting substrate.

Besides of thin layers of the "pure" diblock copolymers, the thin films of ternary blends of a diblock copolymer with corresponding homopolymers were investigated. Here we focused on the surface behavior of the mixtures with composition near the tricritical Lifshitz point, which – because of the possibility to form bicontinuous microemulsions – is an often studied composition for its potential usability in material science. All of the found published comparable studies, however, deal with the behavior of bulk systems, so our thin films-focused experiments can be, as we believe, interesting as the starting point of the next potential studies of the thin films of ternary polymer systems.

In the last part of the work, the dynamic behavior of diblock copolymer solutions in mixtures of two partially miscible solvents A and B was studied by dynamic light scattering (DLS) and small angle X-ray scattering (SAXS); A was selective solvent for one copolymer block and B for the remaining one. Using DLS, we found a number of temperature and concentration dependent dynamic processes which correspond to published ones for solutions of similar diblock copolymers. Using SAXS, we confirmed the presence of hollow micelles which consist of the core ("drop") of A-rich phase (minority solvent) covered with the shell of the diblock copolymer located in B-rich phase (majority solvent). This finding is important since allow us prepare hollow micelles, which can play an important role in theoretical studies or practical applications; *e.g.*, as nanocontainers.

Contents

1 Acknowledgement

The topic of this dissertation was originally a study of various polymer systems with dynamic light scattering, which is a method well-established and verified in our department and widely used in current polymer research.

The first and great part of my dissertation work was the synthesis of diblock- and homo-polymers for further experiments. Because I was pretty new in this field, an experienced leader was recommended for me. I owe a lot for this leadership and at this place I want express many thanks to Ing. Lubomír Lochmann, Dr.Sc., for introduction to the great world of the anionic polymerization and for immense help and leading in laboratory work.

In the course of time other questions and different views appeared so it was appropriate to widen the original path to others directions. A great one was using the Atomic Forces Microscopy for controlling surface behavior of the samples. The detailed study in this field was possible with kind help of people from the Institut für Polymerforschung in Dresden (IPF), namely Prof. Dr. Manfred Stamm and especially Dr. Alexander Sydorenko. At the IPF were obtained all AFM images dealing with vapor annealing of block copolymer thin layers.

According to the (new) trends in polymer science, we found also interesting to extend the research to block copolymer solutions in mixtures of incompatible but selective solvents, and the experiments, results and targets became too large compared to the original aims. Therefore after some consultations, we decided to select one block copolymer system – poly(*n*-butyl methacrylate) and poly(*p*-octylstyrene) – and examine it in details.

The content of this dissertation then includes results of our research of behavior of the mentioned block copolymer system and its mixture with homopolymers and solvents.

Finally, but not lastly, I want to thank my supervisor RNDr. Petr Štěpánek, Dr.Sc., for the help and leading in light scattering methods which are the basis of the presented studies. Thanks to his pedagogical skills and patience in our consultations an originally chemist (me) was steered to try to understand a little of the great physics science.

2 Introduction

In the presented work are summarized our results obtained by investigating the poly(*p*-octylstyrene) (POS) and poly(*n*-butyl methacrylate) (PBuMA) block copolymer system.

This combination was chosen because of several important reasons:

- to continue our previous projects we decided to use in our experiment derivatives of styrene and methyl methacrylate. This helped us to compare the obtained results with work that was (and will be) done and widen the general knowledge of these polymer materials.
- we found interesting to study a hydrophobic diblock copolymer system consisting of two components with relatively low glass transition temperatures, T_g, which makes easier the investigation of the system below and above T_g (T_g of POS is ca -40 °C, T_g of PBuMA ca 50 °C)
- studies of organization in block copolymers with a strong mutual incompatibility of the components is desirable, because of its stabilizing effect on newly created structures in bulk and in thin layers.

Both components also demonstrate high incompatibility, which plays an important role in microscale organization with long organization period. This is important in nanotechnology applications, where a high incompatibility helps to stabilize the created structures. Another motivation for our work was also that we deal with a completely new system, which according to our bibliographic search has never been studied before.

Exploring of systems containing POS has according to our opinion a different, at first sight less noticeable sense: because of its extremely low T_g, comparable with polybutadiene, POS can serve also as a "plasticizer" in otherwise hard polymer blends or copolymers. Here is a great advantage its certain structural similarity with styrene, which can bring a fresh wind in producing of new combination of traditional materials.

Using anionic polymerization we have synthesized poly(*p*-octylstyrene)-*b*-poly(butyl methacrylate) (OB) diblock copolymers and the corresponding homopolymers and we explored these systems from a different points of view: we studied the behavior of the OB diblock copolymer in bulk to see natural organization, in thin layers to have an idea about surface structures and also in solutions in simple and binary solvents to follow its association behavior. We are of course conscious that it is not possible to study all phenomena and interactions and that there still exists many ways for follow up and extension of the presented

experiments. Nevertheless we think that our results on the interesting system of poly(*p*-octylstyrene) – poly(butyl methacrylate), as summarized in this thesis, contribute to the general knowledge of macromolecular chemistry and physics.

3 Abbreviations list

α	: angle tilting of the cuvette with the sample
Γ	: relaxation constant
ξ	: correlation length
λ	: wavelength of the light
η	: dynamic viscosity [$N.m^{-1}.s^{-1}$]
θ	: scattering angle
χ	: Flory-Huggins interaction parameter
ρ	: density
τ	: relaxation time

AFM	: atomic force microscopy
BCC	: body-centered cubic
c*	: polymer solvent critical concentration (the crossover concentration)
d	: regular structure spacing size
D	: diffusion coefficient
DD	: double diamonds
DFE	: 1,1-diphenylethylene
DFMPLi	: diphenylmethylpentyllithium
DLS	: dynamic light scattering
DMF	: N,N'-dimethylformamide
DSC	: differential scanning calorimetry
FCC	: face-centered cubic
g	: normalized correlation function
G	: correlation function
GPC	: gel permeation chromatography
HCPS	: hexagonally closed packed spheres
HPLC	: hexagonally packed cylinders
k	: Boltzmann's constant
l	: trajectory length
LAM	: lamellae
n	: refractive index
N	: degree of polymerization
ODT	: order-disorder transition
OB	: poly(*p*-octylstyrene)-*b*-poly(*n*-butyl methacrylate)
PBuMA	: poly(*n*-butyl methacrylate)
PC	: primitive or simple cubic
POS	: poly(*p*-octylstyrene)

POS-*b*-PBuMA	: poly(*p*-octylstyrene)-*b*-poly(*n*-butyl methacrylate)
q	: scattering vector
r or R	: radius
R_h	: hydrodynamic radius of the polymer molecules
sBuLi	: *sec*-butyllithium
SAXS	: small angle X-ray scattering
SPM	: scanning probe microscopy
t	: delay time
T	: temperature
T_C	: phase separation temperature
T_g	: glass transition temperature
tBuOLi	: *tert*-butoxylithium
TEM	: transmission electron microscopy
THF	: tetrahydrofuran

4 Block copolymers

4.1 General

The presented work deals with synthetic block polymeric materials and their mixtures and solutions. In general, polymers are high-molecular-weight compounds, consisting of monomer units of one or more types. Molecules synthesized from identical monomer units (one kind of monomer units) are called homopolymers, while molecules synthesized from different monomers are called copolymers. Copolymers can be subtly discriminated into different groups according to organization of the monomer units and the chain geometry - we know alternating, random and block copolymers (Figure 1).

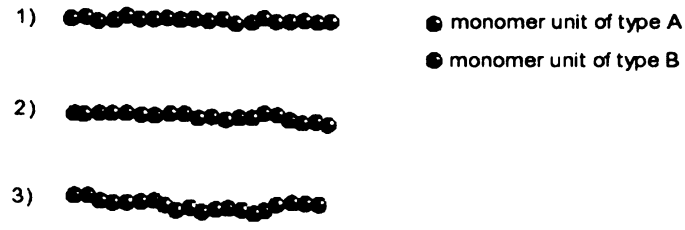

***Figure 1**: Example of copolymer basic types – (di)block (1), alternating (2), random (3)*

The last one can be further separated to linear di- or multi- block copolymers and graft and star-like copolymers (Figure 2).

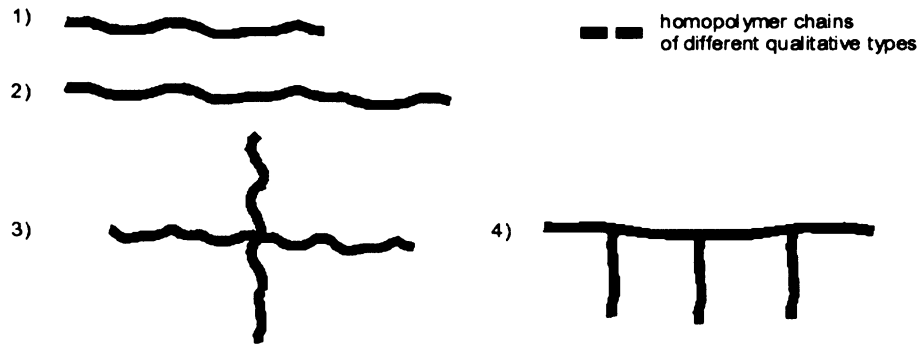

***Figure 2**: Examples of block copolymer structures – (AB) diblock copolymer chain (1), (ABA) triblock copolymer (2), star-like (3) and grafted (4) chains structures.*

By combination of different types of monomer units and homopolymer chains we can widen the possible range of usability of final materials because of combinations of materials

with different properties. The block copolymers, however, bring a new dimension into material science thanks to specific interactions of polymer chains. In a multicomponent polymer system – in mixture of homopolymers – even chemically very similar chains are generally immiscible and strongly incompatible, so at suitable conditions the system is unstable and the originally homogeneous mixture decomposes into phase separate components[1],[2],[3],[4].

4.2 Block copolymers in bulk systems

Copolymers, and especially block copolymers, bring – thanks to chemical bonds between unlike molecules – a desired stability into the system, so we are able to prepare new, tuned materials of target properties simply by the chemical reaction of selected monomers.

The incompatibility of homopolymer chains, even though these are connected through the chemical bonds into one chain, is however still present. The macroscopic phase separation, observable in simple homopolymer systems even by the naked eye, is now moved into a finer level as a self-assembly of block copolymers A-*b*-B, and a microphase separation into various structures (see Figure 3) can be observed using suitable physical methods. The structure and degree of microphase separation of block copolymer systems generally depends on the chain length (given by the degree of polymerization N) on one side and the strength of interaction of components on the other side. The influence of these variables can be drawn to a phase diagram (see e.g. Figure 24 at page 40), where one axis represents the composition of the system *f* and the second the interaction of the components given by the expression χN, where the χ is the Flory-Huggins interaction parameter of the A segment - B segment interaction energy. For theoretical models it s common to distinguish three different regimes depending on the value of χN: the weak-segregation limit (WSL) for $\chi N \leq 10$; the intermediate segregation region (ISR) for $10 \leq \chi N \leq 50$ and the strong segregation limit (SSL) for $\chi N \rightarrow \infty$.

The phase behavior of the final block copolymer can also be fine tuned by addition of small amounts of homopolymers identical to the present blocks, which leads to a system equivalent to a block copolymer with different ratio of blocks. The microphase separation, paradoxically, widens the possible applications of block copolymers into other fields of practical life, and these and similar effects attract nowadays great attention, as can we estimate *e.g.* from reviews[5], [6], [7].

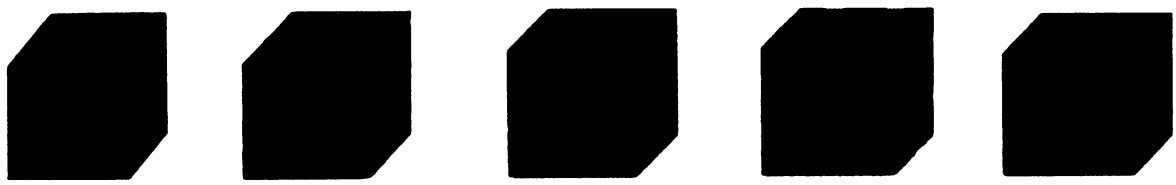

BCC spherical hexagonal cylindrical gyroid (bicontinuous) perforated lamellas lamellar

Figure 3: *Examples of common self-assembled phase structures of block copolymer system. Adopted from [5].*

Self-assembly based polymer structures are useful in various fields. They can be used *e.g.* in optical systems[8], [9], [10], [11] or as base for preparing of microporous structures usable for producing semi-permeable and other membranes (systematically studied *e.g.* by Liu *et al.* in[12], [13], [14], [15] or by the other authors[16], [17]), as well as for preparation of hybrid[18] and semiconducting materials[19] or as regular structures for templates in nanotechnology[20] and nanolitography.

Thanks to theoretically enormous number of possible combinations of usable copolymer systems, we can select materials suitable for a desired application. However, to apply pure block copolymers in all cases is too expensive and often useless. In these cases it is possible to utilize the block copolymers as surfactants and compatibilizers for homopolymer mixtures. In these ternary or more complex systems of homopolymers and block copolymer(s), the block copolymer(s) lower the interfacial tension of homopolymers and the mixture behavior can be compared to the well studied, low-molecular-weight oil/water/surfactant systems[21], [22], [23] (suitable *e.g.* for a drug delivery carriers [24]).

These systems – homopolymer blends combined with a block copolymer to get as much homogeneous system as possible (microemulsion or bicontinuous microemulsion) – have great importance, because of its usability in real life applications. Thank to this technology, we can prepare new materials with targeted quality, often combining exceptional properties from two or more components. The other usable and important application can be also recycling of existing polymer waste, where we are able to omit some (money and/or time expensive) separation processes. From suggested applications, it is logical that in the present time there still exists a wide and intensive research of this field, as can be verified in extensive literature, *e.g.* in [25], [26], [27], [28], [29].

The first approach to understanding the complex behavior of multicomponent mixtures based on block copolymers is studying the simplest and controlled systems formed from ternary mixtures of diblock copolymers of type A-*b*-B and corresponding homopolymers A and B. Most experiments and corresponding theories are focused on the study of equilibrium

bicontinuous polymeric structures near mean-field isotropic Lifshitz point (LP) in ternary blends of two equal molecular weight homopolymers (A and B) and a compositionally symmetric diblock copolymer (see *e.g.*[30], [31], [32], [33], [34], [25], [35], [36], [37]). In such systems LP are located on a plane corresponding to blends with equal proportions of the two homopolymers but varying amounts of copolymer (the isopleth – plane) - see Figure 4.

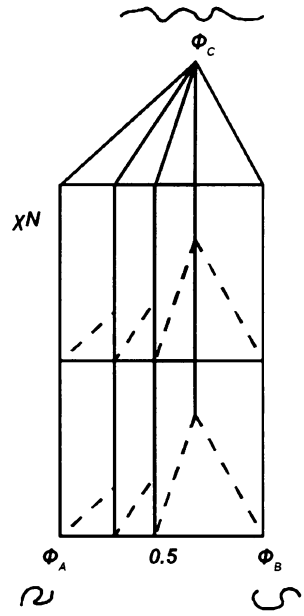

Figure 4: *The phase prism for a ternary blend of two homopolymers and a block copolymer. Homopolymer compositions (volume fraction) Φ_A and Φ_B are measured at triangular base, while copolymer composition Φ_C is measured from the back (hidden)corner of the triangle. The vertical coordinate of the prism is the incompatibility degree χN. The isopleth (plane corresponding to blends with equal proportions of the two homopolymers but varying amounts of copolymer) is the shaded plane cut through the prism at equal amounts of the two homopolymers, $\Phi_A = \Phi_B$. Adopted from [34].*

The detailed behavior of a ternary system can be consequently described by a derived isopleth phase diagram, as is presented in Figure 5 and Figure 6. In[34] is illustratively discussed a mixture of a symmetric A-*b*-B diblock copolymer with a degree of polymerization N and equal amounts of homopolymers A and B with degree of polymerization N_A and N_B: In the absence of copolymer, *i.e.* at the homopolymer volume fraction $\Phi = 1$ (Figure 5), the symmetric homopolymer blend has an upper critical consolute point located at $\chi N = 2$ and the system exhibits a second-order phase transition between a disordered liquid phase (DIS) and two coexisting homogeneous liquid phases ($L_A + L_B$). At copolymer addition to the symmetric mixture, the critical point moves across the "Scott line" (which is a boundary-line between ordered and disordered regions of the phase diagram in Figure 5) to the opposite corner, where $\Phi = 0$ and the pure diblock copolymer melt undergoes an order-disorder

transition (ODT) at $\chi N = 10.5$. When the homopolymers are smaller than the diblock, *i.e.* $\alpha <$ 1 where the α is defined as:

$$\alpha = \frac{N}{N_{AB}} \tag{4.1}$$

(N is average degree of polymerization of homopolymers A and B obtained by a simple equation $N = (N_A + N_B) / 2$ and N_{AB} is degree of polymerization of used diblock copolymer), the line of ODT meets the Scott line at a mentioned multicritical Lifshitz point *L*.

For $\alpha < 1$ and asymmetric diblock copolymer the location of LP can be described by a series of equations[35], [34]:

$$\Phi_A = \frac{N_B^{1/2}}{N_A^{1/2} + N_B^{1/2}} \tag{4.2}$$

where Φ_A is volume fraction of homopolymer A; N_A and N_B are degrees of polymerization of homopolymers. The volume fraction Φ_L of A-*b*-B diblock in the homopolymers blend mixture, required for preparation of LP systems is:

$$\Phi_L = \frac{1}{(1 + 2\alpha^2)} \tag{4.3}$$

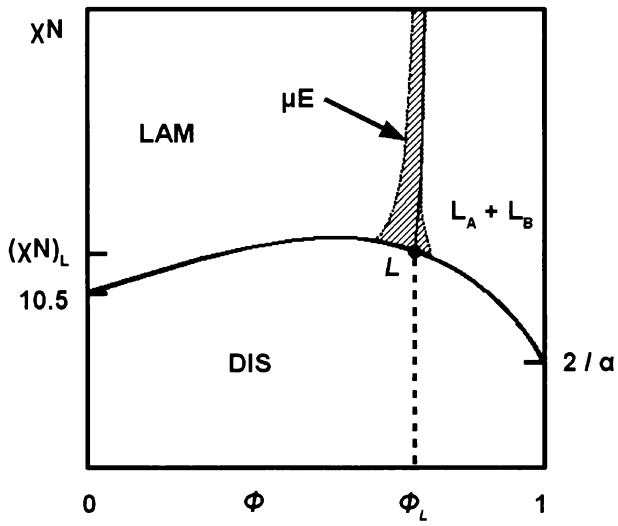

Figure 5: *Phase diagrams in the isopleth plane for $\Phi_A = \Phi_B$ and $\alpha < 1$. The abscissa is the total volume fraction of homopolymer, $\Phi = \Phi_A + \Phi_B$, $[\Phi_L, (\chi N)_L]$ are the coordinates of the Lifshitz point L. LAM is the lamellar region, DIS means disordered liquid, L_A+L_B means coexistence of A-rich and B-rich disordered liquid phases. Fluctuations destroy the L and replace it with a channel (shaded) of highly structured disordered phase – bicontinuous microemulsion (μE). Fluctuations primarily disrupt the lamellar phase to produce the microemulsion channel so this is located just to the left of the mean-field Lifshitz composition. Adopted from [34].*

As was mentioned at the beginning of this section, there exists a lot of experimental studies dealing with critical LP system. Most of the experiments were done using scattering methods (light, X-ray and neutron scattering) in bulk systems, and there also exist a few works where the microemulsion was observed directly by TEM[36], [37], as can be seen at Figure 7.

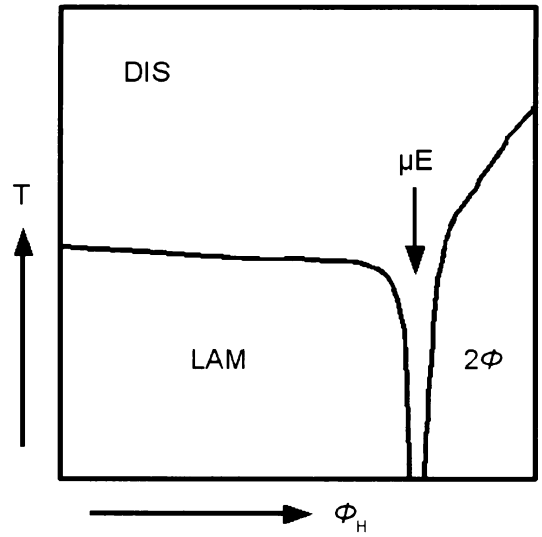

Figure 6: *Scheme of experimentally observed phase diagram for a three-component system A/B/A-b-B. LAM = lamellar phase, DIS = disordered phase, Φ_H = volume fraction of homopolymers, T = temperature, 2Φ = phase separated region, μE = microemulsion channel. Adopted from [37].*

However, up to now we did not find any publication dealing directly with LP ternary blends, focused on their thin layer behavior – even when there exist similar studies focused on other multicomponent systems, *e.g.* in[38], [39], [40], [41].

Because in our projects we also deal with self-assembly of polymer materials in thin layers, we found interesting to try to fill at least a small part of this "vacuum" and prepare a LP microemulsion from POS / PBuMA / POS-*b*-PBuMA ternary system and study its formations in thin films. We think that the described studies can form an additional step to the great world of nanotechnology applications.

Figure 7: *TEM photo of bicontinuous microemulsion morphology; ternary system of polyethylene / poly(ethylene-propylene) / polyethylene-b-poly(ethylene-propylene); 10 % of diblock copolymer. Adopted from [36].*

4.3 Block copolymers in solutions

The block copolymer organization involves also association properties in solutions. The solvent can be simple or a mixture of several solvents. Here the situation is complicated because the solvent can be for a particular chain classified as good, near-θ or bad. In dependence on the polymer concentration and on the solvent quality relatively to the polymer chains a different system behavior can be observed. The polymer chains can be molecularly dissolved, they can form micellar systems of various structures[42] and using incompatible solvents and suitable a block copolymer a quasi-liquid supramolecular systems of high degree of organization[43],[44] can be formed. Exploring these effects is also a part of intensive research in the past decades[45],[46],[47], because of many applications of polymer solutions in various industrial, medicinal and scientific applications.

In non-selective solvents, which are thermodynamically good for all blocks, copolymers can form segregated, core-shell or mixed conformations. Their structures depend mainly on the compatibility of the dissimilar segments and on solution concentration, and there exists a lot of studies focused on this behavior, *e.g.*[48],[49],[50],[51],[52],[53].

In solvents selective for one block, block copolymers structures are formed due the amphiphilicity between the components. The free energy of the system is lower when block copolymers associate into micelles with various structure, which can be observed above the critical micellar concentration (cmc) and below the critical micellar temperature (cmt) (for systems with upper critical solution temperature). In the case of insolubility of one of the blocks, compact micelles are formed, where the insoluble chain is packed in the centre of the micelle - even as a crystalline core[54].

In some other cases, depending on system compatibility and composition[55], the polymer-solvent system can adopt a new structure or preserve the original block copolymer size and organization[43],[56],[57],[58]. This behavior is also known from other systems (*e.g.* surfactant solutions[59],[60],[61]) studied previously, and demonstrates the similarity and variability of liquid systems.

In the case of tri- and higher multiblock morphology of copolymers in selective solvents, studied *e.g.* in[62], [63], [64], [65], [66] the situation is complicated by competition between looping and bridging of the soluble chains given by the ratio of end-block versus inner block solubility[67], and flower-like micelles, bridged micellar networks and gels or other structures can be observed[68],[69],[70],[71],[72],[73]. Micellar and colloid systems generally are in great focus in present because of potential use for drug delivery systems, nanoreactors, coating applications[74],[6] or even as DNA delivery systems, potentially usable in gene therapy[75], *etc.*

In the case of block copolymers in mixture of two immiscible solvents, *e.g.* in the system of diblock copolymer (AB) in solutions (a) and (b) where the (a) is good solvent for block (A) and precipitant for block (B) and vice versa, the behavior is complex.

At (AB) concentrations that exceed a value equivalent to cmc, the system interaction energy drives the block copolymer to the liquid-liquid interface to reduce interfacial tension. In this mixture stable swollen micelles or polymeric emulsions with brush-like interfaces, curved according to (AB) symmetry(see Figure 8), are formed [76], [77], [78], [79], [80]. If the (a) / (b) interface is saturated with (AB) chains, the system also adopts a curvature primarily given by the asymmetry of the (AB) diblock, but is more compact than at low concentrations – for nearly symmetrical copolymers the structure is lamellar, for different blocks ratio spherical or cylindrical domains are predicted.

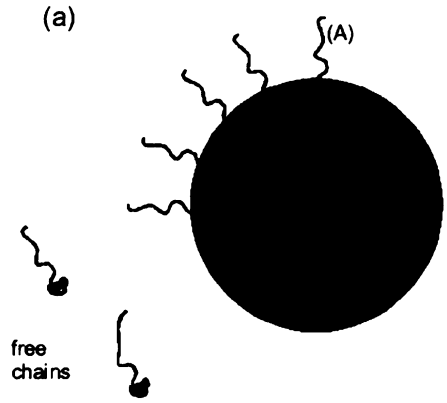

Figure 8: *Diblock copolymer (AB) at liquid-liquid interface; at concentrations above the cmc brushes are forming at the interface of binary mixture of incompatible solvents (a) and (b). The (B) blocks are shorter than (A) and are therefore located on the convex side of the interface. Adopted from [79].*

This ternary system behavior, theoretically studied in details *e.g.* by Cantor[81] and Dan[79], is similar to the well-known three-component water/oil/block copolymer(or generally surfactant) mixtures or to the four-component mixtures of oil/water/alcohol/block copolymer studied *e.g.* by Marie *et al.*[47]. Effects in immiscible solvents/block copolymer systems were in detail examined *e.g.* by Cogan *et al.*[78], who studied radius of micelles of polystyrene-*b*-poly(ethylene oxide) (PSEO) in cyclopentane (CP) (selective solvent for polystyrene) after addition of water (selective solvent for poly(ethylene oxide)). They found that saturated micellar system PSEO/CP/water contains spherical micelles with narrow size distribution and stable aggregation number. At lower water concentrations, anomalous large structures and micelles were found, as was yet observed in some previous works[45], [76] and which can be caused by presence of insoluble or crystallized homopolymer chains in the center of the micelle.

Ternary mixtures of a block copolymer in partially miscible binary solvents can however bring also more complex behavior[80].

After addition of diblock copolymer (AB) to a binary mixture of partially miscible solvents (a) and (b), where (a) can dissolve block chain (A) and (b) dissolve block chain (B), a homogeneous solution is formed at higher temperatures, where the solvents are fully miscible. After cooling below the coexistence curve, solvents without a block copolymer are going into a macrophase separation and a two-layer solvent system is observed. The solvent mixture where diblock copolymer was added, yields a microphase separated system, where (a)-rich domains coexist with (b)-rich domains and the liquid-liquid interface between the domains is – in dependence on diblock copolymer concentration – covered with the swollen, brush-like layer of (AB) copolymer. The morphology of the structure then depends on the

composition and the concentration of diblock copolymer (AB), on the (a) / (b) solvent composition and on the temperature. However, because of the seven interaction parameters in the ternary mixture, the Flory-like system description is non-trivial and we can't easily predict the real structure of the microphase-separated system. According to the new results of Štěpánek *et al.*[80], a long-range-ordered cubic and hexagonal symmetry structure was found in solutions of poly(styrene-*b*-isoprene), poly[styrene-*b*-(ethylene-*co*-propylene)], poly(styrene-*b*-butadiene) block copolymers in binary mixtures of DMF and cyclohexane (CX). The system organization begins above the phase transition temperature of the neat solvents and is probably driven by the selective sorption[82] of solvents to the block which is better soluble in that solvent. The parts of polymer chains, located at the liquid-liquid interface, adopt a conformation corresponding to the one in a good solvent (chain with excluded volume) by which both blocks are surrounded.

As was mentioned before, in this thesis we stay focused on the behavior of one, not so common block copolymer system of poly(butyl methacrylate) and poly(*p*-octylstyrene), *i.e.* poly(*p*-octylstyrene)-*b*-poly(butyl methacrylate) (OB), and by this contribute to the general knowledge of block copolymer systems organization. In this work, we explored the behavior of OB in bulk system to observe its natural organization, in mixtures of selective incompatible solvents to observe possible creation of micelles and supramolecular structures, the behavior in mixtures of corresponding homopolymers, and the behavior in thin layers under various conditions.

5 Experimental methods

The synthesized polymer materials and their mixtures were investigated by a variety of physical methods. Therefore, it was possible to study the material properties of copolymers from bulk samples, through solutions to thin copolymer layers. Moreover, the obtained results by various methods are usually complementary each other and provide complete overview of the studied samples.

5.1 Small Angle X-Ray Scattering (SAXS)

SAXS is one of methods to examine small structures in organized materials, in size ranges of approximately 1 to 100 nm. This method is applicable in solid state as well as in melt and solution, and is widely used in various fields of science. For example it is used[83] to study the organization of membranes and of biopolymers (like DNA and proteins), their interactions, to study the transition and structure organization of different phases in solid materials, gels, latexes *etc.*

The structure information of the explored material is contained in the angular dependence of scattered intensity of X-ray radiation[84] (in the scattering curve). From this and with the help of theoretical relations between structure and scattering, we are able to suggest probable structure model of our sample. This is achieved by comparing theoretical scattering curves of different structures with experimental data, because scattering curves of periodic materials show one or more interference maxima. The list of maxima for known structures[53] is shown in Table 1.

structure	relative positions of maxima (from[53])	values recalculated relative to the first scattering maximum
LAM	1 : 2 : 3 : 4 : 5 : 6 : 7	1 : 2 : 3 : 4 : 5 : 6 : 7
HPLC	1 : √3 : 2 : √7 : 3 : √12 : √13 : 4	1 : 1,7 : 2 : 2,6 : 3 : 3,46 : 3,61 : 4
PC	1 : √2 : √3 : 2 : √5 : √6 : √8 : 3	1 : 1,4 : 1,7 : 2 : 2,2 : 2,45 : 2,8 : 3
BCC	1 : √2 : √3 : 2 : √5 : √6 : √7 : √8 : 3	1 : 1,4 : 1,7 : 2 : 2,2 : 2,45 : 2,6 : 2,8 : 3
FCC	√3 : 2 : √8 : √11 : √12 : 4 : √19	1 : 1,15 : 1,6 : 1,9 : 2 : 2,3 : 2,5
HCPS	√32 : 6 : √41 : √68 : √96 : √113	1 : 1,06 : 1,13 : 1,46 : 1,73 : 1,88
DD	√2 : √3 : 2 : √6 : √8 : 3 : √10 : √11	1 : 1,22 : 1,41 : 1,73 : 2 : 1,22 : 2,24 : 2,35
Ia3d	√3 : 2 : √7 : √8 : √10 : √11 : √12	1 : 1,15 : 1,53 : 1,63 : 1,83 : 1,9 : 2
Pn3m	√2 : 2 : √5 : √6 : √8 : √10 : √12	1 : 1,41 : 1,58 : 1,73 : 2 : 2,24 : 2,45

Table 1: Relative positions of maxima for regular structures adopted from [53]; LAM: lamellae, HPLC: hexagonally packed cylinders, PC: primitive or simple cubic, BCC: body-centered cubic, FCC: face-centered cubic, HCPS: hexagonally closed packed spheres, DD: double diamonds. ia3d, pn3m.

SAXS results are often processed using the Porod's law, which generally predicts a decrease of scattered intensity proportional to q^4 (q is scattering vector defined as

$$q = \frac{4\pi}{\lambda}\sin\left(\frac{\theta}{2}\right) \tag{5.1}$$

where λ is the wavelength, $\theta/2$ is the scattering angle) at large values of the scattering vector q:

$$I(q) = I_e 2\pi\rho^2 S/q^4 \tag{5.2}$$

where $I(q)$ is the scattering intensity, q the scattering vector, ρ the electron density difference between particulate domains and the matrix material, S is a structure factor and I_e is a constant. Figure 9a shows an example of a typical result obtained on one of our systems. In order to see better the behavior at larger values of q, it is preferable to plot $\log q^4 I(q)$ vs. $\log q$ is plotted instead of $\log I(q)$ versus $\log q$ as shown in Figure 9b

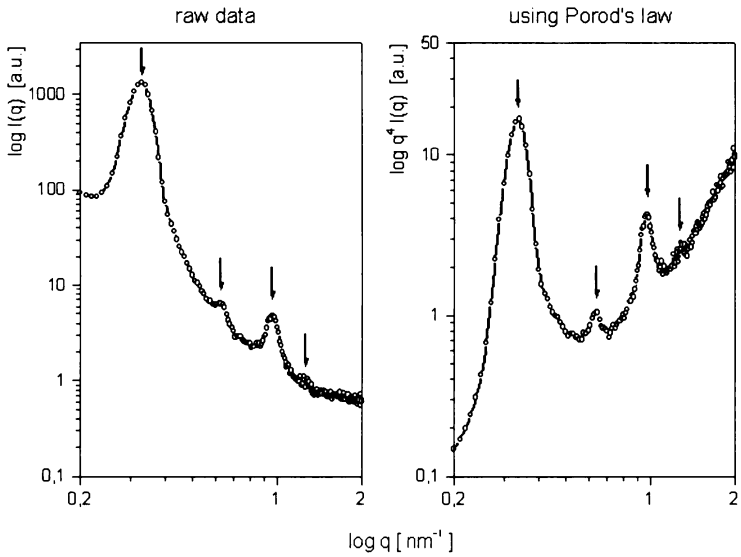

Figure 9: *Illustration of raw SAXS data and data linearized using Porod's law. Thermo-annealed sample of POS-b-PBuMA.*

The SAXS scattering curves were measured in cooperation with Frédéric Nallet from Centre de recherche Paul-Pascal, CNRS, Pessac, France. A Nanostar-U instrument was used (Bruker AXS) with a HiSTAR 2-D detector positioned at 1070 mm from the sample. The X-ray source was a Cu-anode tube yielding a beam with wavelength 1.08 Å, the primary optics was equipped with Goebel mirrors. The resulting 2-D images were found in all cases

to be isotropic, the data were azimuthally averaged to yield an intensity vs. q scattering curve. The scattering experiments were performed at room temperature. The polymer samples were sealed in 2 mm capillaries that were placed in the evacuated chamber of the instrument.

5.2 Transmission electron microscopy (TEM)

Transmission electron microscopy is in general similar to optical microscopy, except that the photons are replaced by electrons. Since the wavelength of electrons is smaller than that of photons a higher resolution is achieved.

Because of strong interactions of electron with matter, gas particles must be absent in the system. Recent advances have allowed samples to be imaged using lower vacuums and with partially hydrated samples, and the use of an electron transparent membrane between a biological sample and the vacuum has been shown to allow fully hydrated samples to be imaged, although there is a reduction in resolution.

Electron microscopy is very suitable for investigation of conductive or semi-conductive materials. Non-conductive materials can sometimes be imaged by an electron microscope, however the electron beam will be absorbed by the material, which will change the physical properties of the material (for example, the material can burn off). A common preparation technique is to coat the sample with a several-nanometer layer of conductive material (*e.g.*, by spattering of gold, *etc.*); however this process may disturb delicate samples.

Transmission electron microscopy results, published in this dissertation, were performed with cooperation with Dr. Miroslav Šlouf. The microscope JEM 200CX (Jeol, Japan) was used for TEM imaging of our samples. All microphotographs were taken at acceleration voltage 100 kV and recorded with a digital camera. Brightness, contrast and gamma corrections were performed with standard software. Ultrathin sections of ca 50 nm were cut from the thermo-annealed bulk sample with the ultramicrotome Leica Ultracut UCT, equipped with cryo attachment. Temperatures during cutting were -110 °C and -50 °C for the sample and the knife, respectively. The samples were stained with RuO_4 to obtain contrast images[85].

5.3 Dynamic light scattering (DLS)

DLS (also known as Quasi-Elastic Light Scattering - QELS or Photon Correlation Spectroscopy) is based on the fact that all particles in dynamic systems, like molecules in solutions and melts, are influenced by the others and demonstrate random motion[86], called Brownian motion.

At the light scattering, particles interact with the incident light and this motion imparts a randomness to the phase of the scattered light, such that when the scattered light from two or more particles is added together, there will be a changing destructive or constructive interference. This leads to time-dependent fluctuations in the intensity of the scattered light[87], [88].

Except for typical static light scattering, the scattered light is influenced also by all dynamic fluctuations and short-ranged forces (*e.g.* from molecules thermal motion), which causes inhomogeneities in microscopic structure of the examined system.

These effects are observable by the Doppler broadening of the spectrum of incident light due to the diffusive motion of molecules. In the case of macromolecules, the broadening is in the range from 1 to 10^5 Hz. Higher frequencies of shift are found at the rotational motion case.

The principle of DLS measurement is monitoring of the time-dependence of the intensity of scattered light *I(q, t)*, which fluctuates about an average value, using a fast photon counter[89]. The rate at which the intensity correlation decays to the average value (relaxation rate) is determined by the dynamical properties of the molecules. Time fluctuations of the scattered intensity may be described by the time autocorrelation function $G^{(1)}(t)$. The correlation function is defined as:

$$G^{(1)}(t)=\langle I_s \rangle g^{(1)}(t) \tag{5.3}$$

where t is the time delay between two observations, $\langle I_S \rangle$ is time-average light intensity and $g^{(1)}(t)$ is the normalized autocorrelation function of the electric field of the scattered light.

The correlation function provides a convenient method for expressing the degree to which two dynamical properties are correlated over a period of time t. A time dependent autocorrelation function is a function describing the correlation of a property with itself over a period of time. A correlation between two different properties is given in a cross-correlation function.

The optical spectrum of scattered light $I_S(\omega)$ is in simple case a Lorentzian function with a maximum at the frequency ω_0 and half-width Γ and is related with correlation function $G^{(1)}$ by the equation:

$$I_S(\omega)=(1/2\pi)\int_{-\infty}^{+\infty} G^{(1)}(t)\exp(i\omega t)\,dt \tag{5.4}$$

and the corresponding autocorrelation function is a single exponential with a decay rate Γ:

$$g^{(1)}(t)=\exp(i\omega_0 t)\exp(-\Gamma|t|) \tag{5.5}$$

The quantity really measured in a correlation experiment is the intensity correlation function $G^{(2)}(t)$, which is related to $g^{(1)}(t)$ by the Siegert relation[90]:

$$G^{(2)}(t)=B(1+\beta|g^{(1)}(t)|^2) \tag{5.6}$$

where $g^{(1)}(\tau)$ is the normalized field correlation function, B is the baseline, and β is the coherence factor, generally considered as an adjustable parameter in the data analysis procedure. This can be rewritten in a normalized form as:

$$g^{(2)}(t)=G^{(2)}(t)/B=1+\beta|g^{(1)}(t)|^2 \tag{5.7}$$

If there are more dynamic processes present in the investigated system, the correlation function is a superposition of many single exponential functions described by an integral relation known as a Laplace transformation

$$g^{(2)}(t)=1+\beta[\int A(t)\exp(-t/\tau)dt]^2 \tag{5.8}$$

where t is the delay time of the correlation function and β an instrumental parameter. Using the inverse Laplace transformation in REPES[91] based programme, $g^{(2)}(t)$ were converted into distributions $A(\tau)$ of relaxation times τ : The relaxation time τ is related to the diffusion coefficient D and relaxation (decay) rate Γ by the relation:

$$\Gamma=\frac{1}{\tau}=Dq^2 \tag{5.9}$$

where q is the scattering vector (see Eq. 5.1).

The hydrodynamic radius R_h of the particles is calculated from the diffusion coefficient using the Stokes-Einstein equation:

$$R_h=\frac{kT}{6\pi\eta D} \tag{5.10}$$

where η is the solvent viscosity, T the absolute temperature and k the Boltzmann constant. In these calculations, it should be kept in mind that the hydrodynamic radius may include a solvatation layer.

In the case of polymeric and other systems without distinctive particles, it is more appropriate using a correlation length (ξ) instead of a hydrodynamic radius (R_h). The correlation length is a measure of the range over which fluctuations in one region of space are correlated with those in another region. Two points which are separated by a distance larger than the correlation length will each have fluctuations which are relatively independent (uncorrelated).

DLS measurements are appreciated as noninvasive and relatively fast method to measure various solutions and colloidal systems to determine translational and rotational diffusion coefficients, as well as for studies of systems mobility. It is applicable also for studying of internal modes of polymer networks and gels[88]. Because of its noninvasive nature, the method is widely usable in bio- science *e.g.* to observe dynamic changes in biological systems *etc.*[92],[93],[94],[95],[96],[97].

For measurement we used a commercially available ALV-5000 and ALV-6000 correlator from ALV GmbH (Germany) with homodyne detection. The used light source was a vertically polarized beam of helium-neon laser with wavelength λ=632,8 nm. The intensity of the laser source was regulated with a rotary gradual-dark filter. From the scattered volume the emitted light was conducted through an optical system with an iris diaphragm to the detection system, consisting of a photodiode or photomultiplier. The signal was then sent to the computer with a special correlator card and processed with a supplied software. The general scheme of the equipment is shown in Figure 10.

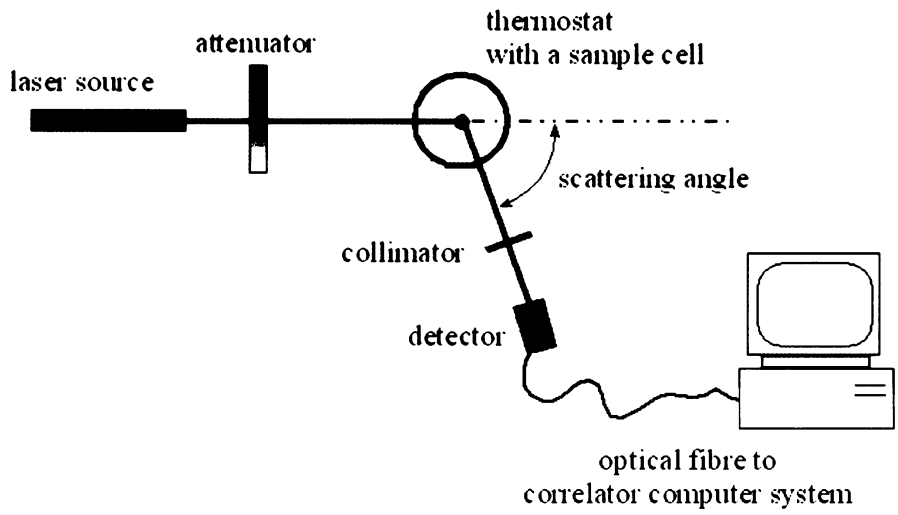

Figure 10: *DLS configuration scheme*

The obtained correlation curves (example in Figure 11a) were transformed by Laplace transformation using home-made program GenR to distribution of relaxation times (Figure 11b) and after that to distribution of correlation lengths (hydrodynamic radius) (Figure 11c).

In the present work it is necessary to show a dependence of three different values, *e.g.* signal intensity/correlation time/temperature. Because a series of simple curves is not too transparent to display it, we decided to use a colored top-view look on a 3-dimensional surface, which is well-known *e.g.* from geographical projection of Earth's surface and is more suitable for our purposes (example in Figure 12).

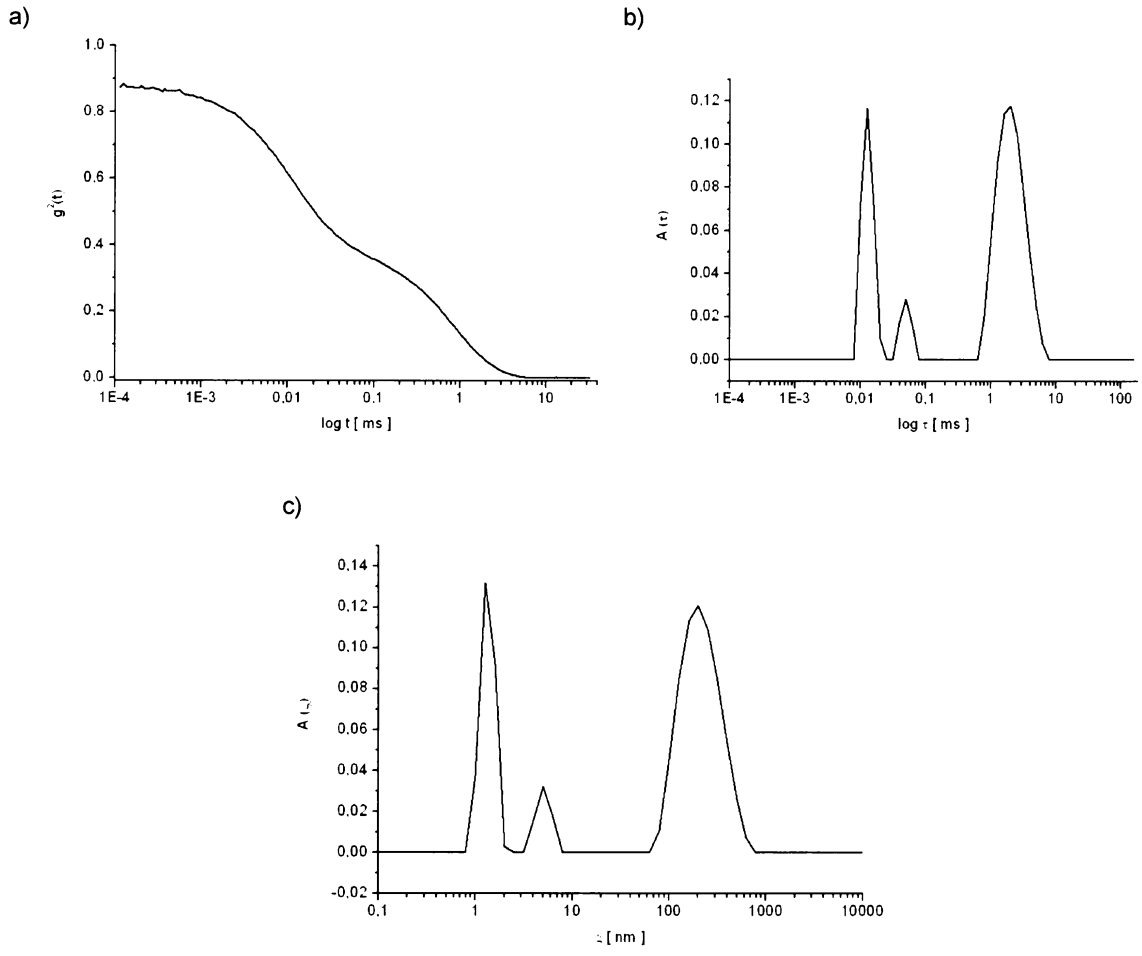

Figure 11: *DLS data processing steps: (a) correlation curve; (b) distribution of relaxation times; (c) distribution of correlation lengths.*

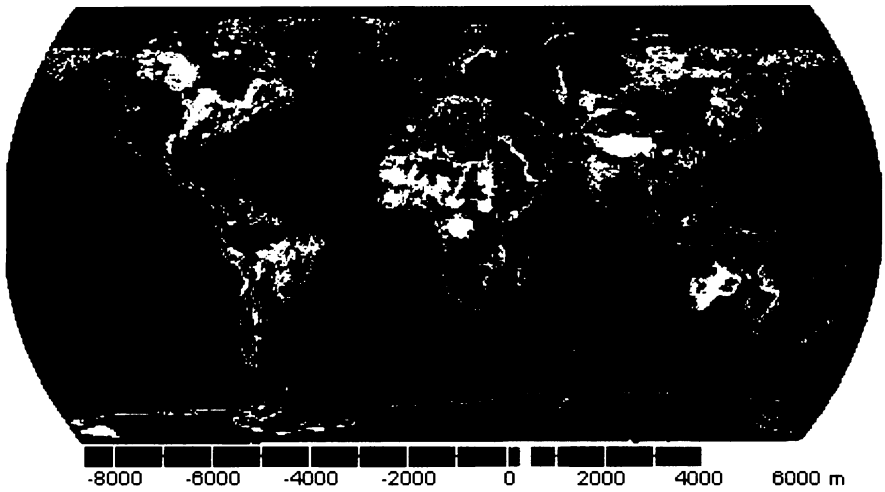

Figure 12: *Example of mapping of 3-dimensional surface.*

5.4 Atomic forces microscopy (AFM)

The Atomic forces microscopy (AFM) is a branch of Scanning probe microscopy (SPM) group and now is used for imaging of surfaces of various materials. Its official history starts in 1986 when Binnig, Quate and Gerber published[98] their progress to measure small forces and introduced it as a new method for detection of atomic scale features[99].

The AFM is based on the surface probing with special, very fine and sharp tip, generally made of silicon or silicon nitride and located on the end of a thin, flexible cantilever. The interaction between the tip and the investigated sample is influenced by surface topography and other forces (adhesion, magnetic domain orientation, domain polarity,...). The position of a laser beam reflected on the cantilever is detected with photodiode position-sensitive detector and transferred to an electronic device for processing. The general schema of AFM scanning is in the Figure 13.

The scanning is running over the sample on a grid system so that this configuration enables getting a 3D view of the surface properties. In good conditions and samples it is possible to obtain an atomic resolution of the scan: in the $x - y$ plane a range of about 0.1 – 1.0 nm and in the z direction about 0.01 nm[99].

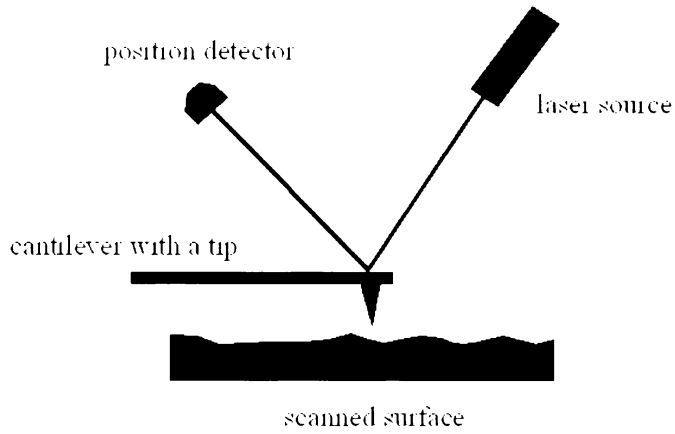

Figure 13: *AFM block schema.*

During the scanning, either the sample or the tip is fixed and the other is moved with a piezoelectric system. The goal is to hold a balance based on initial conditions and given by the user. During the scanning the process is under the control of a feedback system which is, besides of other things, responsible for preventing the tip damage. The established differences between the set state (the "set point") and the "effort" to hold it, is recorded and imaged as the final signal.

As in other methods there exists different adaptations for AFM technique. The two most used are scanning in a contact mode or in a tapping mode.

The contact mode (CM-AFM) means scanning the surface with a sharp tip which is very close – in "contact" – to the sample surface, or precisely, with a thin, fluid layer of adsorbed molecules of gasses and/or vapors on it. The initial set point in this case means selection of an elevation of the tip over the surface and holding this tip - sample distance with help of feedback system during the scanning. The recorded signal represents the deflections of the cantilever given by repulsive or attractive forces between the tip and the probed surface. The disadvantage of this simple and effective method is fast tip contamination on softer materials or the surface destruction and easy tip damaging on surfaces with bigger roughness.

The tapping mode (TM-AFM) is a small modification of the above method, where the tip is held with stable oscillations at the sample surface while scanning. It means that the tip lightly touches the surface only at the lowest position of every oscillation, which is saving both the tip and the surface. The recorded signal covers the preserving of stable oscillations and distance of tip and the sample. In the case of tapping mode we are able to obtain not only the topography signal, but also the "phase" signal which is generally the superposition of sum of all interactions like adhesion, polarity, magnetic fields, conductivity *etc.*, so in good conditions it is possible to "see" material surface distribution into specific domains. The values for phase signal are given in angle units, and here the phase angle is defined as the

phase lag of the cantilever oscillation relative to the signal sent to the piezo element driving the cantilever.

Thanks to the mentioned qualities, in the present time the AFM is often selected as one of the best methods for investigation of polymer self-organization in thin layers.

Part of the AFM measurements, dealing with block copolymer thin layers vapor-annealing, were executed in the laboratories of IPF in Dresden. The samples were examined by TM-AFM using an MFP-3D (Asylum Research) AFM microscope and BS-Tap300-50 tips (Nanoscience Instruments).

The study of thin layers of ternary polymer blends was done in AFM laboratory of Institute of Macromolecular Chemistry AS CR. There was used a multimode AFM Nanoscope IIIa (Digital Instruments) and OTESPA 7 silicone tips.

The final image processing was in all cases done with the software WSxM ® (Nanotec Electronica; http://www.nanotec.es).

The substrate was glossy silicon wafer with a silicon-dioxide layer on the top of one side (ON Semiconductor Czech Republic; 0.4mm, dopant As, orientation <100>). Before using, wafers was cleaned in hydrogen peroxide – ammonium hydroxide bath by a standard procedure:

- degrease plates in methylene chloride in ultrasonic bath (3 baths of 15 minutes)
- then cleaning in the "piranha" mixture from water + ammonium hydroxide + hydrogen peroxide in volume ratio 1:1:1 at 63 °C for 1,5 hours
- washing in millipore water (3x) to remove rests of chemicals
- let through the night in water to obtain an equally hydrated SiO_2 surface
- wafers were stored in the water bath, but at most for a one week period; after that a new series of clean plates was prepared

5.5 Other methods

To obtain physical and chemical characteristic of studied samples we also use a few of temporary methods, like gel permeation chromatography (GPC), nuclear magnetic resonance (NMR), ellipsometry and differential scanning calorimetry (DSC).

6 Results

6.1 Polymerization

6.1.1 Anionic polymerization

All used homopolymers and diblock copolymers were synthesized by anionic polymerization. It is one of the "living polymerization" methods, widely used for precise preparation of polymer materials and with well developed techniques (see *e.g.* [100],[101],[102],[103]).

One of the advantages of this anionic polymerization is that the length of the final polymer chain is easily tuned by the ratio of monomer and initiator amounts. Products synthesized with this polymerization are also characterized by very narrow chain length distribution, so for those reasons we choose it for our purposes. On the other side, the reaction is very sensitive to various impurities as moisture and oxygen, which can "kill" the growing polymer chains, so all monomers and solvents were carefully purified before using. Various synthesis steps with the reaction schemes *etc.* are described hereinafter.

6.1.2 Solvents and polymerization conditions

Before polymerization, the reactor was let overnight in an oven at 120 °C to remove adsorbed impurities. The assembled polymerization system (glass reactor) was then freed from oxygen and rest of moisture by evacuation followed with all glass heating to cca 50 °C and after that a free cooling to room temperature under vacuum. Then argon was filled up to the evacuated system and flushing with argon (now without the heating) was repeated three times to obtain clean, inert system.

The polymerization and all required steps were executed under argon atmosphere. The reaction temperature at all polymerizations was -78 °C. As the cooling agent was used a mixture of $CO_{2(S)}$ and ethanol.

A solution polymerization was used in all syntheses. As the solvent was used tetrahydrofuran (THF) (p.a., Lachema) cleaned by refluxing over sodium (Lachema) and anthracene (Aldrich) complex in argon atmosphere. Freshly distilled solvent was taken for every reaction. For all polymerizations a volume of THF necessary for obtaining ca 3 – 5 % solution of final polymer product was used.

To remove residues of potential contaminants, system was titrated before adding monomer by diphenylmethylpentyllithium (DFMPLi). This agent has dark red colour which bleached after reaction with impurities. This change was used to indicate clean state of the base solvent system in the reactor (THF), where the red colour (from max. 3 drops of DFMPLi) has to be stable for 5 minutes. DFMPLi was prepared from sBuLi and 1,1-diphenylethylene (DFE); reaction schema can be seen in Figure 14. To prepare DFMPLi

solution, we added into an inert flask 40 ml of clean THF, injected 2,3 ml DFE (distilled with calcium hydride in vacuum – ca 1,5 mm Hg, b.p. 86,5 °C) and cooled to -40 °C. Then we carefully (an exothermic reaction) dropped 8,6 ml sBuLi (1,29 M solution in cyclohexane, Fluka) and let the solution overnight in a refrigerator, where it was also stored. Every 2 weeks was prepared a fresh solution. This chemical was – except of titration purposes – used also as the initiator for the methacrylates polymerization. In calculations of initiator amounts in synthesis, the content of s-BuLi was taken into account.

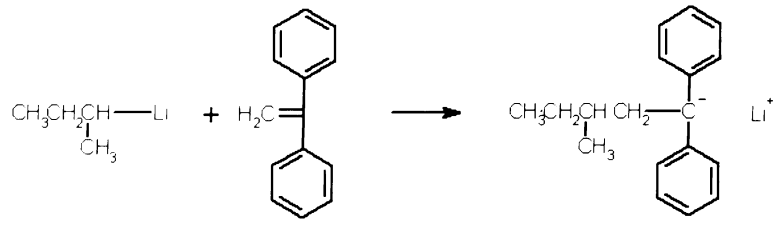

Figure 14: *Reaction of preparation of diphenyl-methyl-pentyl-lithium agent from s-BuLi and diphenylethylene.*

6.1.3 Monomers

The *n*-butyl methacrylate monomer was a commercially available chemical. After purchasing, butyl methacrylate was purified by vacuum-distillation with calcium hydride (Aldrich), stabilized with Irganox 1010 (Ciba-Geigy) and stored in freezer at -20 °C.

The *p*-octylstyrene monomer was synthesized in cooperation with prof. Stibor from VŠCHT in Prague. The product was synthesized from *n*-octylbenzene, which by reaction with acetylchloride and aluminium chloride gives 4-*n*-octylacetofenon. This after reduction with natriumborohydride gives alcohol ethan-1-fenyloctan-1-ol. The last product after dehydration by heating with $KHSO_4$ to 170-220°C, in the presence of antioxidant, finally gives the required monomer. The monomer synthesized by the described procedure was purified by distillation. As the last step, *p*-octylstyrene was recrystalized from ethanol (LACHEMA) at -70 °C, stabilized with Irganox 1010 and stored in freezer at -20 °C.

monomer	"cleaner"	distillation details	
		pressure [mm of Hg]	temperature [°C]
n-butyl methacrylate	trioctylaluminium	15	ca 90
p-octylstyrene	dibutylmagnesium	0,03	ca 150

Table 2: Used monomers details.

Directly before polymerization, the second cleaning procedure was used. The *p*-octylstyrene was distilled in vacuum with dibutylmagnesium (1 M sol. in heptane, Aldrich) and the butyl methacrylate was cleaned by vacuum distillation with trioctylaluminium (25 wt % sol. in hexanes, Aldrich). For every 10 ml of monomer was added 1 ml of cleaning agent.

6.1.4 Polymerization of p-octylstyrene (OS)

As initiator for poly(*p*-octylstyrene) (POS) synthesis was used *sec*-butyllithium (sBuLi) solution (1,29 M sol. in cyclohexane, Fluka).

The required amount of s-BuLi was added into the clean reactor with titrated and cooled solvent and then under vigorous stirring the calculated amount of OS monomer was dripped. The polymerization ran for 3 hours at the temperature of -78 °C and stirring of reaction mixture.

After that, the polymerization was terminated by degassed methanol and the system was heated to room temperature. The solution was then concentrated to ca one quarter of the original volume and the homopolymer product was isolated by precipitation into methanol and after isolation dried in vacuum at 45 °C. The product was characterized by GPC to obtain molecular weight distribution and by DSC to obtain T_g value.

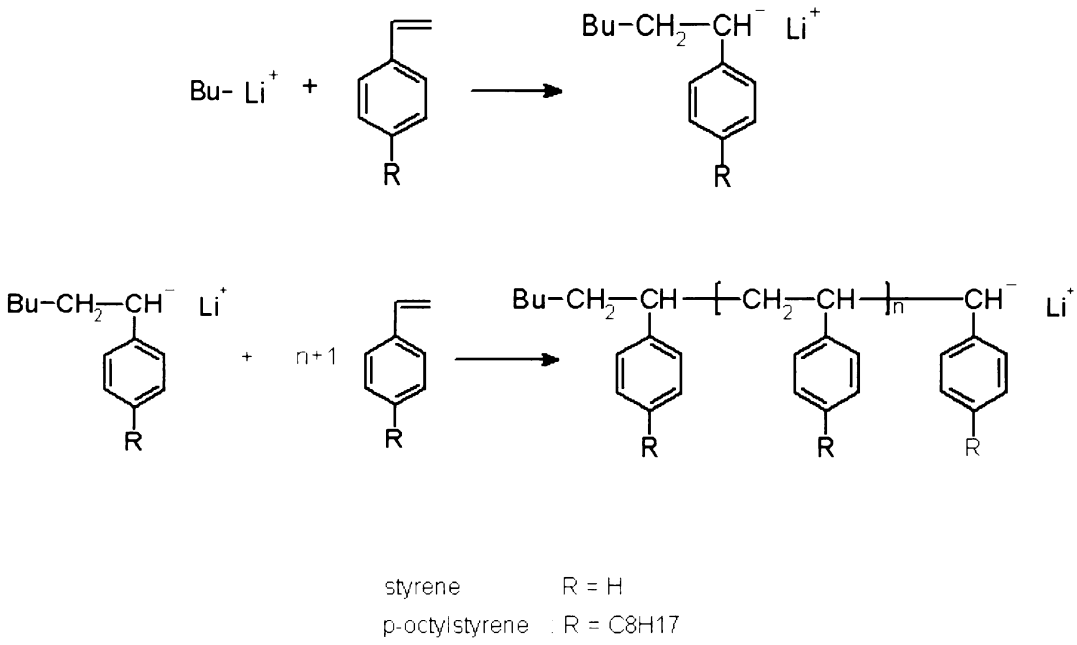

Figure 15: *Polymerization of styrenes – scheme of initiation and propagation steps.*

6.1.5 Polymerization of n-butyl methacrylate (BM)

In poly(butyl methacrylate) homopolymerization we used as initiator DFMPLi (Figure 14).

The reaction steps were similar to the POS synthesis, with one difference: into clean reactor with titrated solvent was added solution of tBuOLi (0.5 M solution in pure THF; synthesized from *tert*-butyl alcohol p.a., Lachema and lithium 99.9%, Aldrich) as reaction stabilizer[100]. A five-fold molar amount of tBuOLi relative to BM was used in all synthesis.

The solution was then retitrated and the calculated amount of DFMPLi was added as initiator. Finally, the required volume of BM monomer was dripped under vigorous stirring. The polymerization was run for 1,5 hour at continuous stirring, followed by termination by degassed methanol.

The reaction mixture was then heated to room temperature and evaporated in vacuum to ca one-third of the original volume. The product was obtained by precipitation to a fifteen-fold volume of methanol. After drying in vacuum at 45 °C, the products were characterized by GPC to obtain molecular weight distribution and by DSC to obtain the T_g value.

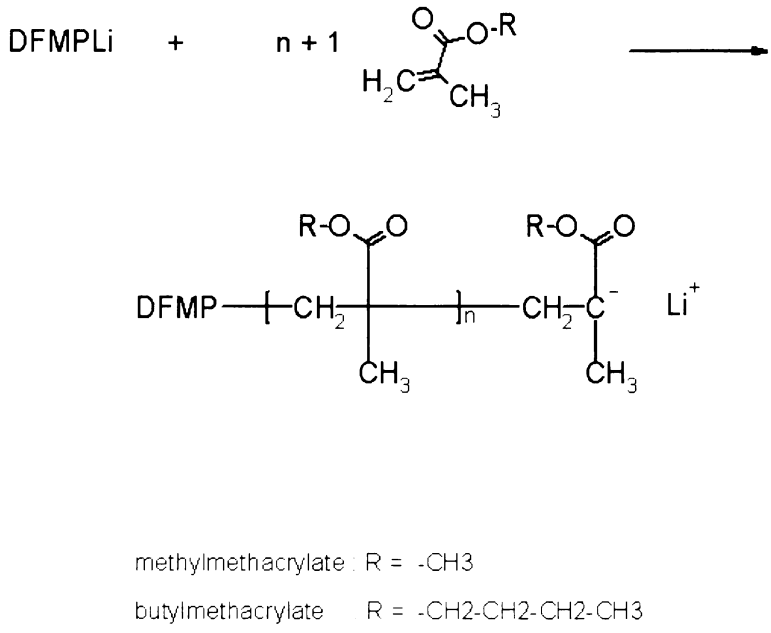

***Figure 16**: Polymerization scheme of methacrylates*

6.1.6 Synthesis of block copolymers

Diblock copolymers were synthesized by sequential copolymerization initiated with sBuLi in THF solutions.

The required amount of initiator was added into a clean reactor with titrated solution of tBuOLi and at -78 °C the *p*-octylstyrene monomer was dripped under vigorous stirring. Polymerization of *p*-octylstyrene chains ran for 3 hours at continuous stirring. Then a defined amount of reaction mixture was taken away and terminated with methanol to have an information about poly(*p*-octylstyrene) chain size and distribution. Immediately after that a calculated amount of butyl methacrylate monomer was slowly dripped (in 5 minutes) into the reaction system and the copolymerization (while stirring) continued for the next 2 hours.

Then the reaction was terminated with degassed methanol, solution was evaporated in vacuum to ca one-third of the original volume and precipitated into a fifteen-fold volume of methanol. To obtain a clean product, precipitation was repeated. The rest of the "killed" *p*-octylstyrene homopolymer present in the final product was removed by a new precipitation into specific solvent - acetone (LACHEMA) that does not dissolve pure POS homopolymer.

The final products – the copolymer and homopolymer collected after the first reaction part - were characterized by GPC and NMR.

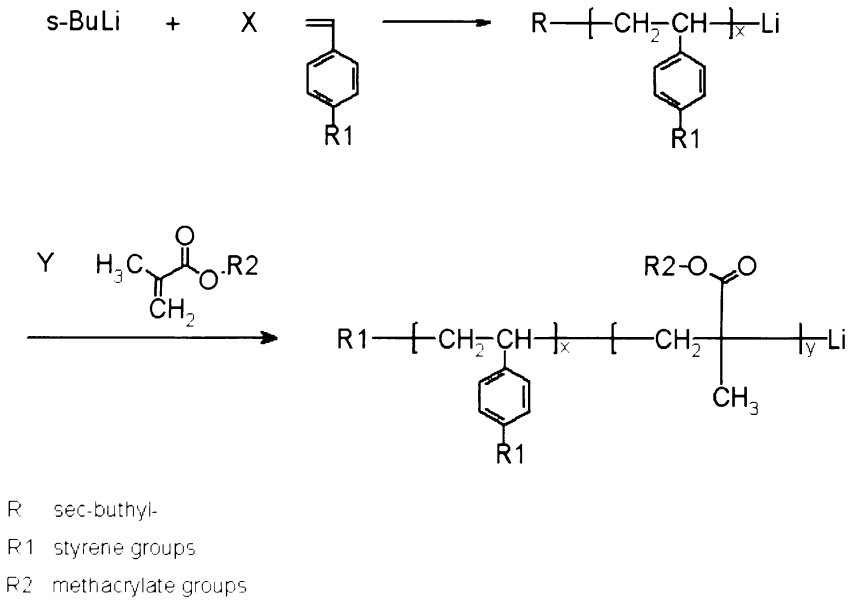

Figure 17: *Scheme of preparation of diblock copolymers.*

product code	total polymer		octylstyrene		butyl methacrylate		total polydisp.	octylstyrene content (w/w)
	M_W	M_N	M_W	M_N	M_W	M_N		
OS-3	-	-	2831	2587	-	-	1,09	-
OS-5	-	-	7898	7227			1,09	-
B5A	-	-	-	-	3735	2634	1,42	-
B8	-	-	-	-	8689	6901	1,26	-
OB2B	12325	9834	5455	4984	6870	4855	1,25	44,3
OB3	23370	22490	11598	11142	11772	11348	1,04	49,6
OB5	35596	29678	21867	20561	13729	9117	1,19	61,4

Table 3: Details of synthesized homopolymers and block copolymers.

6.2 Measurement of block copolymers ODT

An important characteristic of diblock copolymers is their order-disorder transition temperature (ODT), from which it is possible to obtain the Flory-Huggins interaction parameter χ of the pair of blocks. Generally we can say that if χ of the components in the studied system is negative, their mixing is possible (this may be the caused *e.g.* by hydrogen bonding), if χ is positive, the interaction between different segments is repulsive, the system is not compatible and phase separation appears in some temperature range. In most applications the χ is determined experimentally and in symmetric diblock copolymer systems we can use the prediction $\chi N = 10.5$ valid at the ODT. If $\chi N < 10.5$, the system is homogeneously mixed, if $\chi N > 10.5$, the system is phase separated.

To determine the ODT of block copolymers we used a simple home-made equipment based on changing of plane of polarized light (50 mW He-Ne laser, Spectra Physics 125A), which passed through the studied system (see Figure 18). The sample in a flat cuvette (thickness from 0.2 mm to 0.5 mm) was placed between crossed polarizers and its temperature was slowly changed (generally by 1 °C per 1 minute). The ordered sample is birefringent and, therefore, the originally "zero transparency" of the optical systems changes and light starts go through it. The transmitted intensity I_t is then detected by a photodiode detector.

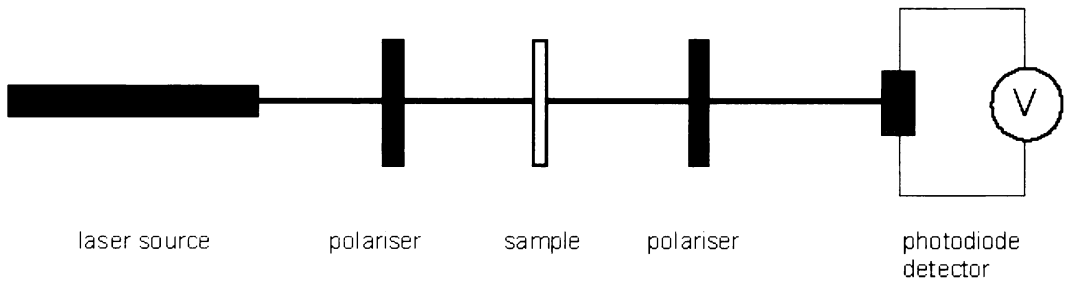

Figure 18: *Schema of equipment for ODT measurement.*

The example of a general result of usually obtained data is shown in Figure 19 (diblock copolymer of polydimethylsiloxane (PDMS) and poly(ethylenepropylene) (PEP): PDMS-*b*-PEP, $M_n = 6300$, $f_{PEP} = 0.48$; a comparative sample of ODT measurements in our laboratory).

To obtain the ODT temperature of OB system we performed experiments with OB2B and OB3 products in temperature ranges up to 180 °C, which was the upper limit for our experimental arrangement. However, this method appears unusable for our samples - the

characteristic change of intensity of transmitted light was not observed and the resultant required ODT temperature was not obtained.

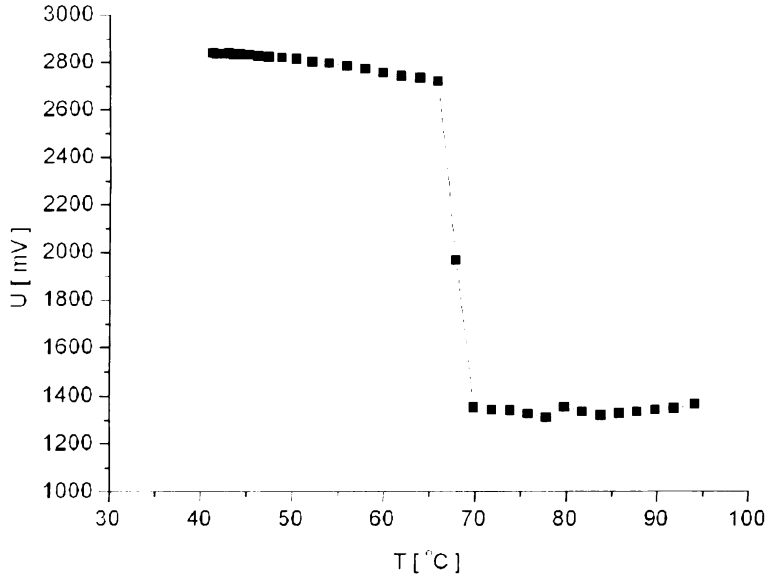

Figure 19: *Demonstration of ODT measurement results for PDMS-b-PEP (M_n = 6300, f_{PEP} = 0.48) diblock copolymer; 0,2 mm flat cell.*

The "obtained" results (see Figure 20) look a little unexplainable at beginning, because a material property[104] of OB copolymers components, compared to the PDMS-PEP etalon sample, are more-less acceptable, as is shown in Table 4.

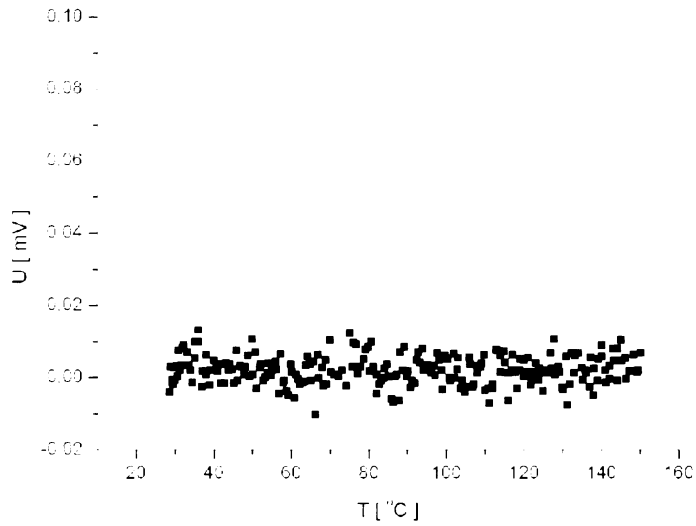

Figure 20: *Example of results from ODT measurement of OB3 sample; 0,5 mm flat cell.*

Also from the TEM examination of our OB samples we have confirmed, that there exists strong, lamellar orientation of presented domains (see Figure 25). However, *e.g.* according to the publications[105], [106], [107], [108] the internal structure of the organized block copolymers consists of irregularly shaped birefringent "grains", with randomly oriented optic axes and the light beam then propagate through a large number of randomly oriented regions. In the cases that the average grains size is small compared to the uses wavelength, the sample demonstrate optical anisotropy and no light polarization occurs - which was also observed in our case.

polymer	POS		PBuMA	PDMS		PEP
refractive index *n*	1,517		1,475	1,39		1,47
ref. ind. difference Δn		0,04			0,08	

Table 4: Refractive indexes *n* of homopolymers used at ODT measurement. The difference of ref. indexes was calculated according to the equation $\Delta n = | n_1 - n_2 |$ where n_i represents refractive index of relevant polymer.

6.3 Compatibility study of homopolymers

Blending polymers is a commonly used method to prepare final materials with suitable physical and chemical properties, thanks to selecting a combination of various components.

The real systems are however generally miscible only when for the Gibbs energy of mixing (ΔG_M) we have $\Delta G_M \leq 0$. The mixing of polymer materials is usually described by the well-known Flory-Huggins equation

$$\Delta G_M = RT[n_1 \ln \phi_1 + n_2 \ln \phi_2 + n_1 \phi_2 \chi_{12}] \tag{6.1}$$

where n_i is the number of moles of component i; Φ is the volume fraction of components; R is the gas constant; T is the absolute temperature and χ is the interaction parameter of components 1 (generally the solvent) and 2 (generally solute), which can be described as:

$$\chi = \frac{(\delta_1 - \delta_2)^2 v_1}{RT} \tag{6.2}$$

where δ_i are the Hildebrand solubility parameters and v_1 is molar volume of the component 1.

Although there exist some homopolymer systems which are mutually compatible and miscible in a wide range of conditions (*e.g.* polystyrene and poly(phenylene oxide) or poly(ethylene terephthalate) and poly(butylene terephthalate)), most polymers don't mix so easily and phase separate into the individual components. The example of ideal phase diagram for a binary mixture of homopolymers (at critical conditions) is presented at Figure 21.

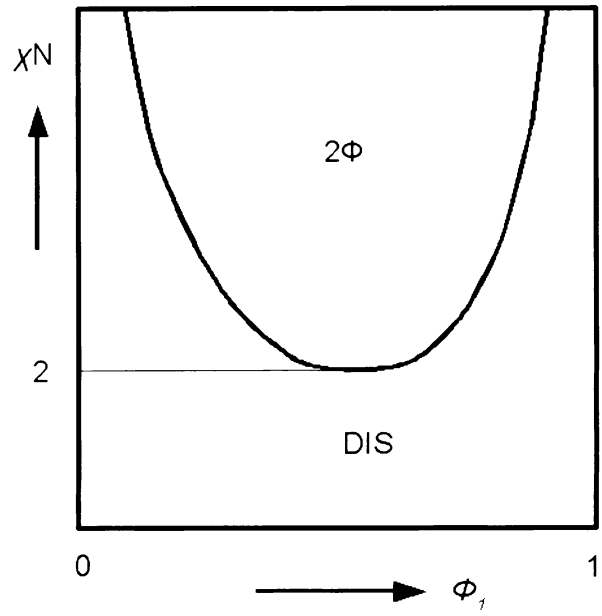

Figure 21: *Phase diagram for a binary blend of symmetric homopolymers. DIS:disordered, homogeneous system; 2Φ: region of coexistence of two separated phases; Φ_1: volume fraction of component 1; N: degree of polymerization; χ: interaction parameter.*

It can be seen that in a binary blend of two symmetric homopolymers at composition $\Phi_1 = \Phi_2$ and the critical temperature, we have $\chi = 2/N$. Because the interaction parameter is an important value to characterize a given homopolymer system, we tried to determine it by observing the phase interface in the critical binary mixture. For this purpose we first prepared a critical mixture of low-molecular weight homopolymers POS and PBuMA, calculated using the equation[109]

$$\Phi_1 = \frac{N_1^{1/2}}{N_1^{1/2} + N_1^{1/2}} \tag{6.3}$$

To do this, a required amount of homopolymer mixture (OS-3 and B-5A) was collected in glass cuvette (5 mm i.d.) by sequential evaporation of mixture solution (5% w/w) in chloroform. The obtained blend was dried in vacuum oven at 70 °C for 24 hour to remove the rest of solvents and the cuvette was after that sealed in vacuum.

After preparation, the system was separated into two distinctly bound layers. To observe created phase interface behavior, the cuvette was placed in a thermostatted bath and during temperature changes was observed by CCD camera.

An example of result image is showed at Figure 22, where is visible that components incompatibility is very strong and even at high temperature (more than 180 °C) the system is still phase separated. Basely on this fact we can conclude, that for OS/PBuMA blend system the critical temperature is higher than 180 °C and the χ value is not obtainable at conditions standardly used in our experiments.

Figure 22: *Example of image from phase behavior experiments (temperature 183.5 °C) . Phase interface (marked with red arrow) is still unchanged and visually observable.*

6.4 Structure of diblock copolymers

After molecular weight and structure characterization with NMR, we explored natural bulk structure of the synthesized diblock copolymers with help of SAXS (small angle X-ray scattering) and TEM (transmission electron microscopy). For these purposes, the block copolymer samples were thermo-annealed in a vacuum oven for 6 hours at 160 °C. After that, natural slow cooling to room temperature was applied. For examination were chosen samples OB3 and OB5 as representatives of two block copolymers with various components ratio (ca 50% of octylstyrene for OB3 and ca 61% of octylstyrene for OB5).

6.4.1 Small angle X-ray scattering results

Scattering curves from measured data are showed in Figure 23 and the corresponding maxima positions are listed in Table 5.

The results for OB5 are clear and the SAXS spectrum indicates the presence of a lamellar phase, even when the sample composition is at the border between lamellar and hexagonal structure, as can be seen in the theoretical phase diagram in Figure 24. The borderline between these two phases is in the vicinty of f = 0.35 which is very close to the composition of OB5.

The same structural result appears for the OB3 sample, where only the first and third maxima are observable. Since OB3 is almost perfectly symmetric polymer (f = 0.5), this result is in good agreement with weak segregation limit theory[110], according to which a nearly symmetric, square-well electron density profile would lead to a negligible second-order intensity[107].

Using the standard equation for lamellar systems to calculate the *d* spacing of structure $d = 2\pi / q$ with scattering vector q defined as $q = (4\pi/\lambda)\sin(\theta/2)$ where θ is the scattering angle, we can obtain a spacing *d* = 15 nm for OB3 sample and *d* = 19 nm for OB5 sample.

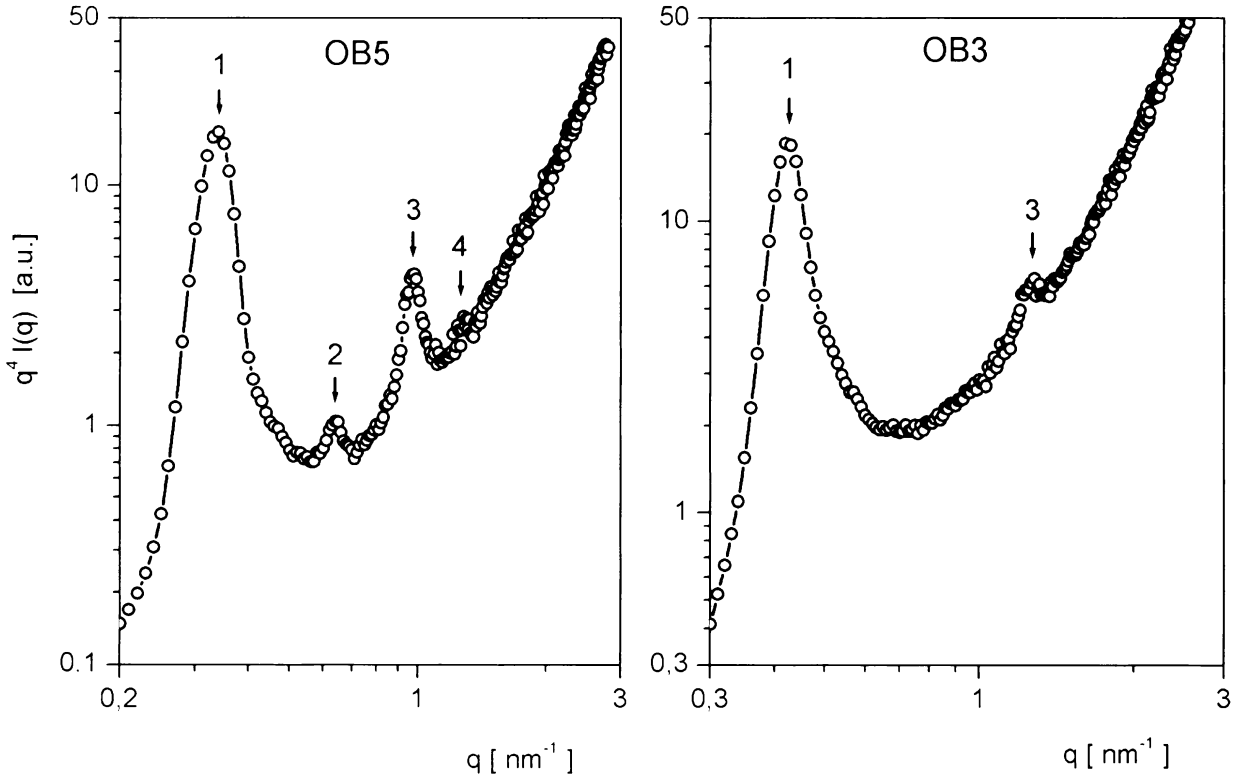

Figure 23: *SAXS measurement of OB3 and OB5 samples. In the images are also demonstrated relative positions of found maxima (see also Table 5).*

sample / maximum	1.	2.	3.	4.
OB3	0,42	-	1,26	-
OB5	0,33	0,64	0,97	1,29

Table 5: SAXS measurement details – numbers at the table head row identify the maxima (relative intensities position given by the ratio: q_i/q_0)from Figure 23. Values in the table body are scattering vector q positions in [nm^{-1}].

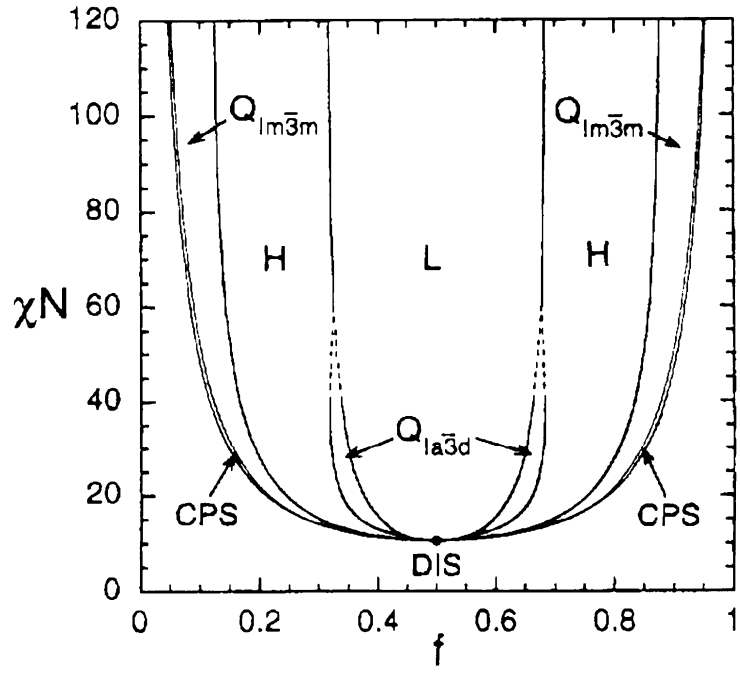

Figure 24: *Example of mean-field phase diagram for conformationally symmetric diblock melts. Phase are labeled - L (lamellar), H (hexagonal cylinders), Q_{Ia3d} (bicontinuous Ia3d cubic), Q_{Ia3m} (bcc spheres), CPS (close-packed spheres), and DIS (disordered). Dashed lines denote extrapolated phase boundaries, and the dot denotes the mean-field critical point. Adopted from [110].*

6.4.2 Transmission electron microscopy results

Slices were cut from the bulk block copolymer samples, prepared as above, and after staining with RuO_4 they were observed by the TEM method. Image processing of TEM photographs was performed using the ImageJ software (http://rsb.info.nih.gov/ij).

The results are shown in Figure 25, where images a) and b) are obtained from OB3 copolymer and images c) and d) are obtained from OB5 copolymer sample. On the basis of previous experiments with RuO_4 staining[85], the black (contrasted) lamellae belong to octylstyrene whereas methacrylates generally remain unstained.

In both OB3 and OB5 samples TEM scanning confirmed lamellar structure supposed from the SAXS method. From these images it is possible (using the above mentioned software) to obtain a lamellar spacing of examined structure, which is ca 17 nm for sample OB3 and ca 22 nm for sample OB5. This sizes also correspond well with the SAXS results.

Moreover, thanks to different homopolymers contrast after staining, it is possible to try to measure the sublamellar ratio of different segments in block copolymers. Because of not sharp-edged interface between the segments and the sample deformation at cutting, the measurement can not be considered as exact, but is still valuable. For the OB3 sample then

we can conclude to stained / unstained length ratio to 8.9 nm / 7.9 nm, which gives octylstyrene volume content as ca 53 %, which is in good agreement with synthesis results of ca 50%. For the OB5 sample, the stained / unstained ratio is ca 14.9 nm / 8.7 nm, which gives octylstyrene volume content in lamellae ca 63 %. Compared to synthesis result (61.4 %) we can also see the good correspondence of these results.

The well-developed lamellar structure in OB3 and OB5 samples, observed both in SAXS and TEM experiments, confirms the strong incompatibility of homopolymers connected into one diblock macromolecule. This immiscibility was also observed in preliminary experiments with OS / BuMA homopolymers binary mixture, where at ca 200 °C the system was still phase separated into two layers. This behavior can also provide usability of the OB system in applications, where the combination of two stable materials with relatively low T_g can bring advantageous properties.

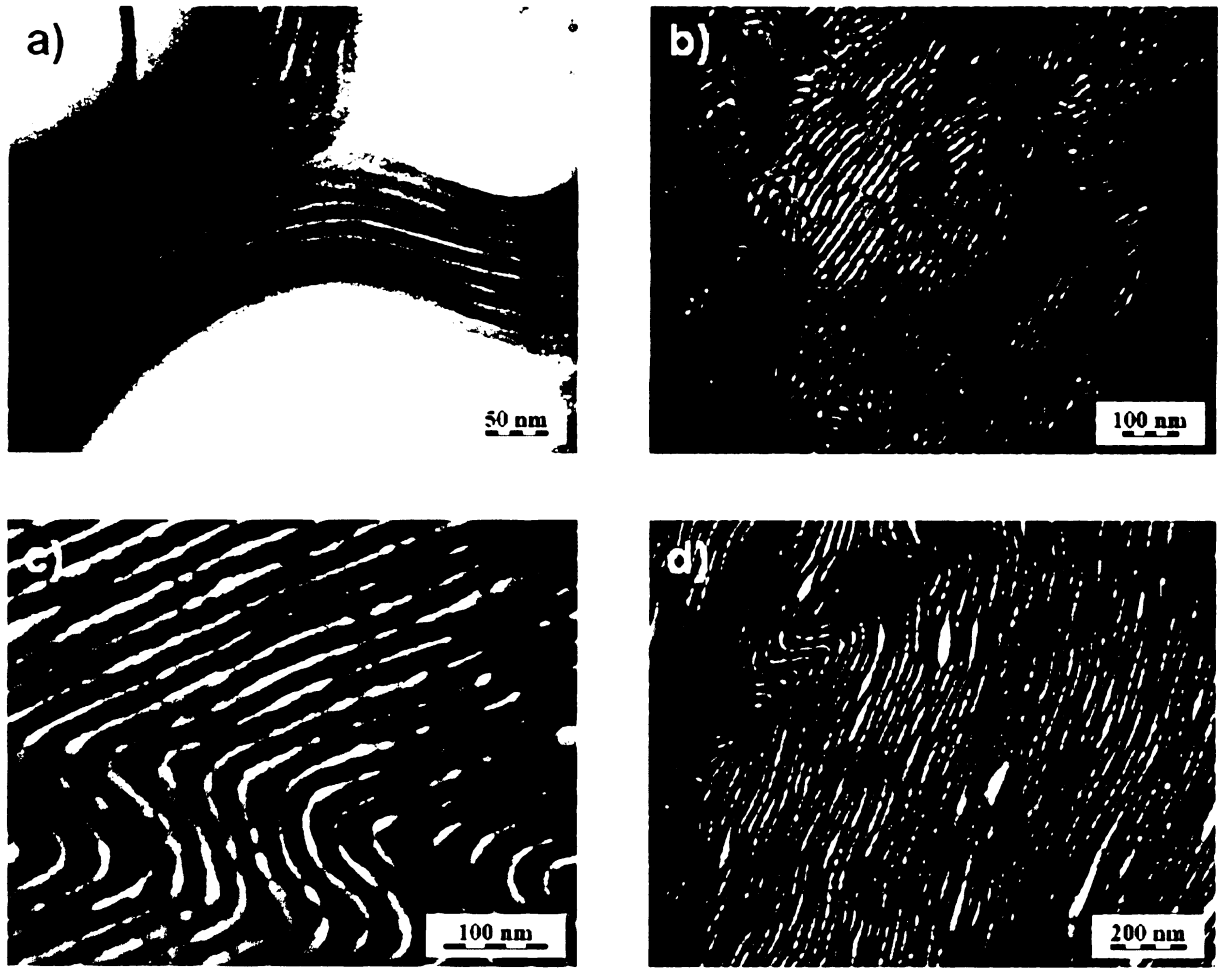

Figure 25: *TEM images of thermo-annealed OB-diblock copolymers. a), b) – OB3 sample; c), d) – OB5 sample*

6.5 Thin layers behaviour

The physical behavior of a polymer system often differs in bulk and in thin layers. The typical self-organization in a block copolymer is caused by a balance between compatibility and miscibility of the homopolymer blocks and the connectivity imposed by covalent bonds. This leads to a grouping of long chains followed by phase separation of the mixtures to qualitatively specific domains, the size of which is limited by the block lengths. This self-assembly can be easily controlled by the synthesis parameters. However, because of considerable influence of interface interaction with supporting material and the surrounding medium (often with air), the behavior in the thin layer can be completely different. Typically, the polymeric component with the lower surface energy will be preferentially accumulated at the surface and the component with the lowest interfacial energy will be situated at the substrate side[111]. Besides, all this can be further modified by other, additional forces or by the history of the thin layers preparation.

Thin layers are currently subject of intensive research, because they have a great potential for various applications, *e.g.* to target membranes preparation, to produce nanodots and nanowires[112],[113] for nanoscience, to form a precision layer[114],[115],[116] or matrix for organic synthesis or to make selective molecular sensors for analytical applications[117],[118].

The scientists in this field have at their disposal a wide range of choices at present time. The simplest way to structural changes is given by different ratio of block chain lengths[119], which, as was mentioned earlier, can be fully controlled by the synthesis. Typical surface patterns of block copolymer formation can be greatly affected also by other effects. An external electric field[120] can be applied to the layer, we can use modification by various solvents[121] or we can control the speed of solvent evaporation[122] during the sample preparation. Also a combination of various techniques can be used to obtain the required organization[123].

The system can be additionally delicately modified, *e.g.* by prewetting the substrate surface with solvents of different polarity[124], by covering the substrate with a defined polymer material[114],[116],[125], by addition of a special chemical compound to the sample[20],[126] and/or by exposure to various solvent vapors[127].

The last mentioned way is very interesting because in a simple manner and with low additional costs, it is possible to highlight or reversibly change existing surface patterns[20]. The behavior of polymers takes into account the "specificity" of the solvent to different monomer units in the polymer chain, so the final swelling ratio can induce unexpected structural shapes by structure deformation.

For these reasons, we made a decision to investigate thin layers of OB copolymer after vapor-annealing in different solvents – chloroform, THF, 1,4-dioxane, acetone and hexane.

The OB5 copolymer was chosen for these experiments; because of its small asymmetry – compared to OB3 – we presumed a richer variability in possible conformations.

Wafers prepared by a standard procedure (described in Chapter 5.4) were dried in micro-filtered air flow and immediately used to be coated with toluene solution of OB5 (concentration ca 1% w/v; filtered through Teflon filter 0.45 μm) by dip casting, to obtain a layer of thickness about 45 nm. The layer thickness was controlled with a microfocus ellipsometer SE-402 (Sentech Instruments GmbH) with a 632.8 nm laser at an incident angle of 70°. Original values for freshly prepared polymer layers (before vapor annealing in solvents) are listed in Table 6.

Solvent to be used	**chloroform**	**dioxane**	**THF**	**acetone**	**hexane**
Thickness [nm]	47	47	45	49	50

Table 6: Thickness of cast copolymer layers before vapor-annealing in solvent.

All samples were vapor-annealed in a small Petri dish divided into four sectors, where two opposite sections were filled with 2 ml of the tested solvent. A sample was placed in one of the remaining sectors. During annealing the dish was covered with a lid. A majority of interaction parameters that would describe the quality of the solvents for individual homopolymers are not known, so simple solubility tests at room temperature have been conducted with all polymer-solvent combinations; they are summarized in Table 7.

polymer / solvent	**chloroform**	**dioxane**	**THF**	**acetone**	**hexane**
poly(*p*-octylstyrene)	G	BP	G	N	BP
poly(butyl methacrylate)	G	G	G	G	BP

Table 7: Homopolymer-solvent solubility. G: good solvent; N: not soluble; B: poor solvent (but slowly dissolving low molecular-weight fractions of homopolymer); P: precipitates at higher concentration or lower temperature. Results are from solubility experiments with ca 3% (w/v) polymer concentration. Room temperature was used as standard and cooling to 3 °C for comparison.

The annealing time was visually checked by layer color changing to blue; the total annealing time used was twice that needed for the first appearance of the blue color. This coloration – according to ellipsometry experiments – corresponded to the swollen thickness of ca 90 nm. According to previous experience, a long exposition (hours) to solvent vapor generally destroys the layers, that were removed by condensed drops, so we did not use a long-time exposition as was done for poly(styrene-*b*-methyl methacrylate)[127]. The annealing time details are described in Table 8.

After vapor-annealing, samples were examined by TM-AFM. For all samples at least three scans were taken to cover different parts of structure formation levels: 1 μm, 5 μm and 25 μm scans. Other sizes were chosen according to actual results. Hereinafter is listed selection of the AFM imaging. The comparison scans of non-annealed samples were smooth both in phase and topography and therefore are not listed in this review.

	Vapor-annealing time [min]			
$CHCl_3$	dioxane	THF	acetone	hexane
4	4	3	18	3,5

Table 8: Annealing time details of studied copolymer thin layers.

6.5.1 Atomic forces microscopy results

Chloroform vapors

According to the previous experiments (Table 7), chloroform is a good solvent for both blocks. Therefore a non-specific swelling and interaction with corresponding homopolymers is expected in this system.

The AFM imaging confirms these assumptions, and on the presented scans (Figure 26) only non-regular patterning on small scales (images a and b) can be observed. The phase image of 1 μ scan shows also sharp phase interfaces, which is in agreement with mutual blocks incompatibility. Because of chains non-specific swelling, together with good polymer solubility and the chloroform evaporation, the sample did not form a regular microstructure. At larger scales (images c and d) a global surface undulation is observed, which can be caused by a tendency to system spinodal decomposition. However, because we have a pure block copolymer system, a phase separation at a bigger scale cannot be observed.

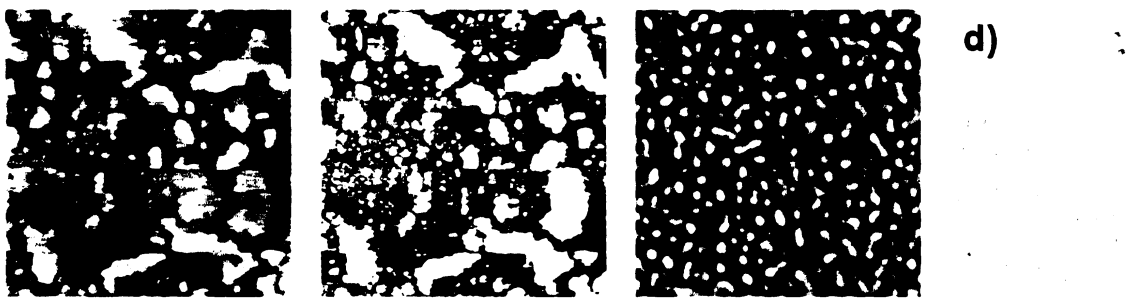

Figure 26: *Annealing in chloroform vapors, a) scan 1 x 1 μm, topography, Z scale 6.3 nm, b) phase of a), Z scale 32° ; c) scan 20 x 20 μm, topography, Z scale 45 nm, d) phase of c), Z scale 73 °*

THF vapors

The behavior of THF/OB system (Figure 27) is similar to the $CHCl_3$/OB one. At higher scale scans (images a and b), the surface looks unorganized and relatively smooth in phase. At smaller scale scans (images c and d), some irregular organization appears. In the case of THF vapors, at 1 μm scans a hole-like structure can be observed both in topography and phase. Because of correspondence of these two images and because we cannot find a sub-organization in smaller scans, we suppose that regular hole structures with diameter around 100 nm, can be residual features from evaporation of solvent. The presence of a perpendicularly-arranged cylindrical phase is not considered, because the diameter size of observed formations is too big relatively to the molecular weight of the used diblock copolymer.

Figure 27: *Annealing in tetrahydrofurane vapors, a) scan 5 x 5 μm, topography, Z scale 49 nm, b) phase of a), Z scale 45 ° ; c) scan 1 x 1 μm, topography, Z scale 8 nm, d) phase of c), Z scale 28 °*

1,4-dioxane vapors

Dioxane is a specific-solvent for PBuMA because it precipitate POS chains. According to this a micellar-like formation in solutions is assumed and influence of this association is expected also on thin layers, because swelling of PBuMA chains will be more distinct then POS chains. However, according to our results, the influence of dioxane solvent vapors on thin layers had a destructive effect, which can be observed on AFM scans on Figure 28. Here on the topography images (a and c) we observe a massive undulation and other deformations of the surface, while the phase structure (images b and d) remains smooth, without a distinct segregation. This can be caused by the fact that the dioxane – although moderately specific for one of the block copolymer chains – is still not enough specific to cause stronger and then sufficient formations. Another explanation can be a parallel organization of potential structures relative to the substrate sheet.

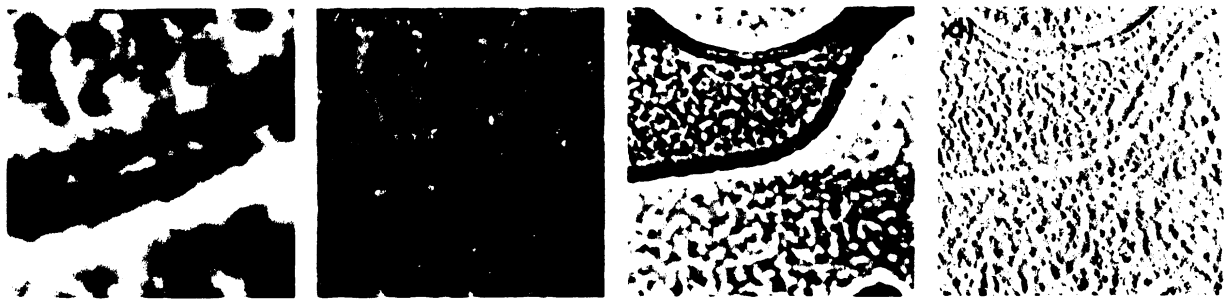

Figure 28: *Annealing in 1,4-dioxane vapors, a) scan 5 x 5 µm, topography, Z scale 69 nm, b) phase of a), Z scale 37° ; c) scan 25 x 25 µm, topography, Z scale 88 nm, d) phase of c), Z scale 68 °*

Hexane vapors

Influence of *n*-hexane vapors is – compared to the previous results – completely different (Figure 29). Some topography morphology is observable, however the corresponding phase separation is very strong, as can be seen on the 1 µm scan result (picture 29d). There is visible a lamellar arrangement of block copolymers, laying perpendicularly to the surface (or substrate). The lamellae are well-developed with clear phases interface.

Figure 29: *Annealing in n-hexane vapors, a) scan 5 x 5 µm, topography, Z scale 18 nm, b) phase of a), Z scale 21.5° ; c) scan 1 x 1 µm, topography, Z scale 7 nm, d) phase of c), Z scale 45 °*

A cross-section through the phase image is shown in Figure 30. From this graph we can measure the lamellae thickness, which give average size for white / coloured lamellae ca 11.5 nm / 16 nm, *i.e.* ca 27.5 nm for the average lamellar spacing. This is more than the size observed by the SAXS (19 nm) or TEM (22 nm), however because the sample preparation is completely different and a thin layer is observed by AFM, we can accept these results.

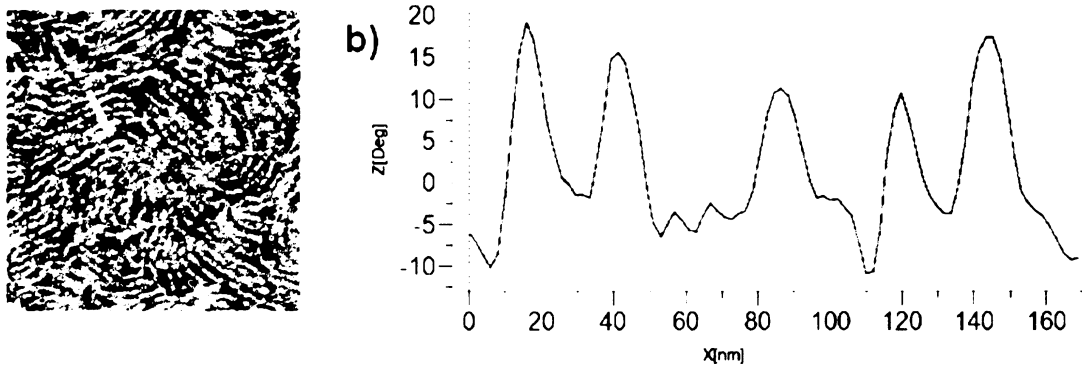

Figure 30: *Hexane annealing OB5 thin layer sample; sectional view from the phase image (details on Figure 29d); a white line on image (a) indicates the presented cut path displayed on the graph at image (b).*

Acetone vapors

Acetone vapors had similar influence on OB system as hexane, however the formations organization is oriented in different direction – parallel to the silicone wafer surface (Figure 31). At small scans the sample does not form a nanometer-scaled structure, but at large scans we can see a kind of lamellar organization. In this case, the surface deformation caused by the solvent vapors is exhibited as crater-like formations or better, terrace formation.

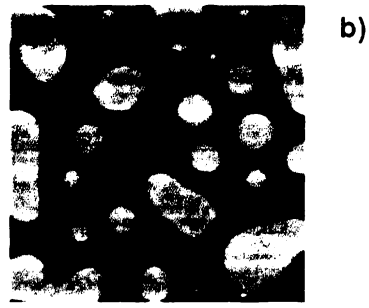

Figure 31: *Annealing in acetone vapors, a) scan 50 x 50 µm, topography, Z scale 153 nm, b) phase of a), Z scale 349 °*

The cross-section of the scan is displayed at image Figure 32. There we can distinctly see that the polymer thin layer is structured into two parallel sublayers. The cracks, caused probably by different swelling ratio of blocks, goes through them and reveals that the final structure after vapor annealing is regularly organized into two levels.

The fact that the phase signal in this and previous cases is often smooth without a phase interface, is probably due to the fact that in systems of diblock copolymers, where the one

chain has a very low T_g and the other has a T_g above the room temperature, the polymer/air interface is usually covered with the softer material. This effect was observed and described also in poly(isoprene)-*b*-poly(styrene) diblock copolymer thin layers[128] and leads to reduction of interface tension at the polymer/polymer interface.

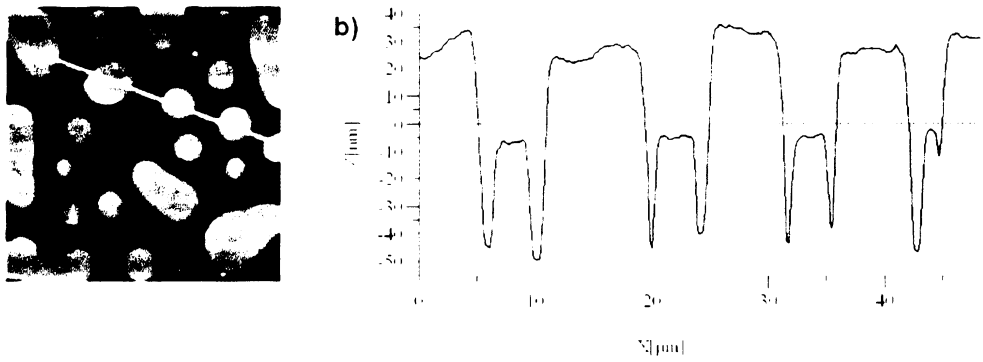

Figure 32: *Acetone annealing of OB5 thin layer sample; sectional view from the topography image (details on Figure 31a), a white line on image (a) indicates the cut path displayed on image (b).*

From the obtained images it is clearly visible that using vapors of various solvents it is possible to obtain a different organization of the originally identical layers of OB diblock copolymer. This can be seen mainly when comparing of the influence of hexane and acetone, where we have obtained lamellar organization. However, in the first case the orientation of lamellae with respect to the silicone substrate was perpendicular, while in the second case it was parallel. Using the other solvents like THF or chloroform had not a so strong self-assembly effect.

From all the results we may conclude that to obtain a structured surface of diblock copolymer it is suitable to use a solvent which can selectively dissolve one of the block, as was already shown in previous experiments[129].

6.6 Ternary polymer blends in thin layer

We have examined structure formation of ternary blends of a symmetric block copolymer (A-*b*-B) and two corresponding homopolymers (A and B) in thin layers.

For these systems there exists a characteristic composition of the polymers called a Lifshitz point (LP), where the blends form a bicontinuous microemulsion (BME). Adding of the different content of the diblock copolymer to the same binary mixture of homopolymers the system undergoes either a macrophase separation or an organization into a lamellar phase (see Figure 5 and Figure 6).

For these experiments we used OB3 as the diblock and OS-3 and B5A as the homopolymers with values (calculated using equations (4.2) - (4.3)):

reference sample: 58.6 % POS + 41.4% PBuMA

LP mixture: 3.89 % of OB3 and 96.11 % of reference sample

To cover thin layer behavior in all regimes, we have prepared three ternary mixtures corresponding to composition (see Table 9):

1. at LP
2. above the LP
3. below the LP

sample name	calculation [mg]				real composition [mg]			
	block copolymer	POS	PBuMA	block [%]	block copolymer	POS	PBuMA	block [%]
LOB5-1	1.9	28.2	19.9	3.9	1.9	28.2	19.2	33,44
LOB5-2	4.5	26.7	18.9	9	4.2	26.9	19.8	33,21
LOB5-3	0.5	29	20.5	1	0.7	33.3	20.3	0

Table 9: Details of composition of samples used for the BME examination on the thin layers.

The mixtures were dissolved in 1 ml of toluene filtered through 0.2 µm PTFE filter to obtain ca 5 % solution. This solutions were spin-coated (40 µl of sample, speed 2000 rpm, ramp 10000, time 60 s) onto polished silicone wafers, prepared by standard procedures described in the section dealing with vapor-annealing.

Immediately after preparation we checked the samples with AFM. All layers were smooth without a surface structure, so we have applied a thermo-annealing procedure to obtain phase separated systems using followed conditions:

- heating of covered wafers in vacuum oven to 150 °C

- keep for 30 minutes at this temperature
- switch-off the heating and let the system cool down to the room temperature (still in vacuum)

The thermo-annealed samples were again examined using AFM and the obtained results are presented hereinafter.

6.6.1 LP system

The LP system shows distinct structural behavior, where the internal microemulsion arrangement probably protrudes on the top of the surface and exhibits a hill-like or shark's-teeth-like structure formation (Figure 33). From these scans we have obtained lateral dimensions of "teeth" of ca 190 nm (measured in the middle of formed cone) with corresponding height of ca 800 nm.

According to our opinion, this formation is clearly visible thanks to extremely low T_g of first homopolymer – poly(*p*-octylstyrene) – presented in the system. OS flows-down at higher temperature and thus reveals the internal structure which is commonly hidden in bulk material. This – hard – structure is probably formed by the stabilized poly(butyl methacrylate) chains present both in the second homopolymer and block copolymer.

We are aware that the system behavior in thin layer after thermal annealing is different from the bulk behavior observable *e.g.* in Figure 7, but up to now we didn't find similar work dealing with A-*b*-B/A/B BME system to compare the results. The developed teeth-like structure can be on the other side extremely useful for the nanotechnology templating, because it shows that it is possible to obtain regular structures potentially fillable or coverable with third-party materials, *e.g.* with metals. Thanks to this we could potentially produce nano- or micro- particles required in other fields of technology.

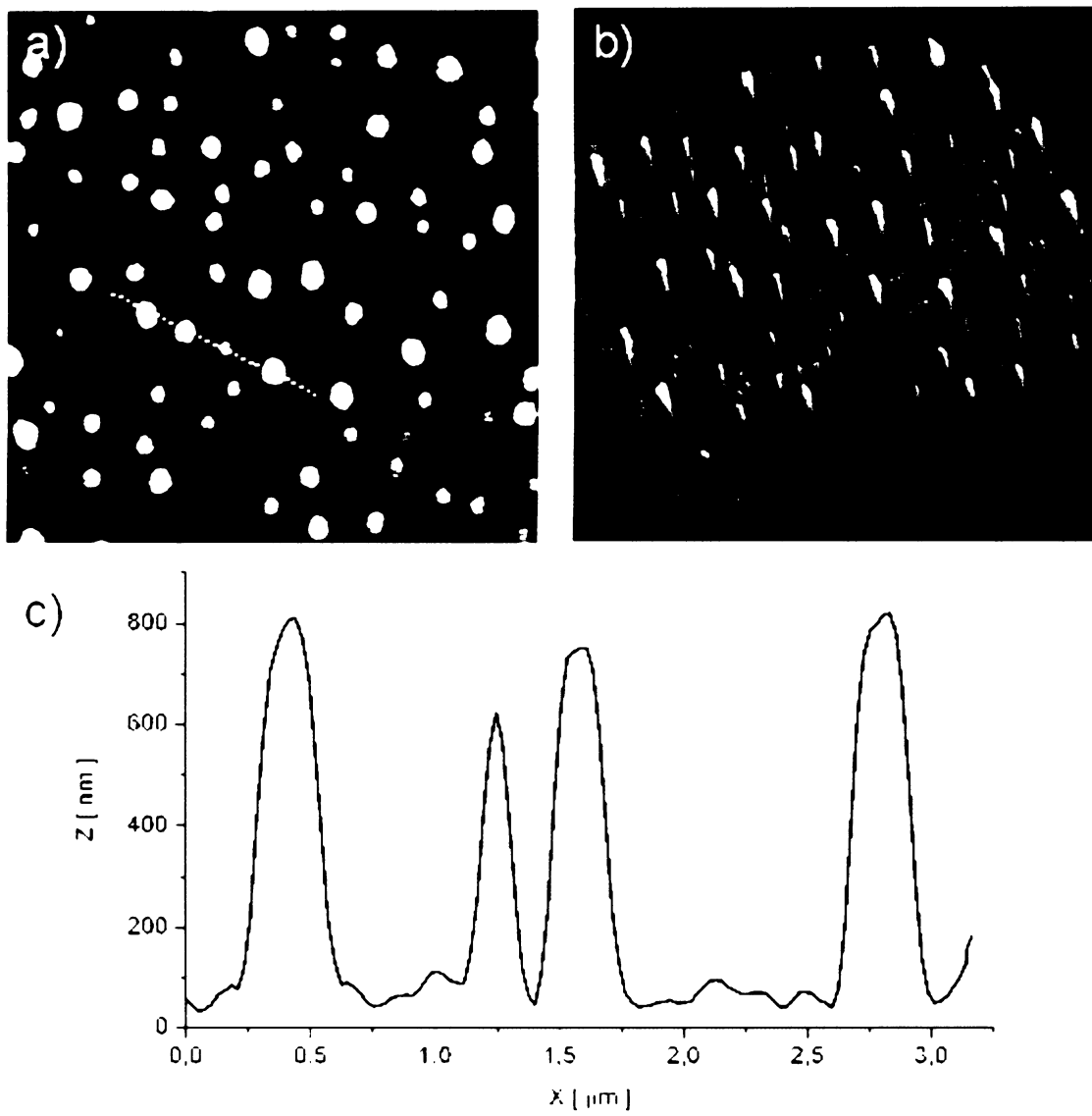

Figure 33: *AFM results of LP (LOB5-1) sample in thin layer. Thermo-annealed sample. (a) 10 µm scan, topography, Z = 1 µm; (b) 3D view of the image (a). (c) a topography profile along the white line in the (a) image.*

6.6.2 Systems with higher concentration of diblock copolymer

All samples with higher concentration of OB3 were smooth under the AFM (Figure 34), without a noticeable surface pattern. It is probably caused by the fact, that according to the phase diagram, the systems with higher concentration of diblock copolymers form lamellae, which may be generally oriented in parallel or perpendicularly to the substrate surface.

In the case of parallel organization, the surface is smooth as was also observed in the experiments dealing with vapor annealing of block copolymers.

Also a presence of distinct content of POS in the system can, thanks to its flow, cause a kind of leveling of the top of the surface. This effect will probably play an important role in the case of flatter surface formations.

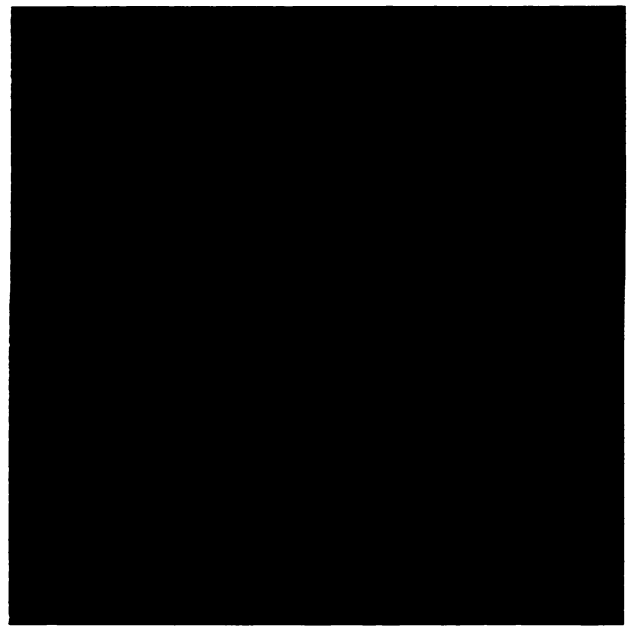

Figure 34: *AFM image of LOB5-2 sample, topography, 10 μm scan, Z = 5 nm.*

6.6.3 Systems with lower concentration of diblock copolymer

In the case of low concentration of diblock in the ternary system, the mixture is unstable and macroscopically separates into two or three phases.

The AFM image in Figure 33 shows a beginning of spinodal decomposition of the thin layer blend into domains rich in either first or second homopolymer.

As in the case of LP system, the observable low-level regions in topography structure are probably caused by the presence of the mobile POS homopolymer with low T_g, surrounding the harder PBuMA material.

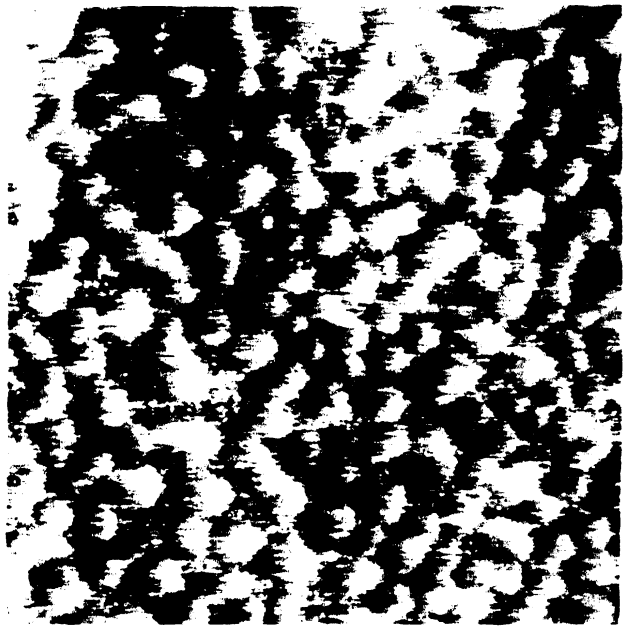

Figure 35: *AFM image of LOB5-3 sample, topography, 20 µm scan, Z = 5 nm.*

6.7 Diblock copolymers solutions in binary mixtures of partially miscible solvents

Block copolymers show a characteristic behavior in different solvents that depends on the thermodynamic interaction between the respective homopolymer chains and the solvent used.

Because of high incompatibility of PBuMA / POS homopolymers, we found interesting to examine the OB diblock copolymer behavior in the binary mixture of partially miscible solvents, namely dimethylformamide (DMF) and *n*-heptane (C7). (To simplify terminology, in further text we will describe this DMF/C7 system as the mixture of two incompatible solvents.)

The behavior of the mixture of these two solvents is described by the phase diagram[130] shown in the Figure 37; the system shows a critical temperature of T_C = 75.3 °C with DMF critical weight fraction w_C = 0.35. Below the coexistence curve two phase-separated regions coexist – an equilibrium of heptane-rich liquid phase with a DMF-rich liquid phase.

In the system, C7 is a preferred solvent for POS homopolymer and is a theta solvent for PBuMA with a θ temperature of ca 65 °C (approximated from[131] as shown in Figure 36). This value is close to the previously published[132] θ temperature for C7 / poly(*tert*-butyl methacrylate) system with θ = 64 °C, so according to our opinion it can be accepted. The other solvent, DMF dissolves PBuMA and precipitates POS.

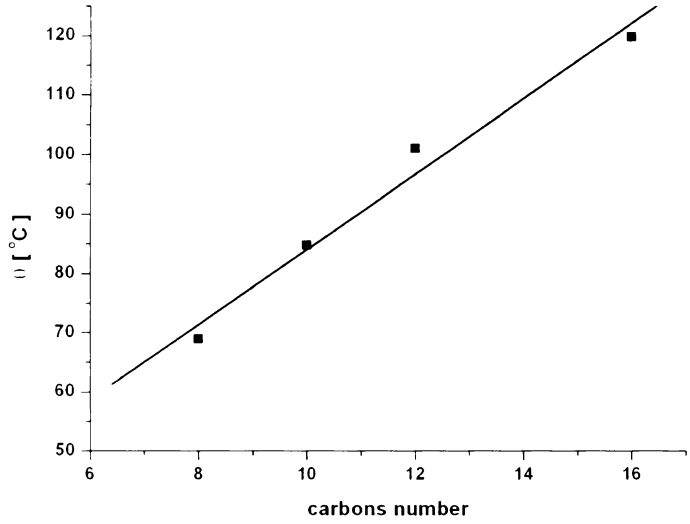

Figure 36: *Theta temperature for PBuMA in n-alkanes. Constructed from experimental data from ref. [131].*

The scheme of the interface structure of a microphase separated solution of OB block in the binary mixture is shown in Figure 38. This scheme refers to local arrangement, on long

distances the interface may be curved to produce, *e.g.*, a cubic or hexagonal morphology. Experiments were performed with both OB3 and OB5 products, to compare symmetrical and asymmetrical copolymer behavior. For this, solutions with different content of DMF and/or OB were prepared, to study effects of different block copolymer concentrations and effects of different binary solvent compositions.

To prepare polymer solutions, we evaporated in vacuum small amounts of filtered (Millipore PTFE microfilter; 0.45 μm) block copolymers solutions in cyclopentane (1% w/w) into a clean, dust-free cell. The operation was repeated until the desired amount of the copolymer was accumulated in the cell. The concentration used was ca 1/5 of c*, the crossover concentration, calculated as $c^* = 3M/4\pi N_A R_g^3$, where M is the polymer molar mass, N_A the Avogadro number and R_g the radius of gyration; for R_g the calculation was for simplification approximated to be that for polystyrene chains with the same M_W dissolved in toluene, using the equation for $R_g \approx 0.0145 M_W^{0.595}$ from[133]; with these assumptions we obtain for OB3 theoretical values $R_g \approx 5$ nm, c* = 7.4% and for OB5 values $R_g \approx 6.4$ nm, c* = 5.4%. Appropriate amounts of filtered selective solvents were weighed in, and the cells were flame-sealed. After that, the mixtures were homogenized at 80 °C to obtain transparent solutions.

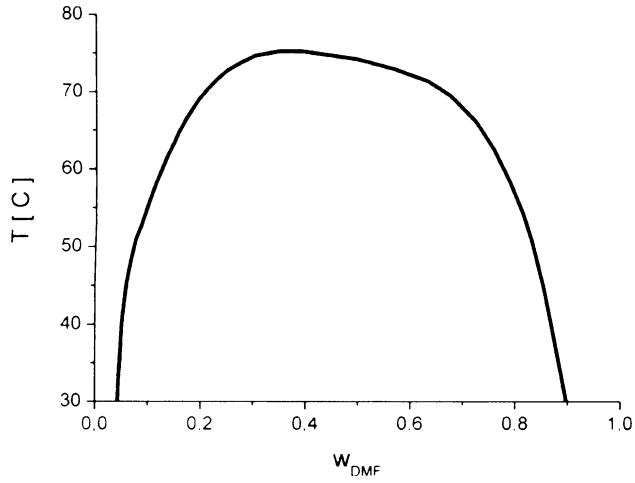

Figure 37: *Phase diagram of the binary mixture of solvents heptane (C7) and dimethylformamide (DMF), constructed from experimental data from [130].*

The samples prepared as above were after homogenization examined by DLS to study temperature and angle dependence of relaxation times of the dynamic processes in these systems. A selected series of samples was also prepared to investigate possible structures in the system by the SAXS method.

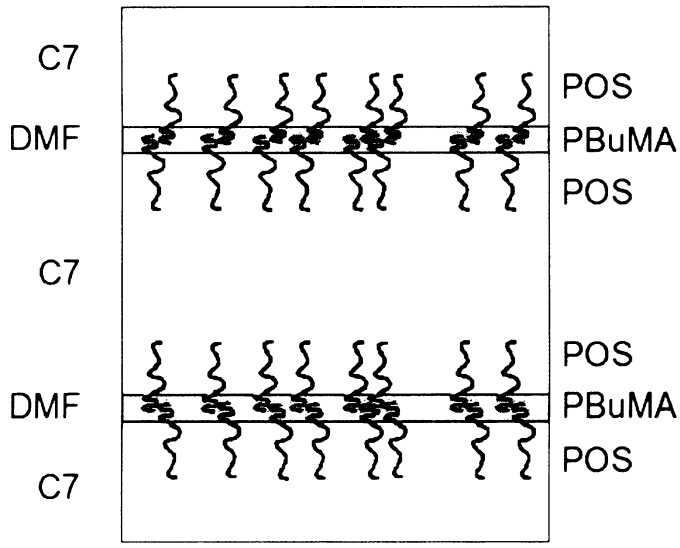

Figure 38: *Scheme of microphase separated structure of OB block copolymer in heptane-rich phase (labeled as C7) and dimethylformamide-rich phase (labeled as DMF) in binary solvents mixture (composition with 10% v/v fraction of DMF). POS blocks form a brush in C7, PBuMA chains form a brush in DMF.*

6.7.1 Viscosity of binary solvent

The temperature dependence of viscosity of DMF/C7 binary mixture was experimentally determined by cooperation with Ing. Jiří Horský, CSc.

A series of solvent mixtures was prepared, and the temperature dependence of viscosity was measured using an Ubbelohde viscometer. The dependence of viscosity on mixture composition was for every experimental temperature described by the equation

$$\eta_x = x_a \eta_a + (1 - x_a)\eta_b + x_a(1 - x_a)(A + B(2x_a - 1)) \tag{6.4}$$

where η_x is the viscosity of the mixture with molar fraction x_a of solvent *a*, η_a is the viscosity of pure solvent *a* (DMF) and η_b is the viscosity of pure solvent *b* (C7). *A* and *B* are experimental constants. Results of the calibration are shown in Table 10.

T [°C]	η_{DMF} [cP]	η_{C7} [cP]	A	B
50	0.61	0.303	-0.1183	0.184
60	0.563	0.276	-0.1116	0.1457
70	0.506	0.254	0.0004	0.2611

Table 10: Experimental results for the viscosity of DMF/C7 mixture.

Using the calibration data and the equation 6.4, viscosity values for a mixture with given composition were calculated, and in next step treated with the Arrhenius equation

$$\ln(\eta) = a + \frac{b}{T} \tag{6.5}$$

where η is the viscosity, *a* and *b* constants and *T* is the absolute temperature. This equation was after linearisation to the form $y = a + cx$ with $y = ln(\eta)$ and $x = 1/T$ solved to obtain coefficients the *a* and c, and the required viscosity at given temperature and composition was calculated.

The values obtained as described above were used to determine the correct correlation length (the hydrodynamic radius) of fluctuations or size of particles from DLS measurements.

The molar and weight fractions of components of the binary mixture for equation 6.4 were converted as needed using the relationships

$$x_a = \frac{w_a \cdot M_b}{w_a(M_b - M_a) + M_a} \tag{6.6}$$

and

$$w_a = \frac{x_a M_a}{M_b - x_a(M_b - M_a)} \tag{6.7}$$

where the indexes *a* and *b* identify the components, *x* is the respective component molar fraction, *w* the weight fraction and *M* the component molecular weight.

6.7.2 DLS results

6.7.2.1 Poly(*p*-octylstyrene)-*b*-poly(butyl methacrylate) copolymer in heptane

We have investigated the temperature dependence of DLS curves from OB3 and OB5 solutions in pure heptane, to obtain a description of block copolymer chains or micelles in the solvent that is used as a majority component in the binary mixtures used in further experiments. For these purposes samples of OB3 and OB5 solutions with w/w concentration of 1% were prepared and measured as a function of temperature. Details of the samples are described in Table 11. The prepared solutions were left overnight at 80 °C to allow homogenization and after that filtered with 0.45 μm PTFE microfilter and measured.

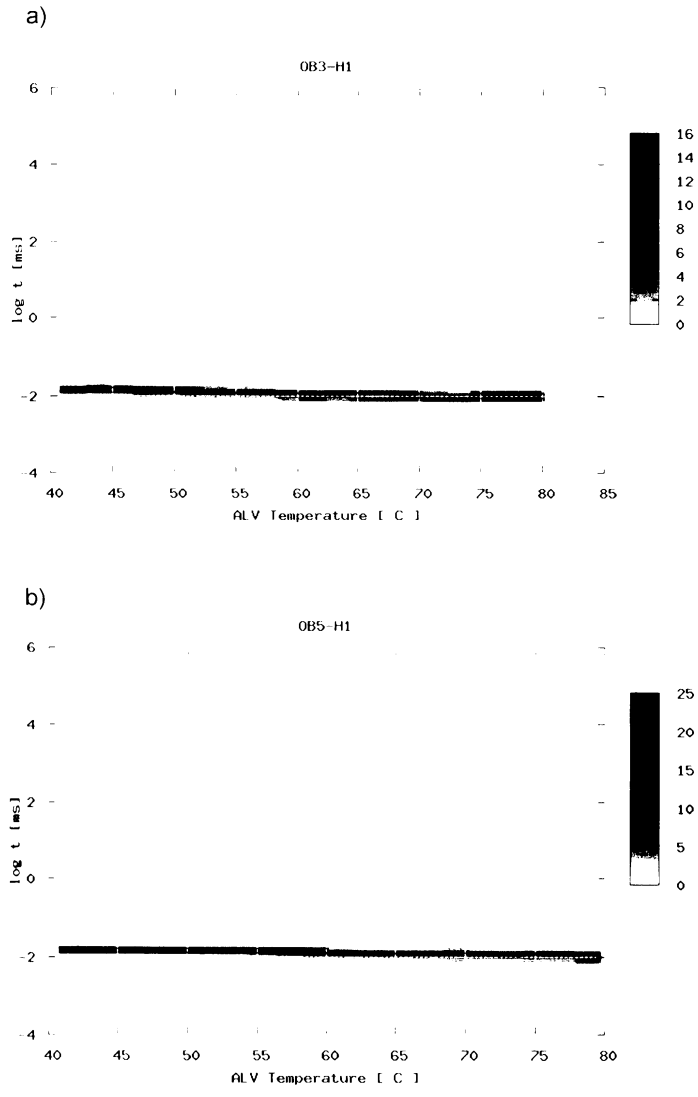

Figure 39: *3D maps of temperature dependence of relaxation time for samples OB3-H1 (image a) and OB5-H1 (image b). In this and all similar figures below, horizontal axis is temperature, vertical axis is relaxation time.*

The results of recalculation of obtained relaxation times (Figure 39) to hydrodynamic radii are shown in Figure 40. From presented images it is clearly seen that in both samples only one dynamic mode is present.

sample name	polymer conc. [%]
OB3-H1	1.0
OB5-H1	1.0

Table 11: OB3 and OB5 block copolymer solutions in n-heptane.

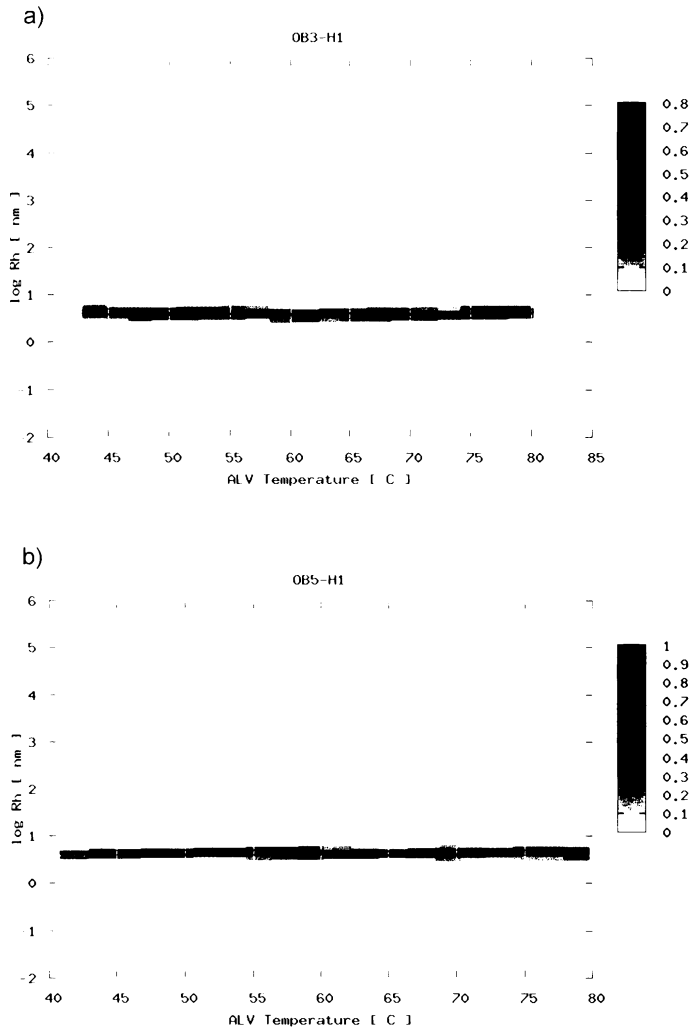

Figure 40: *3D maps of temperature dependence of hydrodynamic radius for samples OB3-H1 (image a) and OB5-H1 (image b). In this and all similar figures below, horizontal axis is temperature, vertical axis is hydrodynamic radius (or correlation length).*

The R_h values of ca 4 - 5 nm obtained in the experiments are in good relation with theoretical values calculated according ref.[133], which gives for polystyrene molecules of the

same molecular weights as that of OB3 and OB5 a radius of 5 nm and 6.4 nm in toluene solutions and 4.4 nm and 5.5 nm in cyclohexane solutions.

According to the sizes obtained from DLS, the only dynamic mode present in the heptane solutions of OB3 and OB5 can be assigned to the molecularly dissolved copolymer chains.

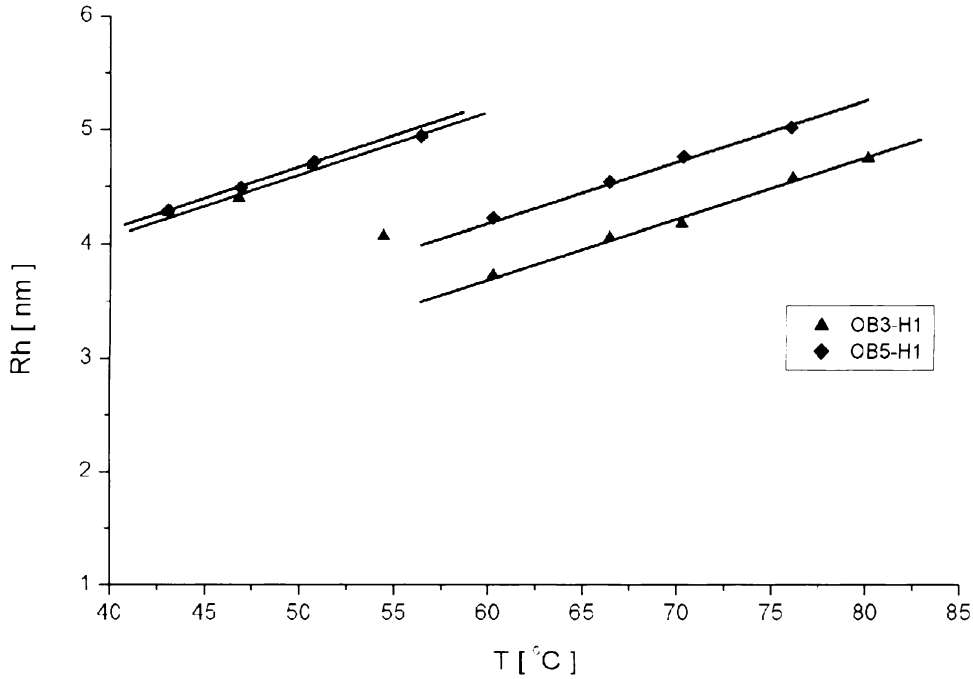

Figure 41: *Extracted data and the corresponding linear fits of OB3 and OB5 solutions in n-heptane.*

The detailed view of the measured R_h values is shown in Figure 41. The observed change of R_h at ca 60 °C on both curves in Figure 41 is similar to the globule-to-coil transition of dissolved macromolecular chains near θ conditions[134],[135],[136], but unlike in that case R_h grows again after the transition. Therefore we suggest a conformational transition in PBuMA chains as an explanation of the measured effect[137],[138]. To check the observed behavior more in detail we performed a series of measurements of the individual homopolymers in various solvents as described later in this chapter.

6.7.2.2 Poly(*p*-octylstyrene)-*b*-poly(butyl methacrylate) copolymer in DMF

To check the dynamic behavior of OB diblock system in the second solvent we investigated DLS of 0.5 % solutions of OB3 and OB5 (for samples details see Table 12). As for all measured samples, the OB-DMF solutions were placed overnight at 80 °C to ensure full dissolution, then filtered with 0.45 μm PTFE microfilter, let stabilize and finally measured.

sample name	polymer conc. [%]
OB3-D1	0.6
OB5-D1	0.7

Table 12: OB3 and OB5 block copolymer solutions in DMF.

In both cases only one dynamic mode was observed. The summary of obtained results, displayed as 3D map of temperature dependence for R_h are shown in Figure 42, where the situation is clearly represented.

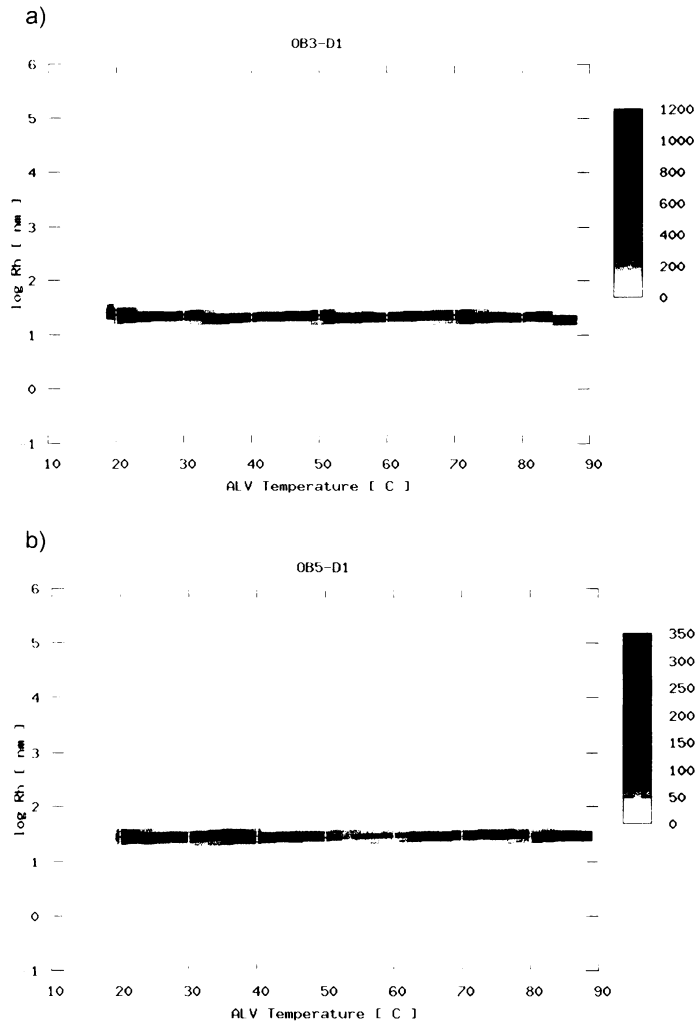

Figure 42: *3D map of hydrodynamic radius of OB3 and OB5 polymer solutions in DMF.*

The temperature dependence of R_h, displayed in Figure 43, shows a distinct difference between the OB3 and OB5 polymer behavior, which can be assigned to the various content of octylstyrene in the block copolymer and to the fact, that DMF is a strong precipitant of POS.

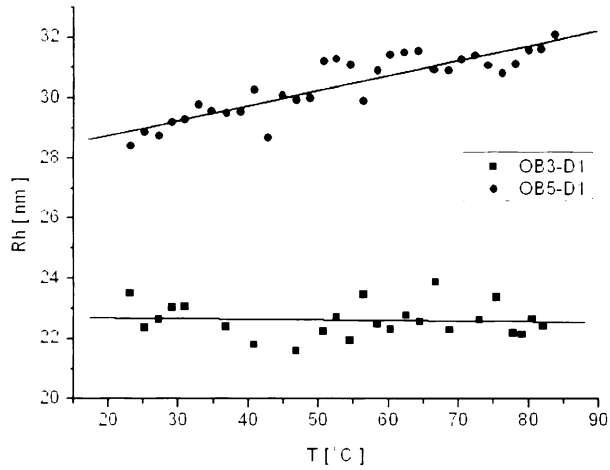

Figure 43: *Temperature dependence of R_h for OB3 and OB5 solutions in DMF. The straight lines are linear fits to the data.*

In these solutions the size of the objects is much bigger (about 5 to 7 times) than in heptane where the polymers are molecularly dissolved (R_h about 4 nm). In DMF, the polymers have a different micellar supposedly core-shell structure with POS core covered with solvated PBuMA shell, as is schematically drawn on the Figure 44.

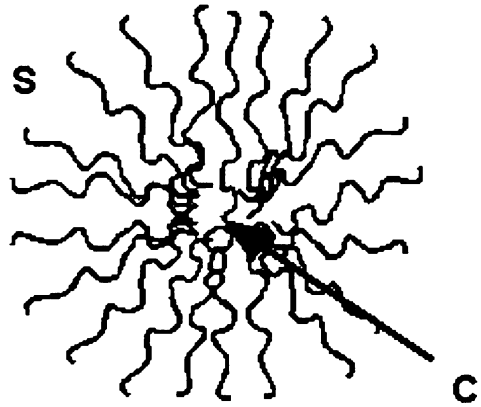

Figure 44: *Micelle of diblock copolymer in a selective solvent. C: core of the micelle; S: shell corona.*

6.7.2.3 Poly(butyl methacrylate) solutions

Because of non-trivial behavior of OB systems in heptane we studied the dynamic behavior of the simple homopolymers in the series of solvents: C7, DMF, THF and acetone, to investigate the possible presence of conformational transition and theta temperatures of PBuMA chains. For this purpose we prepared a series of 3 % (w/w) solutions of B8 homopolymer in these four solvents. The solutions were placed overnight at 80 °C to ensure

full dissolution and after that were filtered with 0.45 μm PTFE microfilter, again let stabilize and measured.

The results of DLS measurement are shown in Figure 45.

For heptane solutions (Figure 45a) we can see a clear, unexpected decrease of polymer size with increasing temperature. This can be a signature of a combination of the transition at a θ-temperature (see Figure 36) and a conformation change in butyl methacrylate chains. Up to ca 60 °C the dynamics of the solution is "ordinary" and the gentle increase of the R_h is probably caused by the thermal expansion of the coils. After the mentioned change we can observe an important decrease of R_h by about 23 % from ca 2.2 nm to ca 1.7 nm. This behavior is usually confirmed also in the other methacrylate systems, as can be seen *e.g.* in the publications[137],[138]. According to the results obtained for OB diblock systems, the effect of change of coil dimension with temperature has also a strong influence on the diblock copolymers where the PBuMA chain forms ca. 40% of the molecule (OB5 system).

In the DMF solution (Figure 45b) the dynamic behavior of the coils is thermodynamic and comparable to the first part of the curve in C7. Here we are also assigning the slight increase of R_h to the increase of thermodynamic quality of the solvent.

In the THF solutions ((Figure 45c) there is observable a soft decrease in R_h, which can be caused by the intramolecular complexation of methacrylates. This idea is in good agreement with results published in[139], where authors studied behavior of solutions of poly(methyl methacrylates) in various solvents.

The behavior of the molecularly dissolved PBuMA in acetone (generally a very good solvent for methacrylates) is again "normal" and no sharp jump as in the case of heptane solutions was observed.

From the obtained results we can confirm the known fact that the thermodynamical behavior of PBuMA is non trivial and is strongly dependent on the quality of the used solvent and temperature of the solution. We can also say that in some cases it is possible to observe a distinct step in the temperature dependence of R_h, which is typical for behavior of some of methacrylate polymers. This step is usually caused by the conformational change in side chains and according to our results it has strong influence on the whole molecule even in the diblock copolymers.

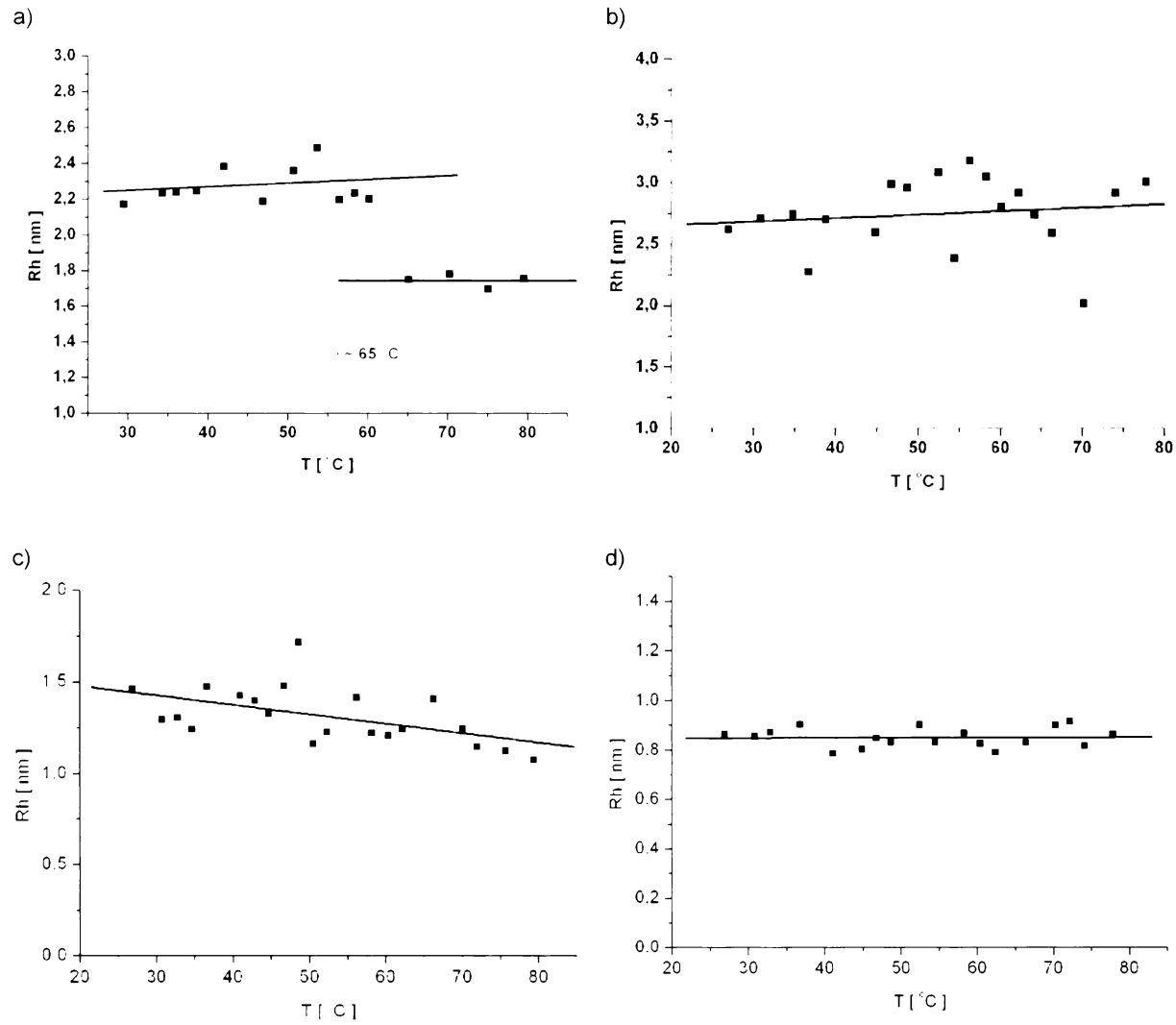

Figure 45: *Temperature dependence of PBuMA size in solutions in a) heptane; b) DMF; c) THF; d) acetone.*

6.7.2.4 Poly(*p*-octylstyrene) solutions

The temperature dependence of hydrodynamic radius of POS homopolymer was measured for 3 % (w/w) solutions (prepared in the same way as in the PBuMA case) of O5 in C7 and DMF.

In POS-C7 system also only one dynamic process was observed. According to the small size it can be again assigned to molecularly dissolved polymer chains with coil R_h of ca 2.3 nm. The temperature dependence of chain sizes has a slow increasing tendency (Figure 46a), which again represents the temperature expansion of the polymer.

Since, compared to the PBuMA, the aromatic structure in POS carries the long alifatic chain without tendencies to intramolecular clusterization, no "steps" of $R_h = f(T)$ are visible in the examined solutions.

Because POS is not soluble in DMF, it was not be possible to measure the size of single polymer chain in such solutions – the majority of the POS material remains undissolved in the scattering cell. Because of this, we tried to investigate the dynamic behavior of the extremely diluted solution above the undissolved homopolymer.

In the results it was not possible to find any signal assignable to molecularly dissolved chains, only scattering of a big clusters with size of ca 4 µm were observed (Figure 46b) This is, however, near the size limit of dynamic light scattering and the obtained information has therefore only a limited value.

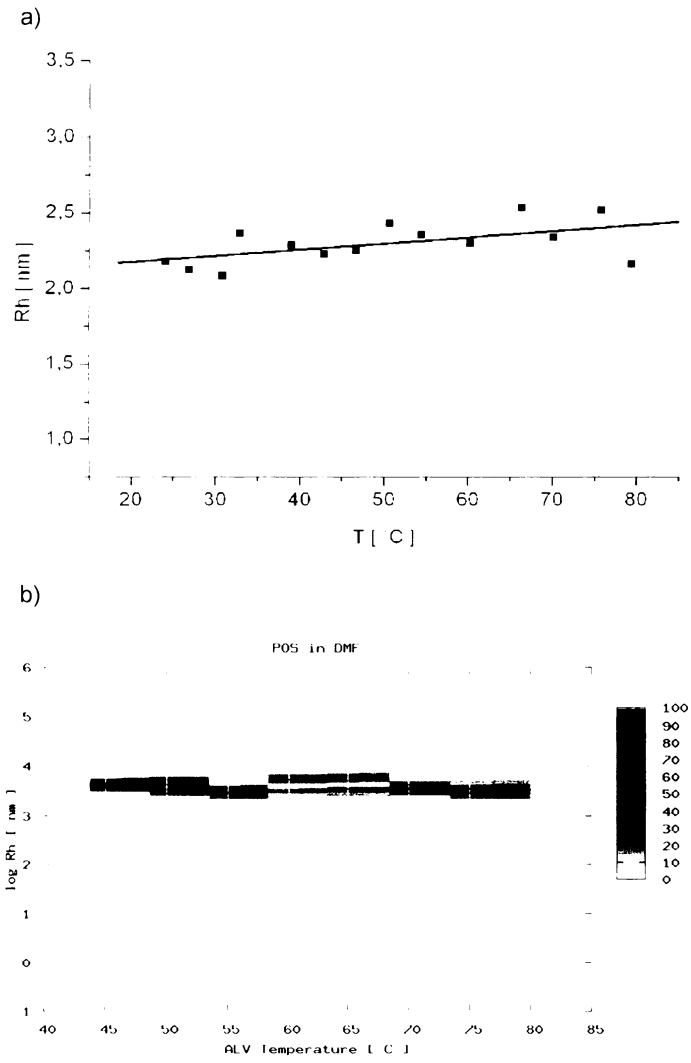

Figure 46: *Experimental results of dynamic behavior of POS homopolymer in C7 (a) and DMF (b) solvents.*

6.7.2.5 Diblock copolymer in a binary solvent; variable copolymer concentration

In this section we examine the influence of diblock copolymer concentration in the binary mixture on the solution properties. For this, we have prepared a series of solutions with variable copolymer concentrations and fixed solvent composition.

As the basic composition for binary solvent was chosen a mixture of C7/DMF with 15% (w/w) of DMF. The phase separation temperature T_c of this mixture is 63.9 °C. Also a control sample of this binary solvent mixture without polymer was prepared and measured using dynamic light scattering, to verify the phase separation temperature of the solvent mixture in our experimental conditions. Our result, measured as the increase in scattered intensity caused by the system clouding at phase separation temperature (Figure 47), gave T_c = 63.7 °C. This value is in good correspondence with a value T_c = 63.9 °C approximated from published data[130] (Figure 37).

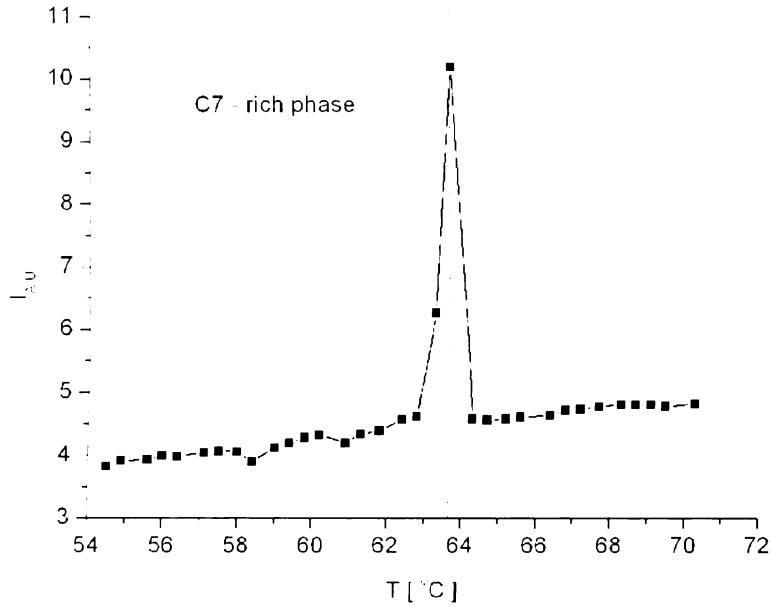

Figure 47: *DMF-C7 binary mixture, 15.3% DMF; temperature dependence of scattering intensities.*

The list of examined OB-solutions is shown in the Table 13. The block copolymer concentrations were ca 1%, 2%, 5%, 10%, 15% (w/w). The samples were after preparation homogenized in the oven at 80 °C overnight, and after that used in light scattering experiments.

For all prepared samples we have measured correlation curves as a function of temperature and scattering angle.

The influence of temperature was investigated for the scattering angle 90° in a temperature range from 90°C to 40°C, with a step of 2°C. An example of correlation curve is

displayed in Figure 48. The presence of two dynamic modes is visible, which implies a more complex behavior of studied solutions than in the case of simple solvents (10.3.1, 10.3.2)

system	sample name	DMF fraction [%]	polymer conc. [%]
OB3	OB3-A1	15.3	0.9
	OB3-A2	15.5	1.9
	OB3-A3	15.4	5.0
	OB3-A4	14.9	9.9
	OB3-A5	18.1	13.9
OB5	OB5-A1	15.7	1.0
	OB5-A2	15.1	2.0
	OB5-A3	14.8	4.9
	OB5-A4	15.3	9.9
	OB5-A5	14.2	15.0

Table 13: Composition of OB3 and OB5 samples used to investigate the effect of block copolymer concentration. "*DMF fraction*" is w/w fraction of DMF in binary mixture of DMF/C7. "*polymer conc.*" is w/w concentration of diblock copolymer, dissolved in the binary mixture.

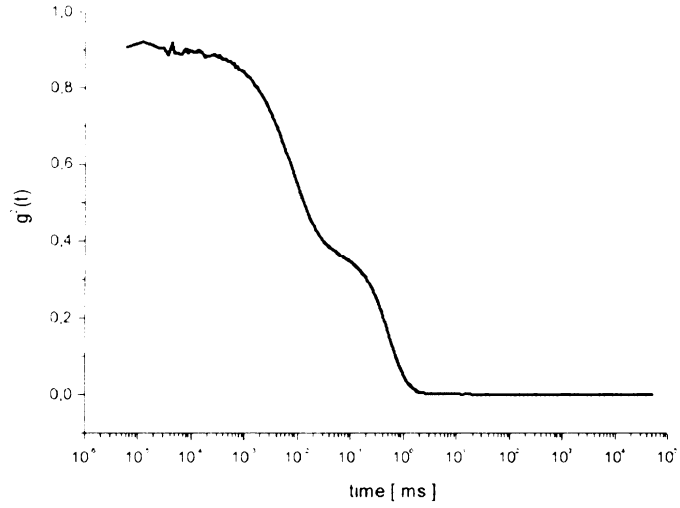

Figure 48: *Correlation curve example, sample OB3-A4; T = 78 °C, measurement duration 180 s, angle 90°.*

Next, Figure 49 shows the temperature dependence of normalized intensities of scattered light obtained from all samples. On the graphs is observable a stabilizing effect of block copolymer in the binary mixture[80], exhibited as a shift of the binary mixture T_C to the lower temperature values. The segregation temperature of DMF and C7 is in all solutions decreased - from the theoretical value of ca 64 °C below ca 60 °C. The mentioned effect is, as in the case of mixture of pure solvents, generally measurable as a solution cloud point.

The decreasing of relative intensity at the T_C, observable on samples with higher copolymer concentrations, is probably caused by a multiple light scattering and absorption in cloudy solutions. The signal instability and second decrease of the intensity of the scattered light often present after the T_C, is on the other hand probably caused by the fluctuation and sedimentation of "precipitated" micelles and agglomerates.

This behavior – the sedimentation of excluded agglomerates – was observed in all samples after cooling the solutions under the system cloud point. After this, during ca 5 hours the sedimentation is finished and the mixture is separated into two layers – at the bottom layer is the precipitated block copolymer together with DMF; in the upper layer is the slightly clouded C7 fraction with the rest of DMF and block copolymer. Because of this effect, it was necessary to perform the measurements in as short time as possible and the applied temperature program every time ran from the higher to the lower temperatures.

The solutions remain at all temperatures (both over and under the T_C) very liquid, without any observation of tendency to gelation, in contrast to some other systems, (*e.g.* studied in[80]), where gelation was caused by the long-range orientation of dissolved macromolecular chains into organized lattices.

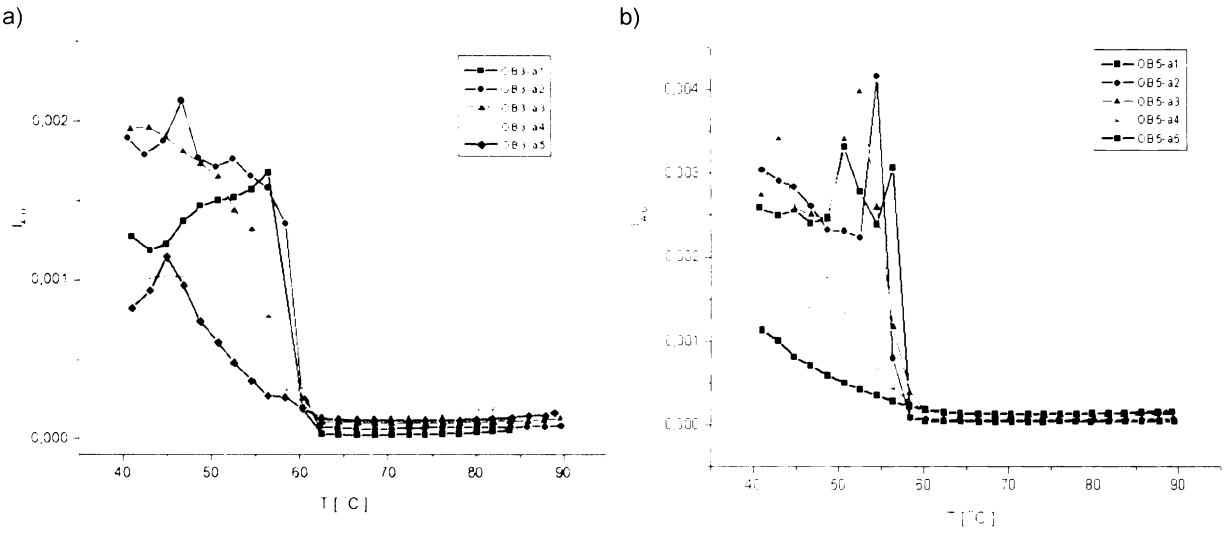

Figure 49: *Normalized intensities of scattered light at angle 90° as a function of temperature for: (a) – OB3 solutions, (b) – OB5 solutions.*

DLS results displayed as 3D graph maps of sample OB3 are shown in Figure 50 as a dependence of relaxation time on temperature. For the system OB5 the relevant 3D graphs are shown in Figure 51. (In further text subscript "A" will be used for descriptions of dynamics "above" the phase separation temperature and subscript "B" to describe behavior "below" the phase separation temperature; an example of this notation is indicated in Figure 50e.)

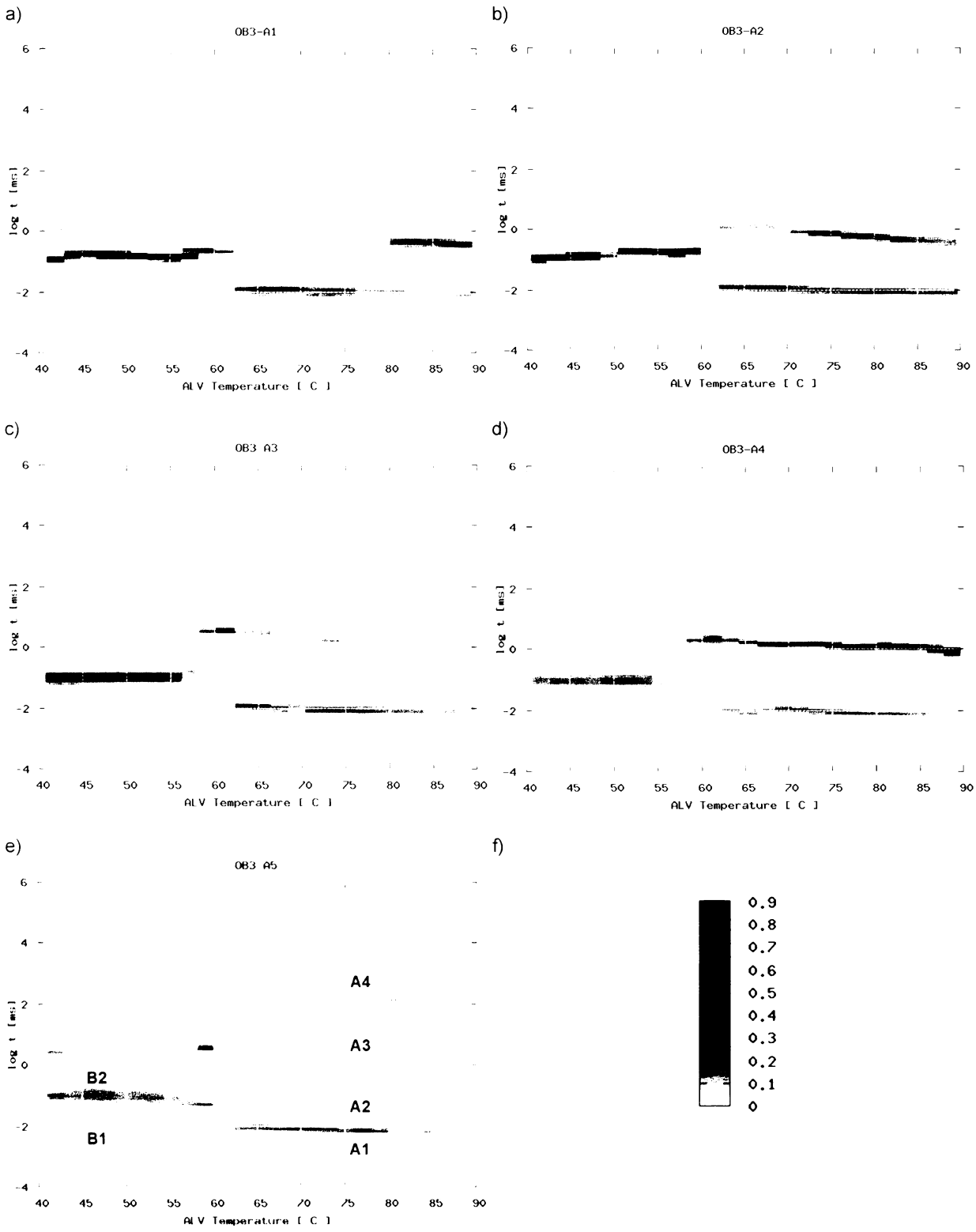

Figure 50: *DLS results for OB3 samples with fixed solvent composition (ca 15% (w/w) DMF in binary solvent mixture) and variable block copolymer concentration; OB3 content in a), b), c), d), e) is 0.9%; 1.9%; 5.0%; 9.9%; 13.9% (w/w) respectively; X vs. Y graph coordinates describe log of relaxation time [ms] vs. sample temperature [°C].The Z-scale displayed in f) belongs to all maps. In the image e) is indicated naming of dynamic modes described in further text.*

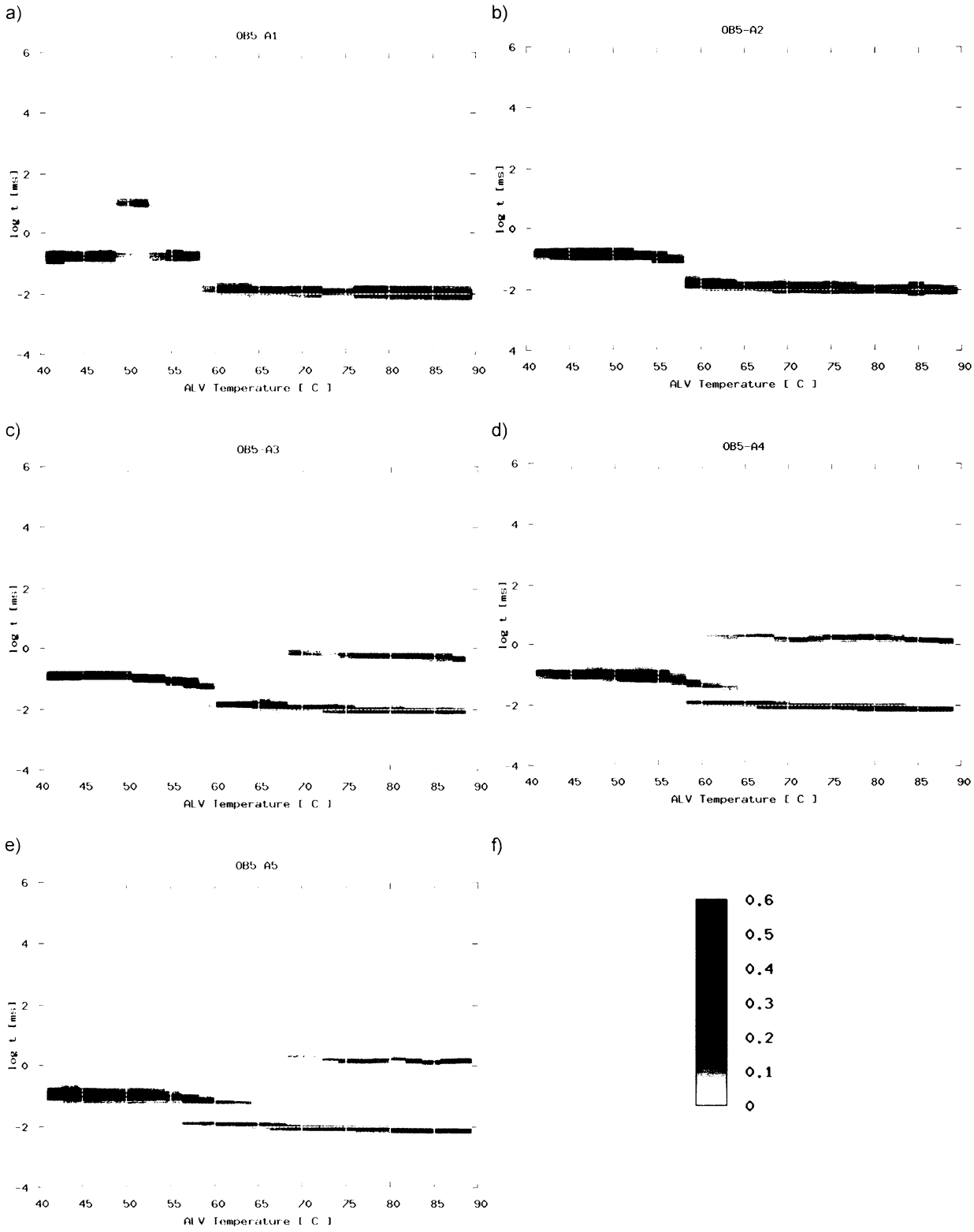

Figure 51: *DLS results for OB5 samples with fixed solvent composition (ca 15% (w/w) DMF in binary solvent mixture) and variable block copolymer concentration, ; OB5 content in a), b), c), d), e) is 1.0%; 2.0%; 4.9%; 9.9%; 15.0% (w/w) respectively; X vs. Y graph coordinates describe log of relaxation time [ms] vs. sample temperature [°C]. The Z-scale displayed in f) belongs to all maps.*

In the case of OB3, it is clearly seen, that above the phase separation temperature, for block copolymer solutions with concentrations up to ca 10% (samples OB3-A1...OB3-A4), two main modes are present. The faster has a relaxation time of about τ_{A1} ~ 10 μs and the slower τ_{A2} ca from 450 μs to1 ms. Below the phase separation temperature, the two modes merge into one mode with relaxation time τ_{B1} of about ca 150 μs. In the sample with 5% concentration of OB3 a second one slow mode appears, probably as a continuation of the τ_{A2} and is observable as τ_{B2} at ca 10 ms.

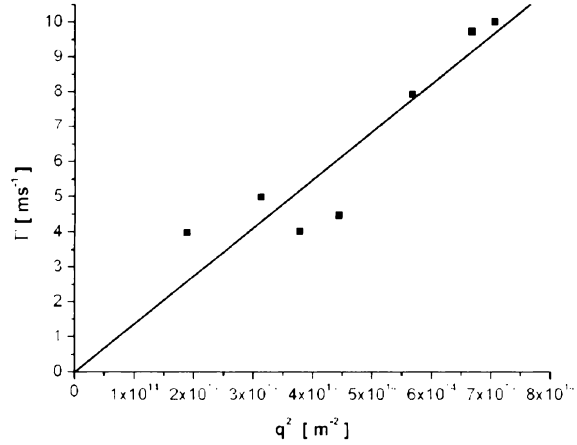

Figure 52: *Dependence on q^2 of decay rate of dynamic mode B1 for OB3-A1 sample at 50 °C.*

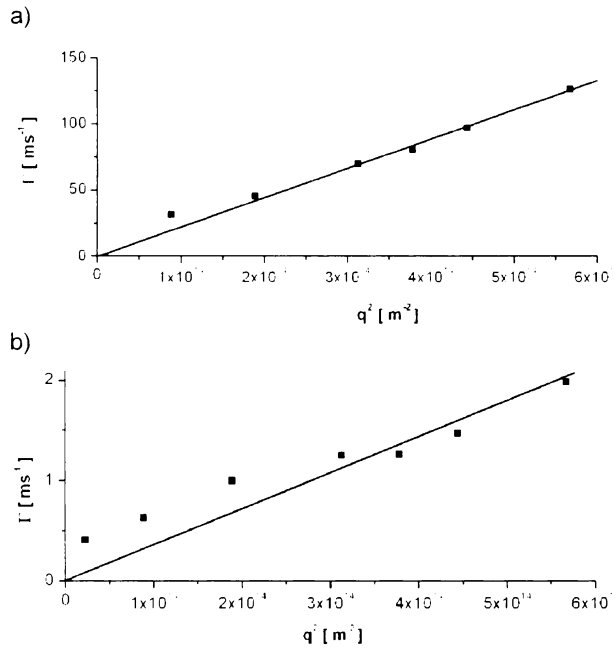

Figure 53: *Dependence on q^2 of decay rates for OB3-A1 sample at 70 °C. a) dynamic mode A1; b) dynamic mode A2.*

At higher block copolymer concentration – in 10% solution (sample OB3-A4) – above the phase separation temperature the dynamics remains unchanged. Below the phase

separation temperature the fastest mode splits into two individual components with τ_{B1} ~ 20 μs for the first component, the second mode ("parent") with τ_{B2} ~ 100 μs remains unchanged and is present in all systems. Also the third, slowest, mode present in this solution remains (or disappears and the new one appears), however is shifted from 10 ms observed in OB3-A3 to the faster values at τ_{B3} ~ ca 600 μs.

In the most concentrated solutions with ca 15% of OB3 (sample OB3-A5) a more complex behavior is observed. Above the T_C four modes are present. The fastest mode is now clearly separated into two components with τ_{A1} ~ 10 μs and τ_{A2} ~ 30 μs. The third dynamic process with τ_{A3} ~ 1-10 ms again remains mostly unchanged as was observed in more diluted solutions. However, in addition a completely new, slow mode (τ_{A4} ~ 100 ms) not previously observed in more diluted solutions appears. Because the polymer concentration is higher than the c*, it implies the existence of large-scales inhomogeneities or clusters in the system.

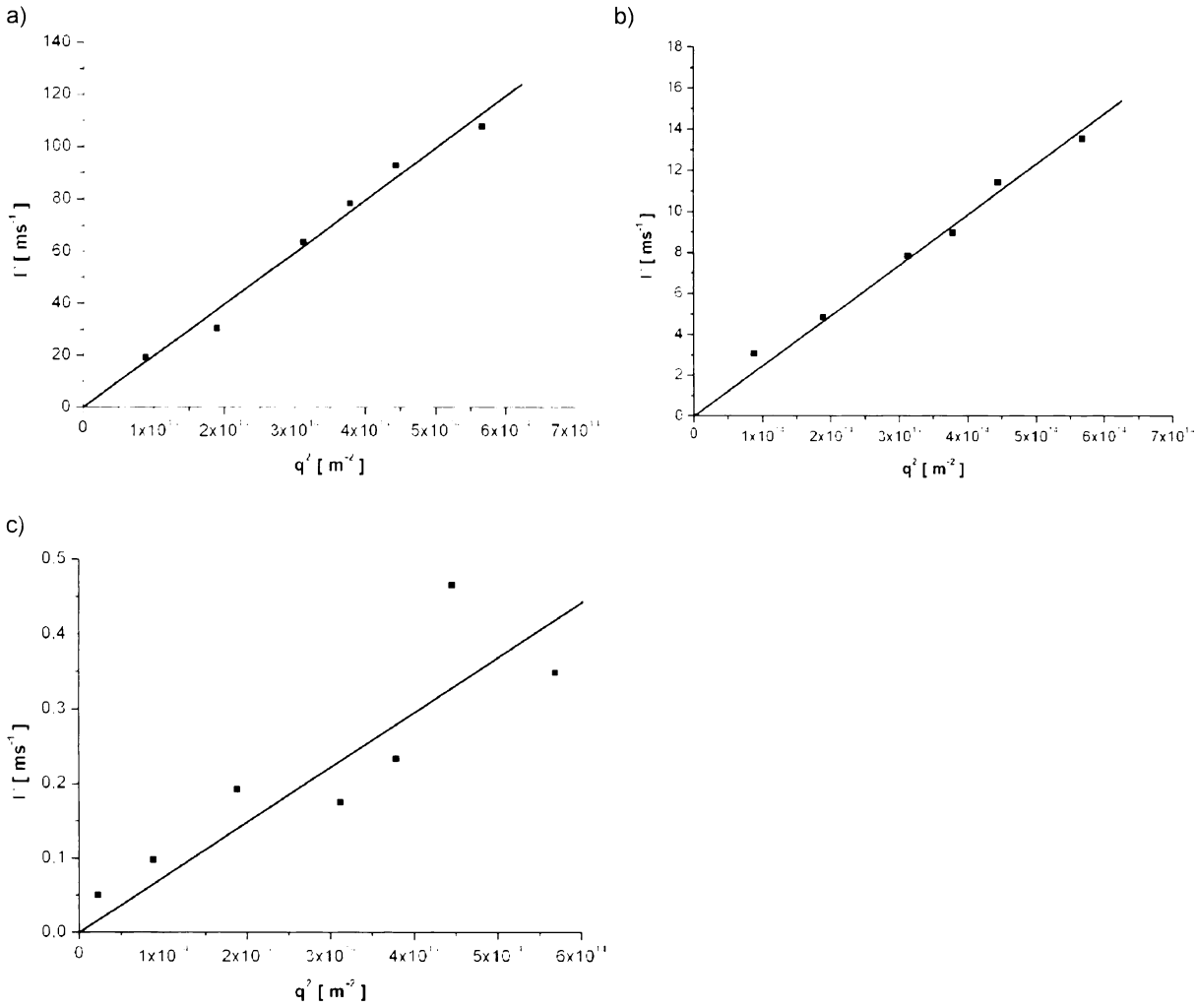

Figure 54: *Dependence on q^2 of decay rates for OB3-A5 sample at 50 °C. a) dynamic mode B1; b) dynamic mode B2; c) dynamic mode B3.*

To check whether these dynamic modes have a diffusive character (*i.e.* the relaxation rates (Γ) – given by equation 5.9 – are q^2 dependent) angle dependent measurements for several temperatures were performed. We use 70 °C to study the behavior above the phase separation temperature and 50 °C to study behavior below the phase separation temperature. As representative samples was chosen the solution OB3-A1 as the dilute system below c* and the solution OB3-A5 as the concentrated solution above c*.

For dilute samples with polymer concentration below c* (OB3-A1) the dynamics in all cases – *i.e.* both below and above the phase separation temperature – is diffusive. Individual modes are there presented in Figure 52 (B1) and Figure 53 (A1, A2).

In Figure 54 it is visible that for concentrated solutions above c* (*i.e.* sample OB3-A5) and below the phase separation temperature (50 °C), all dynamic processes B1, B2 and B3 are diffusive.

The behavior of the same sample at temperatures above the phase separation temperature (70 °C) is shown in Figure 55. The character of all dynamic processes is also clearly diffusive, except for A2.

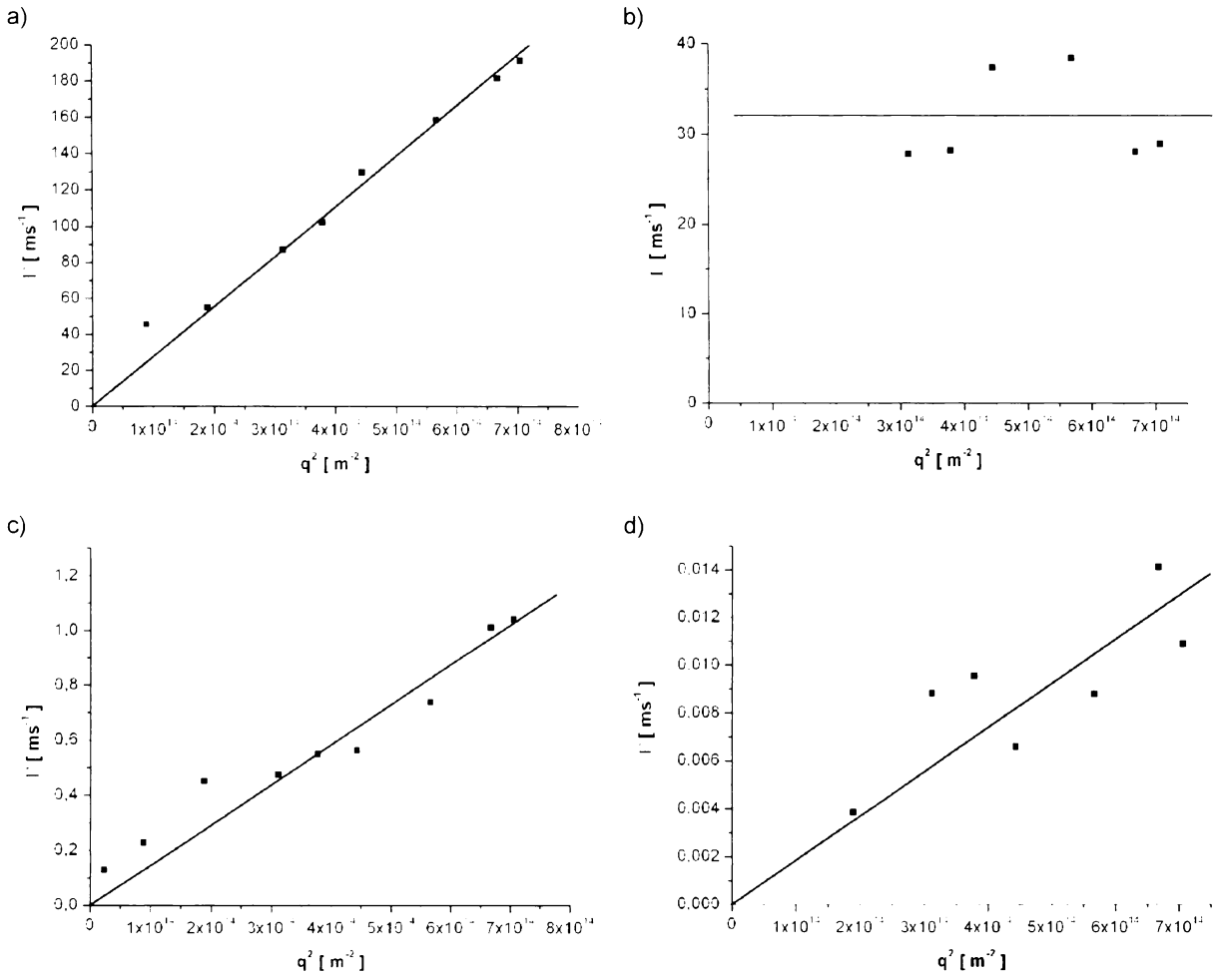

Figure 55: *Dependence on q^2 of decay rates for OB3-A5 sample at 70 °C. a) dynamic mode A1; b) dynamic mode A2; c) dynamic mode A3; d) dynamic mode A4.*

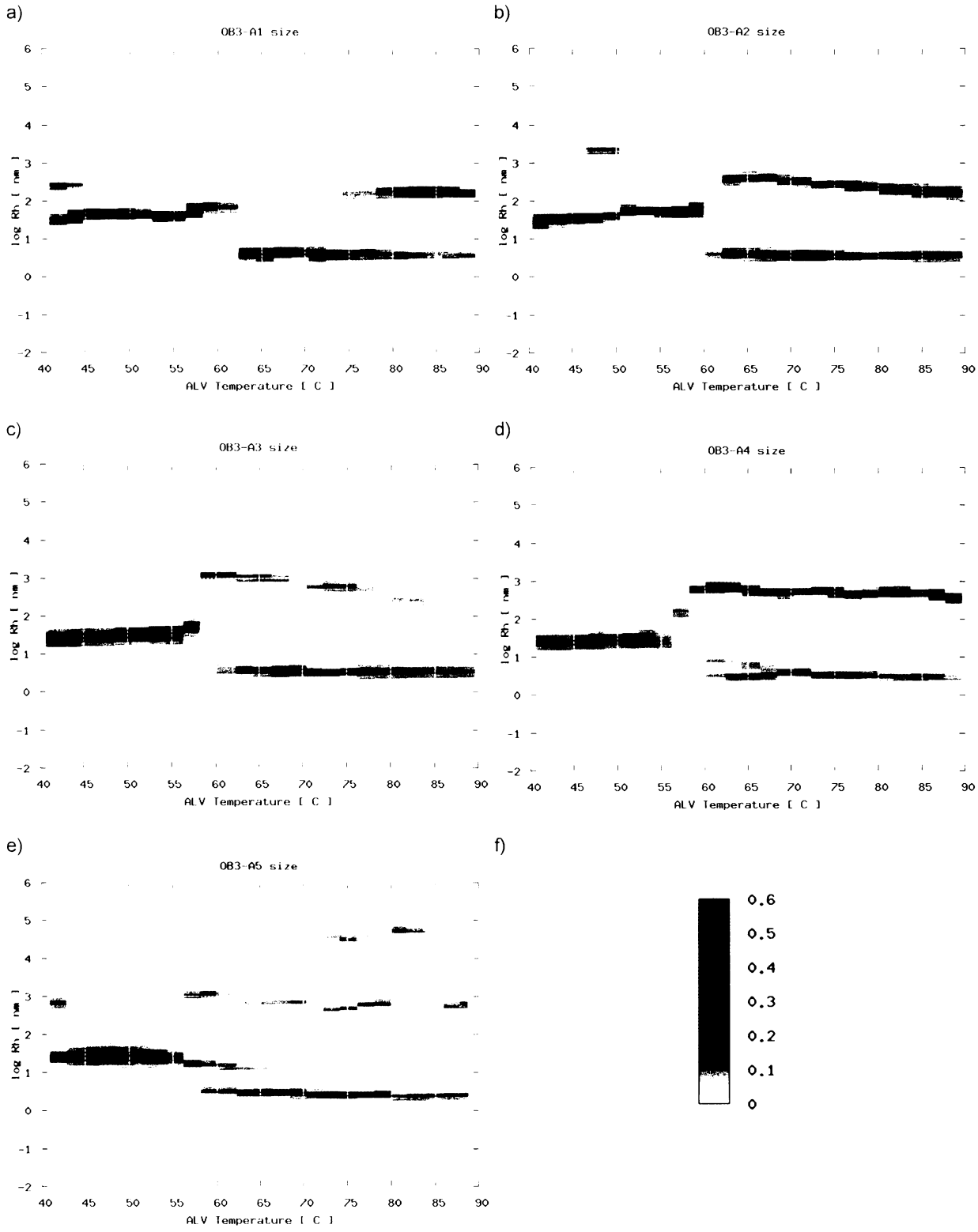

Figure 56: *DLS results for OB3 samples with fixed solvent composition (ca 15% (w/w) DMF in binary solvent mixture) and variable block copolymer concentration; OB3 content in a), b), c), d), e) is 0.9%; 1.9%; 5.0%; 9.9%; 13.9% (w/w) respectively; X vs. Y graph coordinates describe log of correlation size [nm] vs. sample temperature [°C]. The Z-scale displayed in f) belongs to all maps.*

The results are therefore in good agreement with the theory of Semenov[140], according to which in solutions of diblock copolymers there generally occur at least three dynamic modes, and the correlation function is influenced by contribution of relaxation rates Γ given by Γ_I, Γ_C, Γ_H from

- internal mode (Γ_I) which reflects the relative motion of the centers of mass of the two blocks on a single chain; it does not depend on q^2
- cooperative mode (Γ_C) which is essentially identical to that observed in homopolymer solutions and is thus, at least to a first approximation, independent of the copolymer nature of the chain; it is dependent on q^2
- heterogeneity mode (Γ_H) which is caused by fluctuations in the relative concentration of A and B segments in diblock copolymer chain; it depends on q^2

According to this we can characterize (for the sample OB3-A5, 70 °C; description of the other samples is similar) the mode A1 as the cooperative mode, A2 as internal mode and A3 as heterogeneity mode. The fourth slowest mode A4 according to our opinion comes from the diffusion of large clusters or aggregates and was described previously[141], [142] but is not so important for our studies.

From these data we can generally accept a linear dependence of Γ on q^2 for almost of all observed modes, which entitles us to use equation 5.10 and to calculate the hydrodynamic radius (for dilute solutions) or correlation length (for concentrated solutions) corresponding to the measured diffusion coefficient. The results of those calculations are presented in 3D maps in Figure 56.

We are aware of the fact that to create size graphs we used DLS data in form “as is”, so there were done calculations also with non-diffusive dynamic processes. This helps with a clear and easy identification of the corresponding modes, available by simple comparison of corresponding relaxation time vs. size images. The parts of the 3D graphs that do not make sense in a size representation can be identified from the $\Gamma = f(q^2)$ dependencies.

Similar measurements as a function of temperature and scattering angle have been performed also for the OB5 solutions.

The results for relaxation time are shown in Figure 51, where it can be seen that the dynamic behavior of both copolymer systems (OB3 and OB5) is almost identical and the observed variations can be assigned to the differences in composition (ratio of PBuMA and POS in blocks) and in molecular weight – M_w ~ 23.4 k for OB3 and M_w ~ 35.6 k for OB5. The only distinct difference is that the dynamic mode B2 (at τ_{B2} ~ 7.5 ms) occurs – compared to OB3 samples – also at lower concentrations of diblock copolymer in binary solvent.

For the characterization of diffusive behavior of obtained dynamic modes an angle dependent measurement was also performed. For those purposes were selected samples OB5-A1 as the representative of dilute solutions and the sample OB5-A5 as the representative of solutions above the overlap concentration.

Results from the experiments with sample OB5-A1 are shown in Figure 57 for 50 °C and at Figure 58 for 70 °C. For the dilute solution the diffusive character of the both relaxation modes is again confirmed, both below and above the phase separation temperature.

The concentrated sample OB5-A5 has a similar behavior as in the OB3-A5 case. At low temperatures all modes are diffusive; above the phase separation temperature the relaxation rate of the A2 mode does not dependend on q^2 and we again assume his "internal" character.

However, again most of studied fluctuations in solutions of OB5 have diffusive character and because of this the transformation of relaxation times to the hydrodynamic radius respectively to the size of fluctuations in solution is applicable. The general result of this transformation is shown in Figure 61.

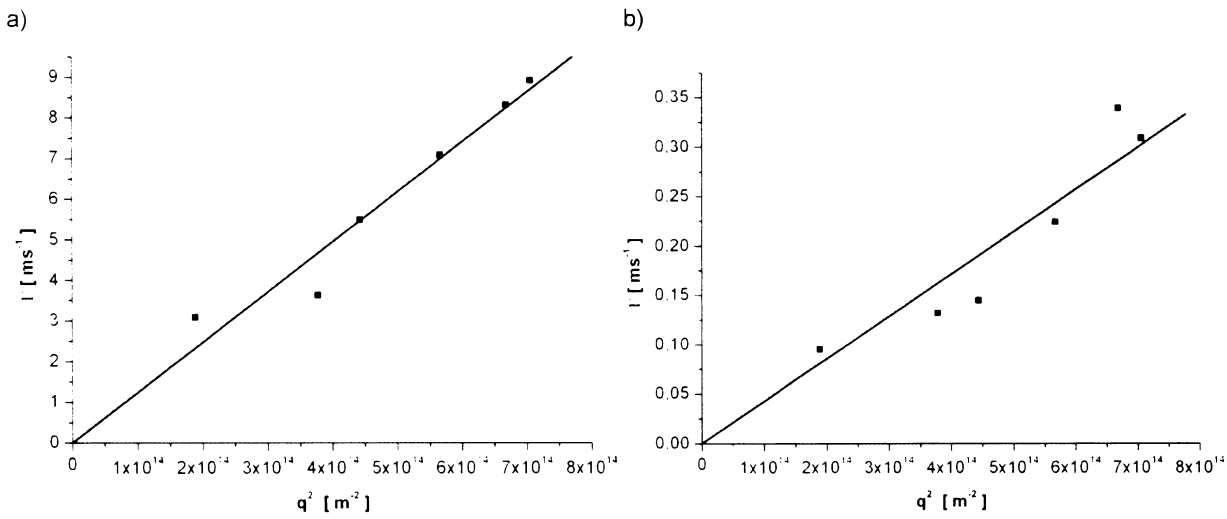

Figure 57: *Dependence on q^2 of decay rates for OB5-A1 sample at 50 °C. a) dynamic mode B1; b) dynamic mode B2.*

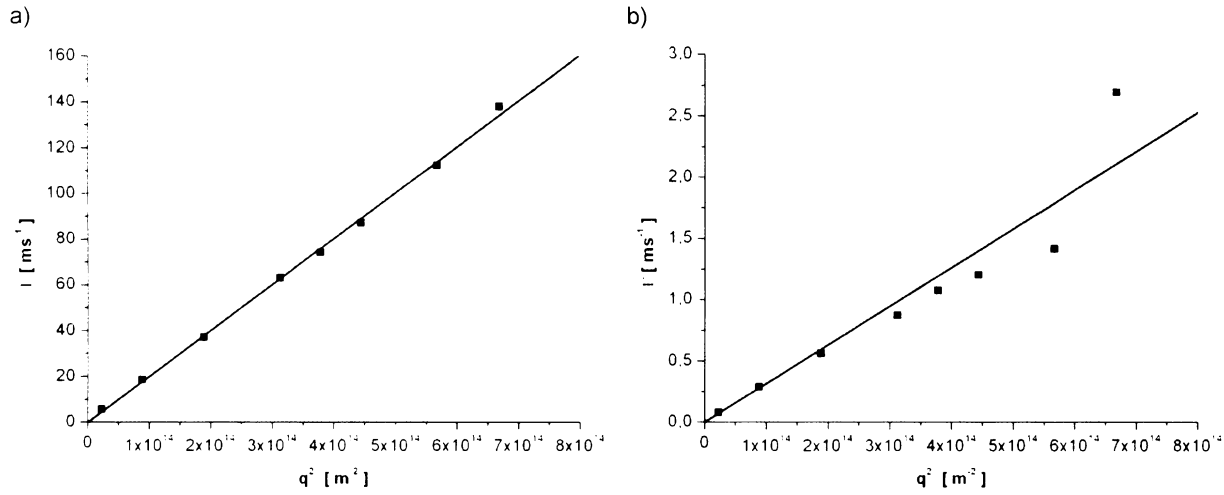

Figure 58: *Dependence on q^2 of decay rates for OB5-A1 sample at 70 °C. a) dynamic mode A1; b) dynamic mode A2.*

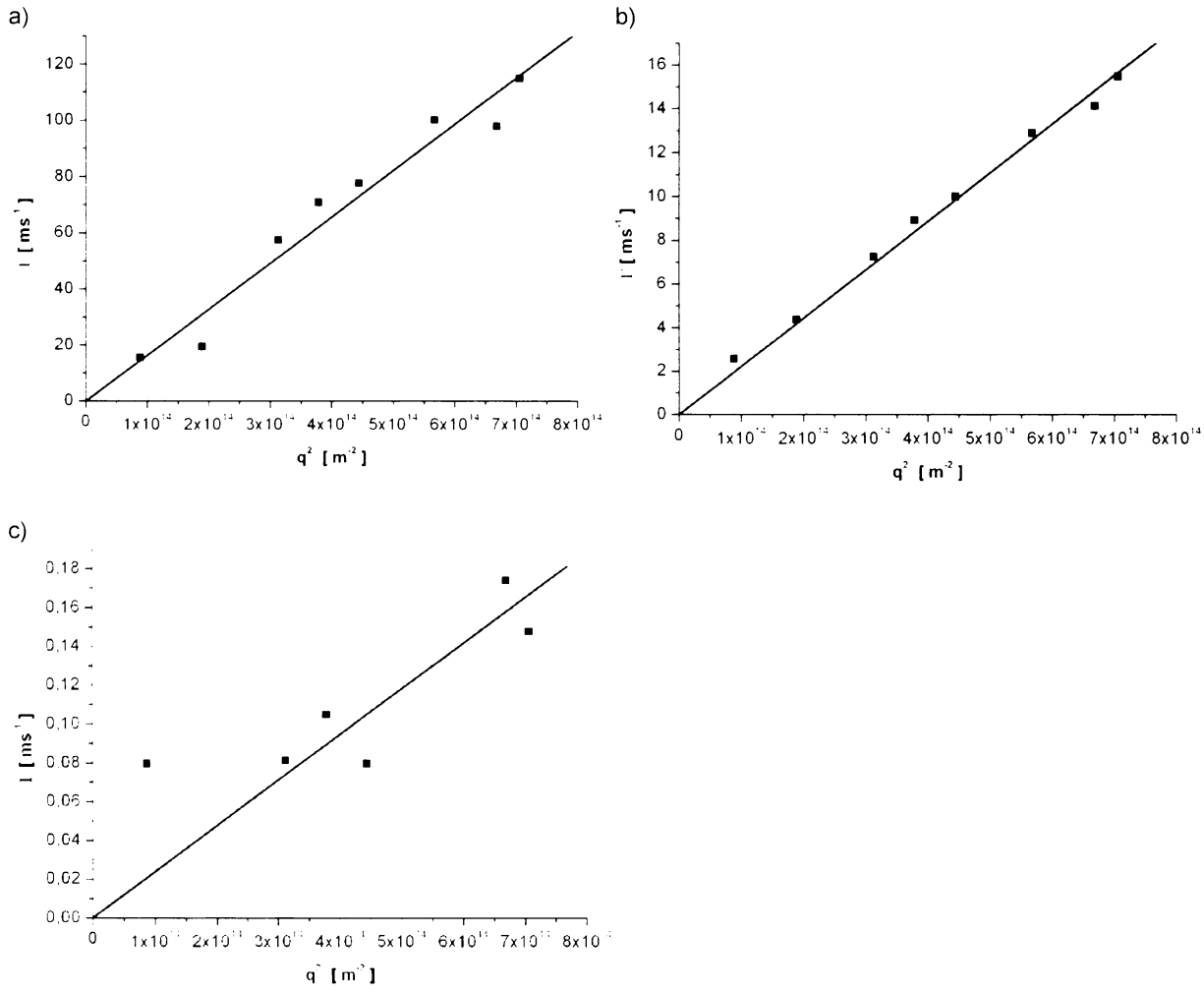

Figure 59: *Dependence on q^2 of decay rates for OB5-A5 sample at 50 °C. a) dynamic mode B1; b) dynamic mode B2; c) dynamic mode B3.*

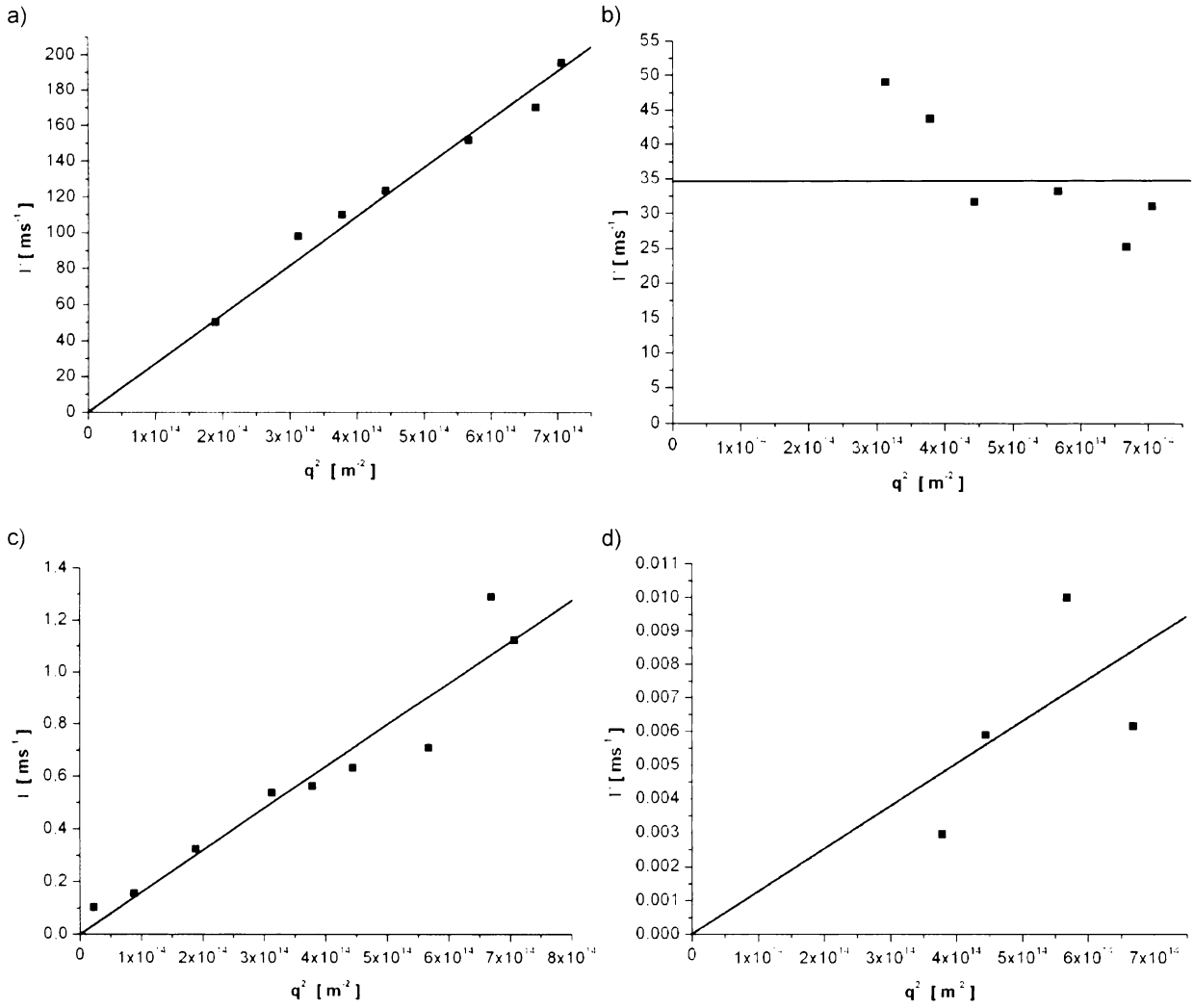

Figure 60: *Angle dependence of decay rates for OB5-A5 sample at 70 °C. a) dynamic mode A1; b) dynamic mode A2; c) dynamic mode A3; d) dynamic mode A4.*

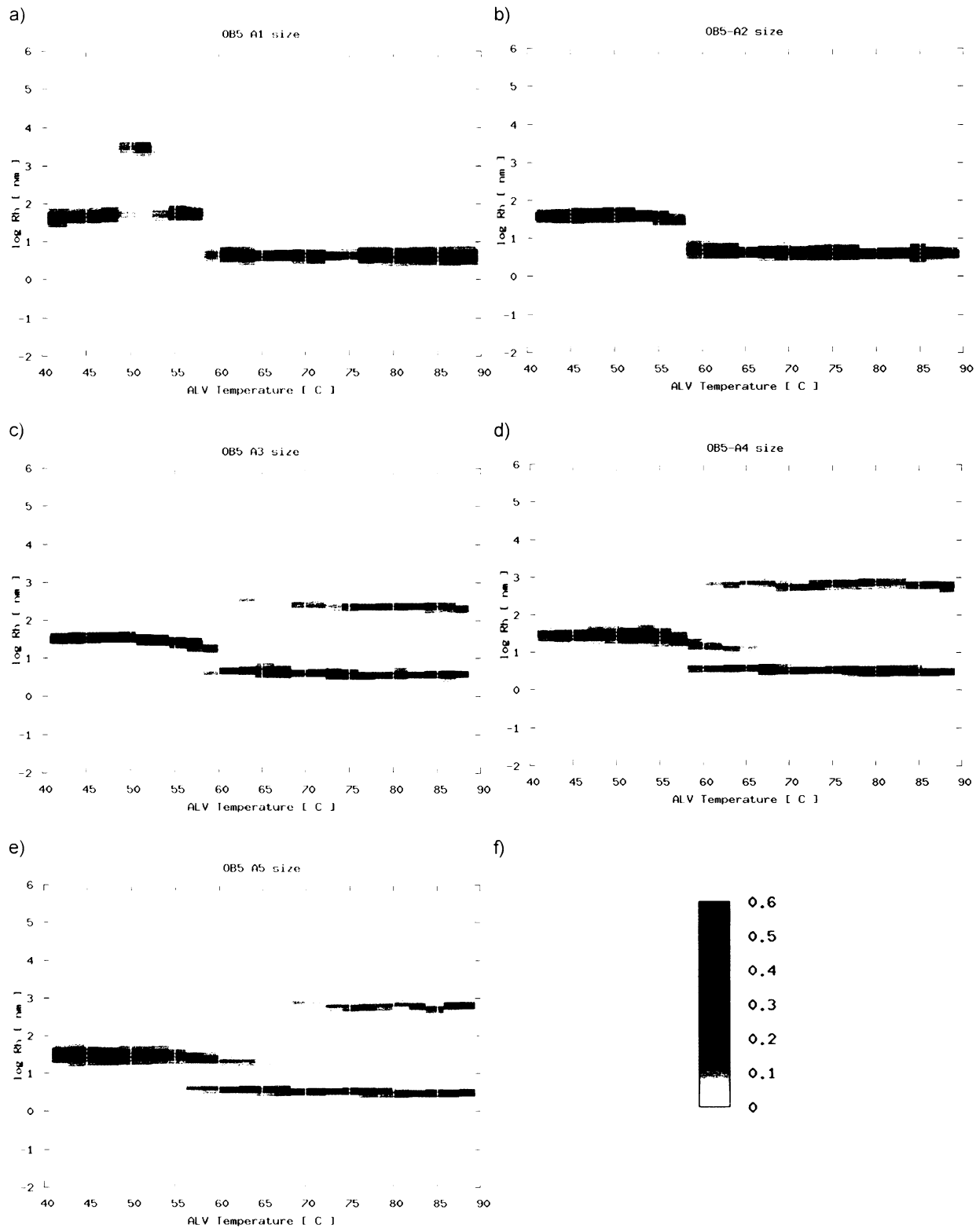

Figure 61: *DLS results for OB5 samples with fixed solvent composition (ca 15% (w/w) DMF in binary solvent mixture) and variable block copolymer concentration; OB5 content in a), b), c), d), e) is 1.0%; 2.0%; 4.9%; 9.9%; 15.0% (w/w) respectively; X vs. Y graph coordinates describe log of correlation size [nm] vs. sample temperature [°C].The Z-scale displayed in f) belongs to all maps.*

Examples of details of selected dynamic modes and R_h for dilute solutions OB3-A1 and OB5-A1 are shown in the Table 14 and Table 15 ,

mode	temperature [C]	R_h [nm]
B1	50	48
A1	66	4
A2	66	200

Table 14: Overview of diffusive dynamic modes and corresponding R_h in OB3-A1 solution.

mode	temperature [C]	R_h [nm]
B1	50	70
A1	66	4
A2	66	600

Table 15: Overview of diffusive dynamic modes and corresponding R_h in OB5-A1 solution.

From the presented data we can deduct that the fastest modes (corresponding to A1) can be assigned to the diffusion of molecularly dissolved chains of diblock copolymers. This is also supported by the fact that the obtained R_h is in good correspondence with the dimensions obtained from solutions of diblock in one solvent. The slower dynamic modes (corresponding to B1) with size of about 50 nm can be assigned to micelles formed in the binary mixture after cooling of the system below the phase separation temperature. The third type of objects (corresponding to A2) with size of hundreds of nanometers, present in solutions above the T_c, are probably larger clusters or "animal-like" micelles[63], [71].

The values for concentrated solutions OB3-A5 and OB5-A5 are mentioned in Table 16 and in Table 17. For the OB3 sample it is clear that the size corresponding to the diffusive A4 component has no real physical sense, because the obtained dimension (70 μm) is out of DLS resolution (which is ca 3 μm). This unrealistic result was caused by high concentration of examined solutions and by the motion of large objects governed by friction, which is not given by the solvent but by the influence of the other surrounding chains. Because of this, the viscosity of solvent used in the calculation of R_h (see Eq. 5.10) does not give usable results. The described effect can be corrected by measuring the right viscosity of the solution in a special apparatus, which, however, was not available in our experiments.

mode	temperature [C]	ξ [nm]
B1	50	3.4
B2	50	29
B3	50	3200
A1	66	3.3
A3	66	700
A4	66	70000

Table 16: Overview of diffusive dynamic modes and corresponding ξ (correlation length) in OB3-A5 solution.

mode	temperature [C]	ξ [nm]
B1	50	3,9
B2	50	32
A1	66	3,7
A3	66	960

Table 17: Overview of diffusive dynamic modes and corresponding ξ (correlation length) in OB5-A5 solution.

From the Tables 16 and 17 it is also visible, that the molecularly dissolved chains (corresponding to the modes A1 and B1) now remain also in systems cooled under the T_c. This means that there exists an equilibrium between polymer chains bound in a complex micelles and free polymer in solution, as in the case of the other micellar systems[143], [144].

The size of micelles is lower than in more diluted solutions, which can be again explained by the fact, that more micelles can be formed with a higher concentration of block copolymer therefore at a constant content of the minority solvent each micelle must be smaller.

In further steps we also studied the concentration dependence of sizes of the objects for OB3 and OB5 systems at temperatures both below and above the phase separation temperature of the binary mixture, where we focused on the behavior of the molecularly dissolved chains and micelles.

For this purpose we chose the samples OB3-A1 and OB5-A1 as basic system to identify the modes of interest, because according to the DLS results, both contain solely diffusive fluctuations (processes B1, A1, A2 in Figure 52, Figure 53, Figure 57 and Figure 58 and the corresponding processes from the other concentrations) that appear also in the other samples (OBX-A2, OBX-A3, OBX-A4, OBX-A5, where "OBX" means OB3 or OB5).

The obtained results are shown at Figure 62 and Figure 63. From the graphs it is visible that the dimension of objects in solution is inversely related to the diblock copolymer concentration.

It is interesting to note that also the size of the molecularly dissolved chains decreases with increasing concentration. This can be explained by the dependence of the cooperative

diffusion coefficient D on the solution concentration, where for D we can (in simple approximation) write[140]: $D = D_0(1 + k_d c)$ where k_d is the virial coefficient of diffusion and c is the concentration of the solution. From this is visible that in the case of positive value of k_d (as is the case in thermodynamically good solvents), D increases, which using Eq. 5.10 causes a decrease of the obtained size.

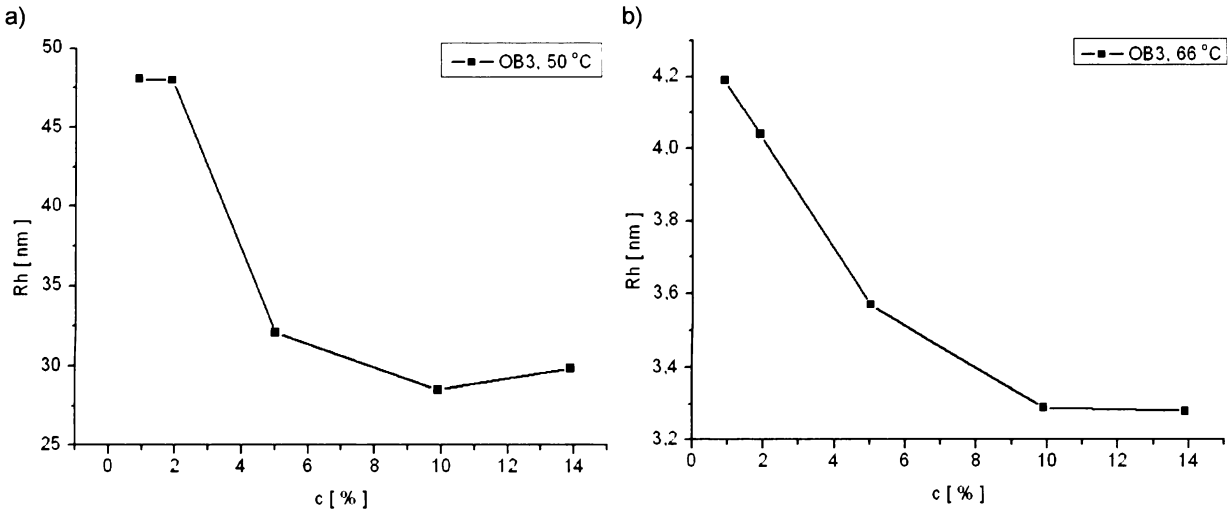

Figure 62: *Concentration dependence size of a) micelles and b) molecularly dissolved chains for OB3 diblock copolymer in DMF / C7 binary mixture.*

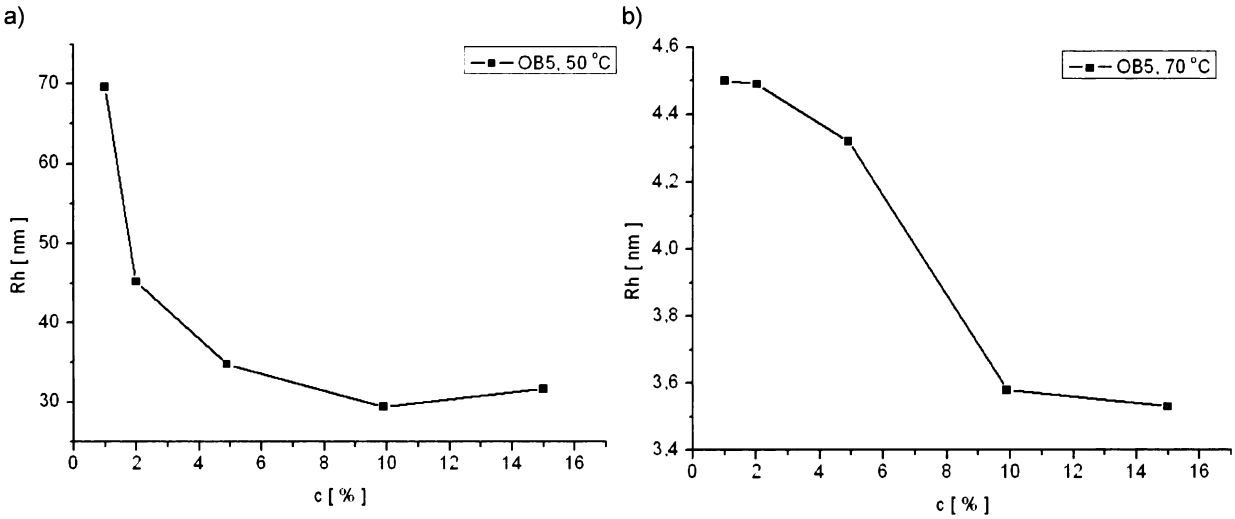

Figure 63: *Concentration dependence size of a) micelles and b) molecularly dissolved chains for OB5 diblock copolymer in DMF / C7 binary mixture.*

6.7.2.6 Diblock copolymer in a binary solvent; variable content of DMF

The composition of samples used to explore the influence of solvent composition is displayed in Table 18. We prepared a series of ca 10% (w/w) solutions of OB3 and OB5 in C7 / DMF mixture with solvent composition from 5 to 25% (w/w) of DMF. The samples were homogenized at 80°C overnight and after that used for experiments.

For all samples we measured correlation curves as a function of temperature and scattering angle. The temperature dependence was measured from 90 to 30°C with a step of 2°C and at a scattering angle of 90°. The angular dependence was measured for temperatures from 80° to 20°, with a step of 20°, and in selected cases for temperatures from 90°C to 30°C with a step of 10°C.

system	sample name	DMF fraction [%]	T_c [°C]	polymer conc. [%]
OB3	OB3-1	7.7	50.8	10.0
	OB3-2	9.6	54.9	8.8
	OB3-3	15.1	64.4	9.8
	OB3-4	20.4	69.6	9.9
	OB3-5	25.7	73.1	9.5
OB5	OB5-1	5.0	37.9	9.2
	OB5-2	10.1	56.6	9.0
	OB5-3	16.3	65.9	9.3
	OB5-4	22.4	71.3	9.1
	OB5-5	25.5	73.1	9.7

Table 18: Composition of OB3 and OB5 samples used to evaluate the effect of solvent composition (DMF content). "*DMF fraction*" is w/w fraction of DMF in binary mixture of DMF/C7. T_C is the phase separation temperature for the binary solvent at given DMF fraction in the mixture. "*polymer conc.*" is w/w concentration of diblock copolymer, dissolved in the binary mixture.

Graphs of normalized intensities for all samples, measured at a scattering angle of 90°, are displayed in Figure 64. For all curves we can see the stabilizing effect of addition of diblock copolymer to the binary mixture. Generally we can say that the phase separation temperature is in all cases decreased by ca 10 – 15 °C, which is in good agreement with results obtained in previous experiments with variable content of block copolymer.

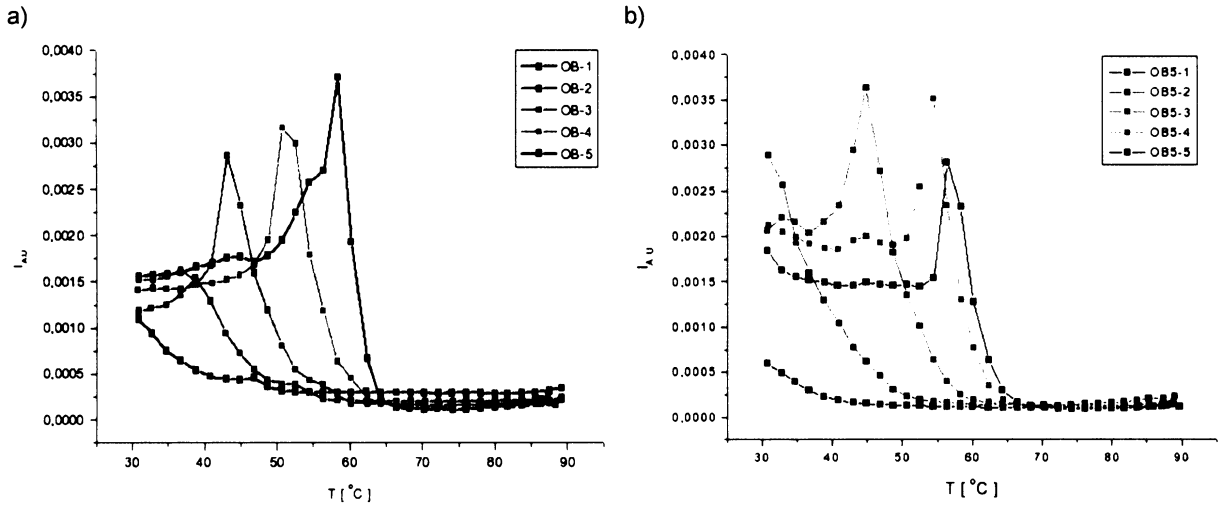

Figure 64: *Temperature dependence of normalized intensities of scattered light from solutions of (a) – OB3 diblock copolymer , (b) – OB5 diblock copolymer .*

The temperature dependence of the distributions of relaxation times displayed in 3D graph maps, is represented below. Figure 65 shows relaxation time graphs for OB3, Figure 66 shows the results of calculations of corresponding correlation lengths. For system OB5 the relaxation time is shown in Figure 67 and correlation lengths in Figure 68.

In both systems it is evident that the scheme of dynamic behavior remains identical and similar to the results obtained with variable concentration of copolymer, but the phase separation temperature is (as supposed) strongly dependent on the DMF concentration in the binary mixture of incompatible solvents. We can conclude that the number of dynamic modes is related to the concentration of diblock copolymer and does not depend on the DMF content. At temperatures below the T_c both micelles and high molecular clusters are present. Above this temperature we can – again – find the cooperative mode A1 and the slower heterogeneity mode A3. The internal mode A2 is also present.

It is also visible that the higher amount of DMF in the mixture helps to differentiate between the two fastest modes above the phase separation temperature (dynamic processes described as A1 and A2 using the same identification as at experiments with variable OB content).

The other observable fact is, that at neither map from Figure 65 nor from Figure 67 are observable large scale inhomogeneities as was in the case of samples OB3-A5 and OB5-A5. This implies that the presence of those object is a matter of high concentration of diblock copolymer and does not depend (in range of used conditions) on the composition of the binary solvent.

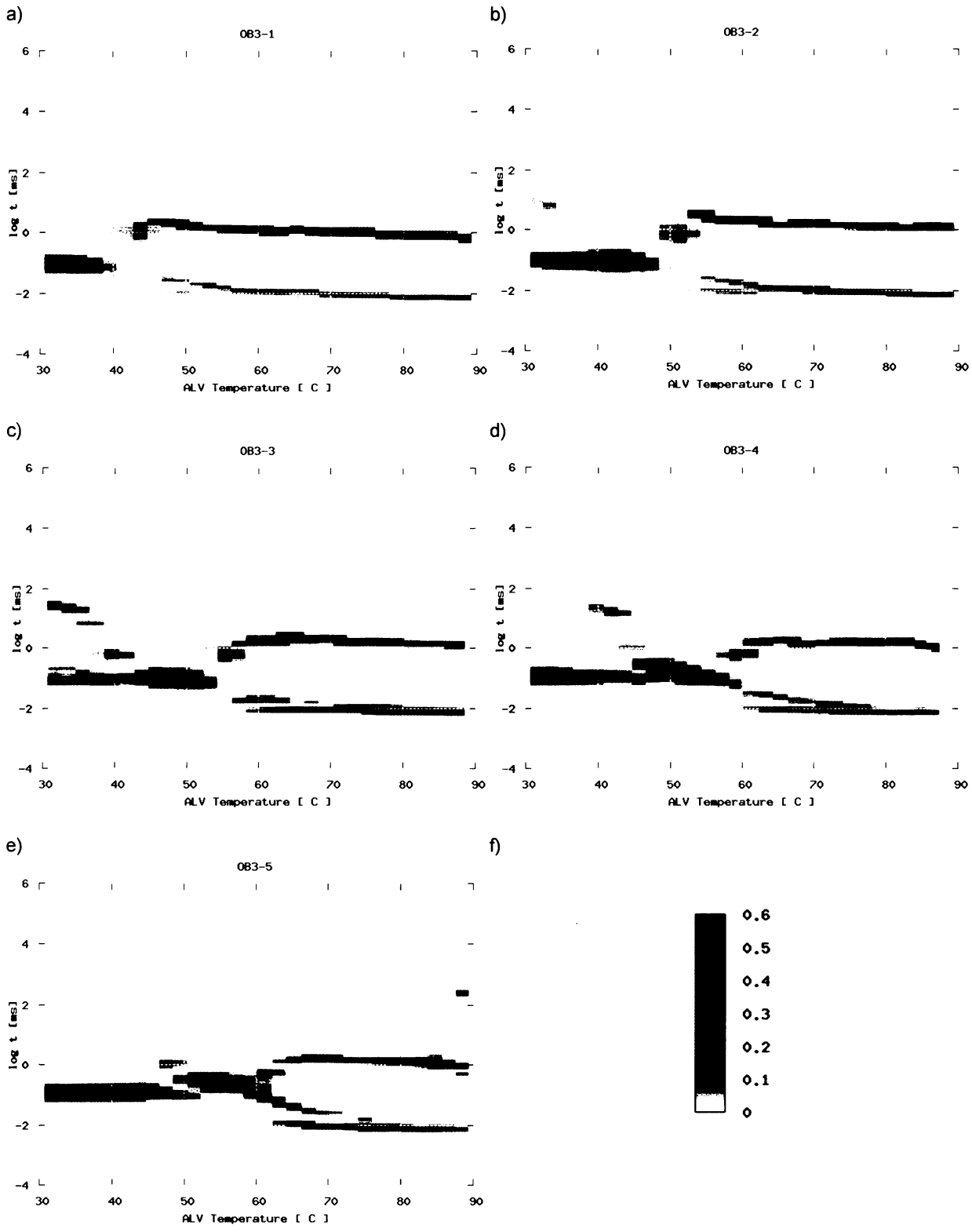

Figure 65: *DLS results for OB3 samples with variable DMF concentration, ca 10% (w/w) OB3 in binary solvent mixture ; DMF content in a), b), c), d), e) is 7.7%; 9.6%; 15.1%; 20.4%; 25.7% (w/w) respectively; X vs. Y graph coordinates describe log of relaxation time [ms] vs. sample temperature [°C]. The Z-scale displayed in f) belongs to all maps.*

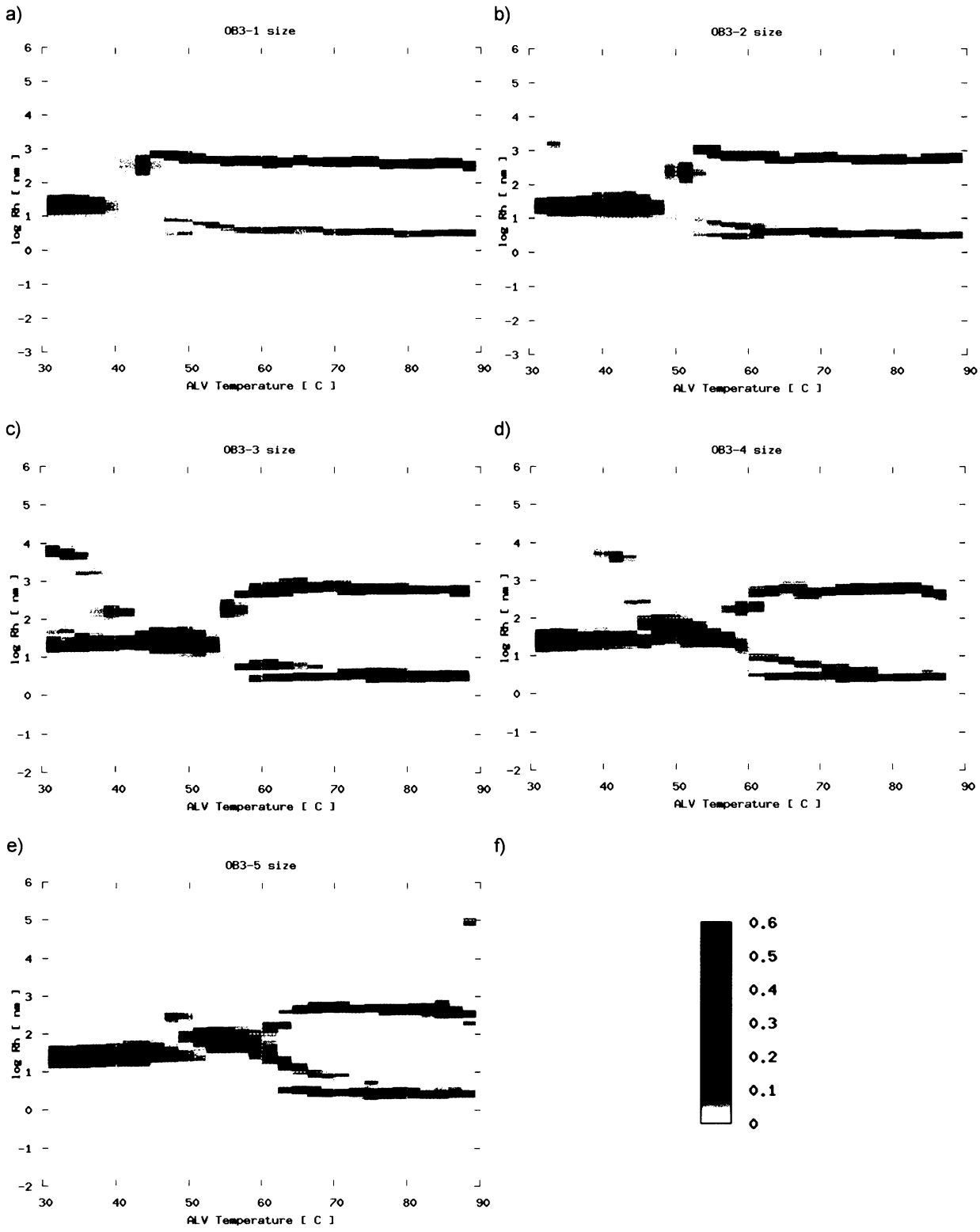

Figure 66: *DLS results for OB3 samples with variable DMF concentration, ca 10% (w/w) OB3 in binary solvent mixture ; DMF content in a), b), c), d), e) is 7.7%; 9.6%; 15.1%; 20.4%; 25.7% (w/w) respectively; X vs. Y graph coordinates describe log of correlation length [nm] vs. sample temperature [°C]. The Z-scale displayed in f) belongs to all maps.*

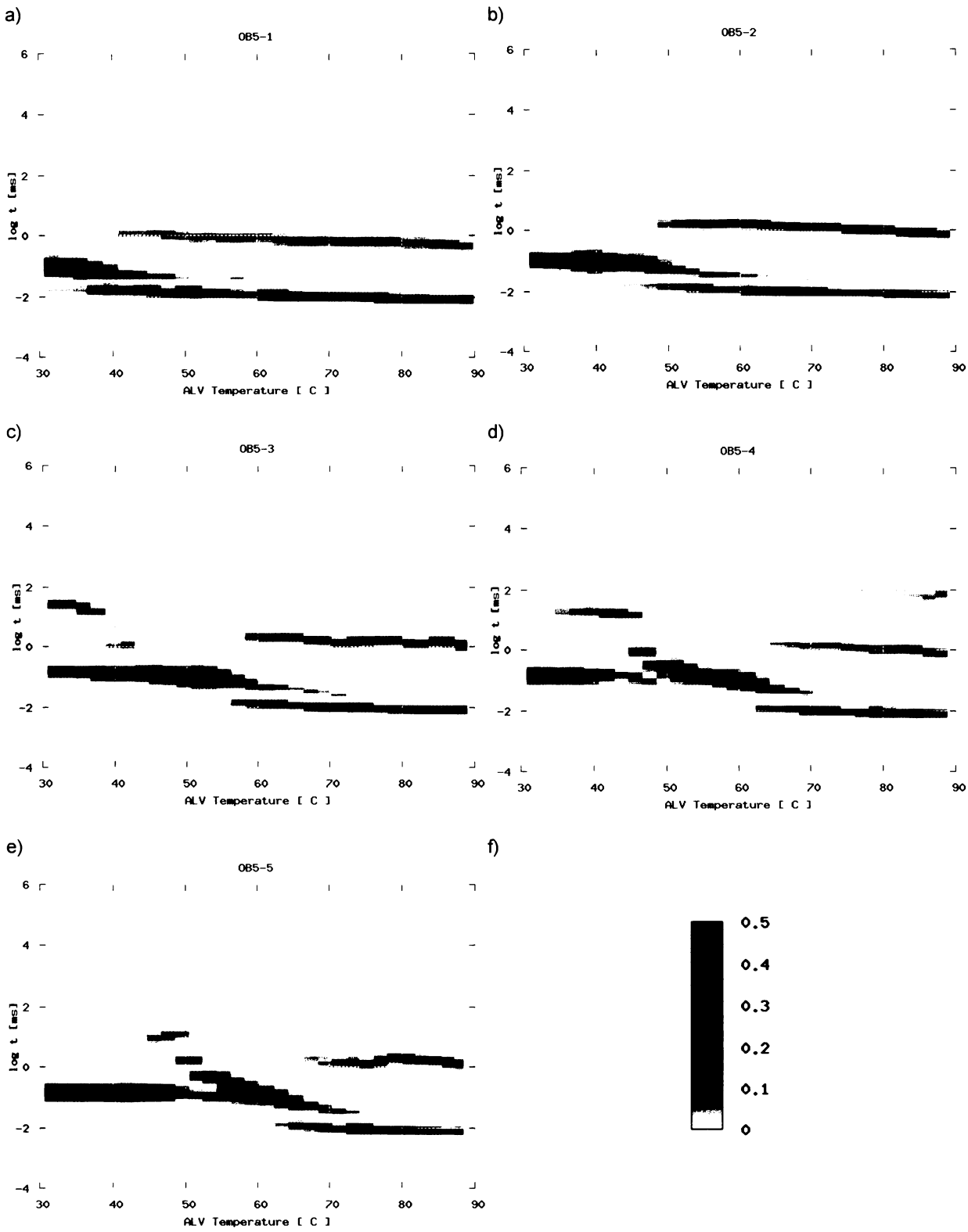

Figure 67: *DLS results for OB5 samples with variable DMF concentration, ca 10% (w/w) OB5 in binary solvent mixture ; DMF content in a), b), c), d), e) is 5.0%; 10.1%; 16.3%; 22.4%; 25.5% (w/w) respectively; X vs. Y graph coordinates describe log of relaxation time [ms] vs. sample temperature [°C]. The Z-scale displayed in f) belongs to all maps.*

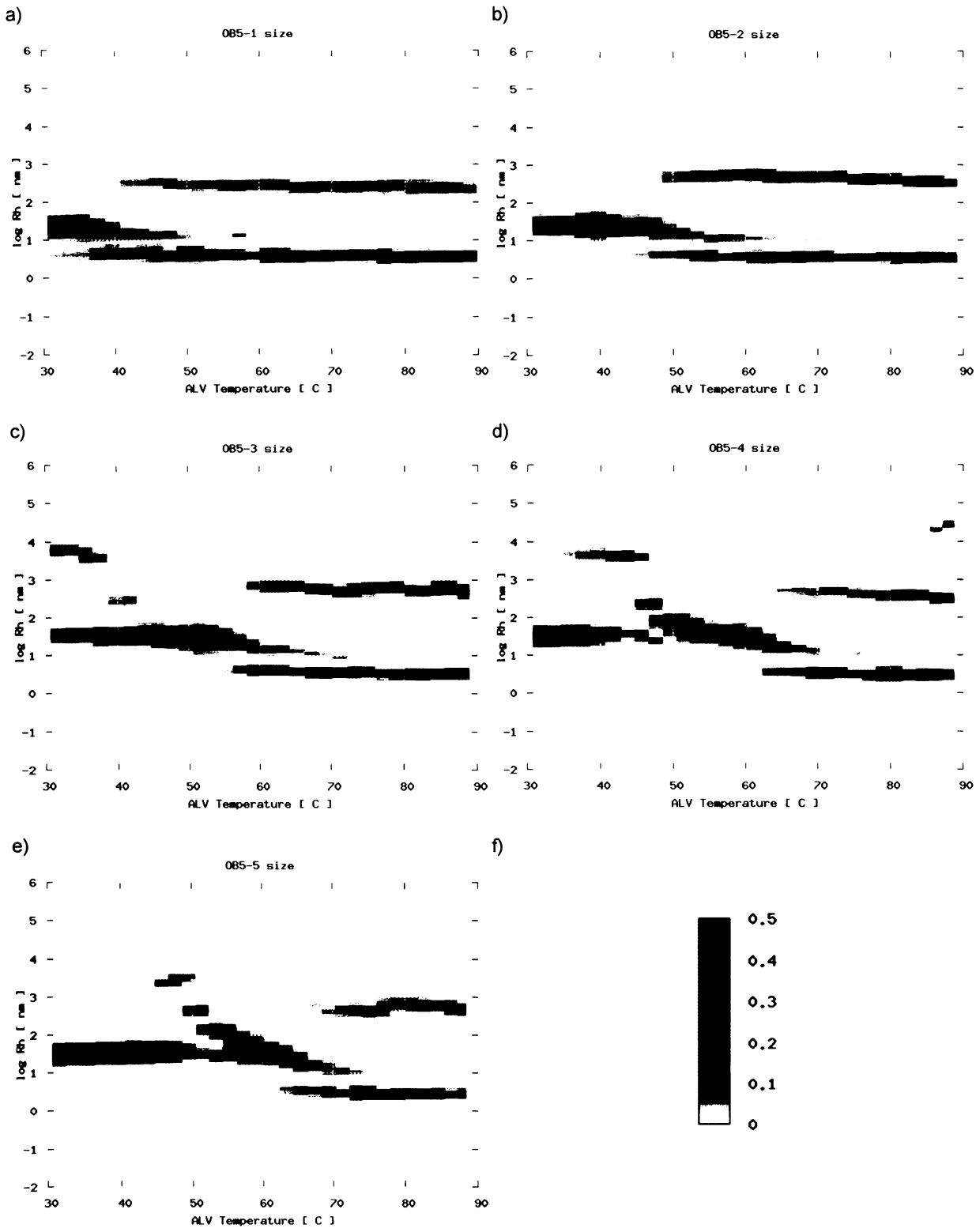

Figure 68: *DLS results for OB5 samples with variable DMF concentration, ca 10% (w/w) OB5 in binary solvent mixture ; DMF content in a), b), c), d), e) is 5.0%; 10.1%; 16.3%; 22.4%; 25.5% (w/w) respectively; X vs. Y graph coordinates describe log of correlation length [nm] vs. sample temperature [°C]. The Z-scale displayed in f) belongs to all maps.*

6.7.3 SAXS results

In some systems composed of two immiscible and inversely selective solvents and a diblock copolymer it was confirmed[79], [80], [81] that in depending on the symmetry of the used block copolymer, the system can self-organize into three dimensional networks and/or into microemulsion nanoparticles encapsulating the minority solvent in the majority matrix. In our case we can obtain a phase separated system at low temperatures, where a part of the used polymer and solvent is precipitated. However, in the supernatant micelles are still present. For the investigation of structure and mass distribution in this system, we examined the OB / DMF / C7 ternary systems by the SAXS method.

For this purpose new samples with 5 % and 10 % (w/w) concentration of either OB3 or OB5 in binary solvent(15 % content of DMF) were prepared, as is described in the Table 19.

sample name	polymer [mg]	DMF [mg]	C7 [mg]	polymer [%]	DMF [%]
OB3-B1	25.00	77.5	403	5.0	16.1
OB3-B2	50.05	67	381	10.0	14.9
OB5-B1	25.00	75	403	5.0	15.7
OB5-B2	49.48	71.5	385	9.8	15.7

Table 19: Composition of OB3 and OB5 samples used for SAXS investigation.

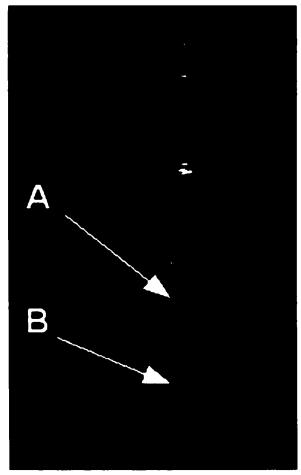

Figure 69: *A photo of a sample used for SAXS examination of OB / DMF / C7 system. A: micellar solution; B: precipitated phase.*

The solutions were explored below the phase separation temperature, where the binary solvent is separated into its components and micelles are present in the solution. To do this,

the samples were placed in 2 mm quartz X-ray capillaries, homogenized at 80 °C, cooled to desired temperature and investigated in the thermostatted chamber.

We have used three different temperatures (35 °C, 40 °C, 50 °C), to cover the temperature behavior for each of OB3 and OB5 samples (with two different diblock concentration).

The SAXS curves were measured both for micellar solutions and the precipitated suspension from the bottom (Figure 69, B) of the cell, however meaningful results were obtained only from the micellar solution so only those will be discussed below. An example of the scattering curve is presented in Figure 70.

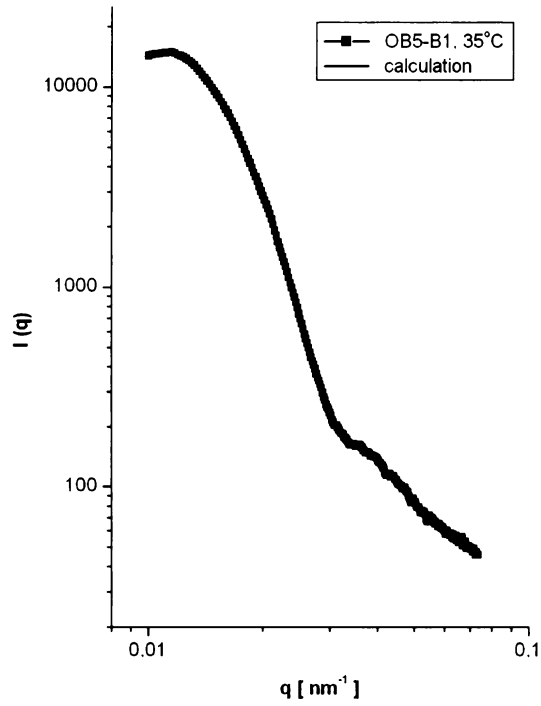

Figure 70: *SAXS curve for OB5-B1 sample.*

The obtained results do not demonstrate any higher self-assembly into more organized structures as lamellae or cylinders, however using the standard relation $d = 2\pi/q_0$ we can from the position of the structure peak q_0 obtain the average distance of the micelles in the system.

By fitting and modeling the real data we can obtain the form factor of the scattering objects. The best description corresponds to hollow spheres of inner radius R_1 and outer radius R_2. The solution can then be described by a model shown in Figure 71 and Figure 72. According to the composition of solution we suppose that the internal volume of the micelle is formed by the encapsulated drop of DMF (to be precise DMF-rich phase), which is

covered by the solvated corona of the diblock copolymers chains. The copolymer molecules are oriented by the PBuMA part of chain into the inner area of the micelle, while the POS part remains oriented into the outer surrounding, which is formed by the majority solvent – heptane (C7) (to be precise heptane-rich phase).

The complete details of SAXS results are shown in Table 20 for OB3 system and in Table 21 for OB5 system.

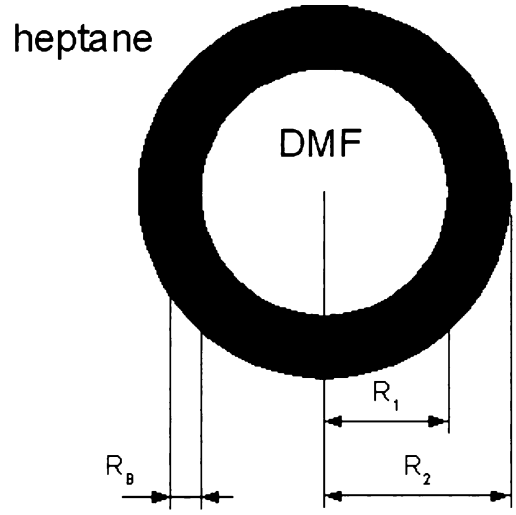

Figure 71: *Hollow micelle image. R_1: diameter of the internal hole/cavity, which is in our case formed by the DMF-rich solvent. R_2: outer diameter of the micelle, which includes the internal DMF core of the micelle and the corona (green color) formed by the presented OB coils. R_B: ideal radius of one diblock coil in micelle corona (one half of the corona thickness). Label "heptane" represents a heptane-rich solvent phase; label "DMF" represents a DMF-rich solvent phase.*

sample	temperature	q_0	d	R_1	R_2
OB3-B1	35	0.0113	55.6	12	22.8
	42	0.0119	52.8	11.9	22.8
	50	0.0115	54.6	13.5	24.4
OB3-B2	35	0.0131	48.0	12.7	20.9
	42	0.0131	48.0	12.8	21.6
	50	0.0130	48.3	12.7	22.7

Table 20: Results for SAXS measurement of OB3-B1 and OB3-B2 samples. q_0 = position of first maximum in SAXS data; d = average distance between centers of micelles; R_1 = radius of internal (DMF) core; R_2 = radius of micelle.

sample	temperature	q_0	d	R_1	R_2
OB5-B1	35	0.0111	56.6	13.4	23.5
	42	0.0113	55.6	13.7	23.6
	50	0.0112	56.1	12.8	21.8
OB5-B2	35	0.0128	49.1	12.9	21.8
	42	0.0134	46.9	13	21.8
	50	0.0128	49.1	13.3	22.7

Table 21: Results for SAXS measurement of OB5-B1 and OB5-B2 samples. q_0 = position of first maximum in SAXS data; d = average distance between centers of micelles; R_1 = radius of internal (DMF) core; R_2 = radius of micelle.

From the values of d, R_1, R_2 and a few preconditions we can calculate the other interesting parameters of the measured solutions:

1. according to the d value we can hypothesize that every one micelle appears in the center of a cubic space of volume: $V_S = d^3$
2. from the R_1 value (from tables before) we are able to calculate the real volume of the DMF presented in the cubic space described by: $V_D = (4\pi R_1^3) / 3$
3. from step 1. and 2. we can calculate real content ([%] in V/V) of DMF in the micellar solution c_D
4. the corona of the hollow micelle is formed by the diblock copolymers coils (see Figure 72), of which the radius (R_B) is in the case of symmetric copolymer equal to the ½ of the corona thickness ($R_B = (R_2 - R_1) / 2$); the volume of the single coil is then: $V_B = (4\pi R_B^3) / 3$
5. it is possible to calculate the total volume of the corona as a simple difference of total volume of micelle and the volume of the internal DMF core, using an equation: $V_C = (4\pi(R_2^3 - R_1^3)) / 3$
6. according to 4. and 5. we can calculate the approximate aggregation number of diblock copolymer chains in studied system: $A = V_C / V_B$
7. using the A from 6. and copolymer M_w we can calculate the weight of the molecules in corona and in next step with using of the volume V_S we can obtain the real concentration of the copolymer c_B in studied solution (w/V or w/w as needed)

The complete summary of results of all samples obtained according to the mentioned considerations is presented in the Table 22.

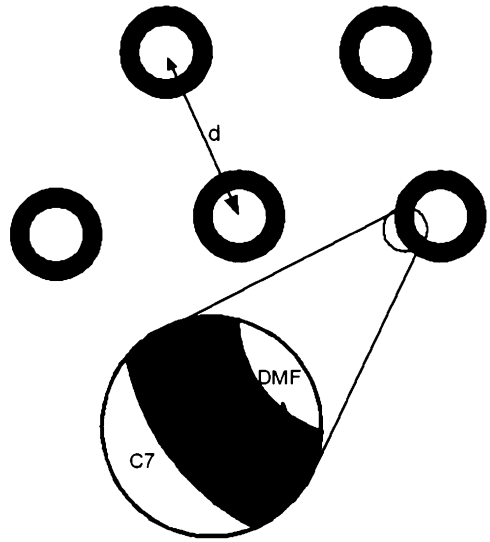

Figure 72: *Schema of the solution and micelle corona organization.*

value	OB3-B1			OB3-B2			OB5-B1			OB5-B2		
T [°C]	30	42	50	30	42	50	30	42	50	30	42	50
d [nm]	55.6	52.8	54.6	48.0	48.0	48.3	56.6	55.6	56.1	49.1	46.9	49.1
R_1 [nm]	12	11.9	13.5	12.7	12.8	12.7	13.4	13.7	12.8	12.9	13	13.3
R_2 [nm]	22.8	22.8	24.4	20.9	21.6	22.7	23.5	23.6	21.8	21.8	21.8	22.7
R_h [nm]	-	27.8	32.1	-	25.8	28.6	-	31.8	34.8	-	28.5	29.5
V_S [nm^3]	171911	147197	163097	110338	110338	12904	181372	171911	176557	118280	103092	118280
V_D [nm^3]	7238	7059	10306	8580	8785	8580	10079	10771	8785	8992	9203	9855
c_D [%]	4.2	4.8	6.3	7.8	8.0	7.6	5.6	6.3	5.0	7.6	8.9	8.3
R_B [nm]	5.40	5.45	5.45	4.10	4.40	5.00	5.05	4.95	4.50	4.45	4.40	4.70
V_B [nm^3]	660	678	678	289	357	524	539	508	382	369	357	435
V_C [nm^3]	42409	42588	50544	29661	33429	40416	44283	44288	34612	34405	34194	39142
A	64	63	74	103	94	77	82	87	91	93	96	90
c_B [%]	1.5	1.8	1.9	3.8	3.5	2.8	2.8	3.2	3.2	5.0	5.9	4.8
c_F		5			10			5			9.8	

Table 22: Summary of calculations of OB3 and OB5 solutions based on the obtained SAXS data (for details see text and the other tables above). *T*: temperature; *d*: average distance of micelles; R_1: radius of inner DMF core; R_2: radius of micelle; R_h: hydrodynamic radius of micelle obtained by DLS experiment; c_D: real concentration (v/v) of DMF in the micellar solution; V_S: space volume of ideal cube calculated according to *d*; V_D: volume of DMF core; R_B: ideal radius of one diblock coil appearing in micelle corona; V_B: ideal volume of the coil; V_C: volume of the corona of the micelle; *A*: aggregation number; c_B: real concentration of OB diblock copolymer in micellar solution (w/w); c_F: original OB diblock concentration in freshly prepared solution.

From these data it is visible, that the temperature has no significant effect on the system characteristics.

Unlike this, the polymer concentration (at constant content of the DMF in the binary solvent) has observable influence and both the average distance between micelles and outer radius of spheres decreases with increasing of OB concentration, which is in good correspondence with results observed by DLS. The difference in sizes obtained by both methods is easily explainable by the fact, that in DLS we "see" not only pure (co)polymer coils, but also their solvating layer and the obtained result is hydrodynamic radius R_h, while using the SAXS we have as result the radius of gyration R_g.

It is also clear that after preparation of the solutions and their cooling to the measurement temperature, a distinct part of both DMF and OB is precipitated at the bottom of the measurement cell and the micellar solution above the sediment is – compared to the original composition – significantly diluted.

This fact is in good correspondence with the theoretical paper of Dan and Tirrell[79], according to which in the case of asymmetric diblock copolymers ($N_A / N_B \neq 1$, *i.e.* the most of real systems) the microemulsion domains coexist with the "bulk" phase. This phase is formed by the macroscopically separated liquids, where their interface is again covered by the oriented diblock copolymer chains.

7 Summary

Poly(*p*-octylstyrene) and poly(*n*-butyl methacrylate) systems have been studied from various points of view.

In the synthetic part of this work we synthesized homopolymers of *p*-octylstyrene and *n*-butyl methacrylate by anionic polymerization initiated by *s*-butyllithium or diphenylmethylpentyllithium. In the following steps we successfully synthesized a series of diblock copolymers by sequential anionic copolymerization (also initiated by *s*-butyllithium). All products were isolated and characterized by GPC to obtain molar mass distribution and for homopolymers we also measured T_g (glass transition temperature) using DSC method.

We tried to obtain the order-to-disorder transition (ODT) temperature of synthesized symmetric diblock copolymers, in order to calculate the Flory-Huggins interaction parameter χ. However, as we finally found from homopolymer blends compatibility studies, in the used temperature range (up to ca 200 °C) it was not possible to obtain the disordered state of the studied systems. According to our results, both homopolymer blends and block copolymer systems exhibit a high incompatibility and the samples are either permanently ordered (block copolymers) or phase separated (homopolymer blends). Since our experimental setup does not allow using of higher temperatures and exclusion of presence of oxygen to prevent decomposition of polymer materials, the exact location of ODT remains still open.

Diblock copolymers synthesized by anionic copolymerization and used further in other experiments were investigated by SAXS and TEM methods. Both methods confirmed that the natural organization of the copolymers OB3 and OB5 is lamellar with regular internal structure. Observation by TEM showed that the structures are clearly formed with long range organization. This can play an important role in potential applications focused on microphase separation.

The OB was also explored in thin layers, where we investigated the behavior after exposition to vapors of simple organic solvents.

Like in SAXS and TEM experiments, in thin layers we also observed an intensive separation into lamellae, which is caused by the strong incompatibility of both blocks. The main difference is in orientation of thin layers, where from AFM samples a perpendicular arrangement in hexane vapors and parallel in the case of acetone is evident.

Chloroform and tetrahydrofuran vapors have no remarkable structural effect except for a weak variations in the shape and size of the characteristic terrace formations. Vapors of 1,4-

dioxane on the other side cause massive undulation and deformation of the surface, which forms an irregular patterning of the thin layer. A common attribute of the mentioned solvents is also the fact that the phase structure of all images remains smooth. This indicates that the lamellae parallel to the surface are covered by the softer polymer material, here probably polyoctylstyrene, because of a higher mobility of this block. Similar behavior of a polymer system was observed *e.g.* in ref. [128] for the polystyrene / polyisoprene system.

More intensive surface changes were observed after exposition to *n*-hexane and acetone vapors.

Here we can say that hexane on one side can serve as a highlighter of natural lamellar structure and on the other side causes perpendicular organization of lamellae to the surface plane. A nice phase separation is also visible on all hexane-treated images, where the average lamellae size is bigger than the dimensions observed by TEM and SAXS method. But because of physical history and because the preparation technique of thin layers is not the same as for thermo-annealed samples, this difference is possible and we propose that the bigger dimensions are caused by swelling effects of solvent vapors.

Unlike in the case of hexane, acetone vapors cause organization of lamellae into a parallel direction to the surface plane, with a terrace-formation typical for block copolymers as mentioned *e.g.* in ref. [145],[20],[146]. The influence of solvent vapor together with the ratio of chain segment lengths and the swelling properties disrupted the original smooth structure to island-like arrangement with a very regular height profile. In the topography image and the attached profile graph (Figure 32), we can clearly see the presence of two main height distributions, markedly isolated by cracks through the layers. As noticed before, in this samples it is also not possible to distinguish detailed structure in the AFM phase image. This effect is clear in the lowest positions where phase does not extend to the original wafer surface, where the contact with the silicone surface would be immediately visible. Also in this case we propose that the surface of the sample is covered with the poly(*p*-octylstyrene chains).

Except for relatively simple studies of thin films of pure diblock copolymers under various conditions, we also dealt with thin layers of ternary systems POS / PBuMA / POS-*b*-PBuMA. At mixtures composition out of the values calculated for Lifshitz point (LP) we found a typical behavior like phase decomposition or lamellar phase organization. However, at components ratio corresponding to the tricritical LP we found a distinct structure formation which creates a teeth-like shapes on the top of the thin layer surface. Because of the characteristic properties of used components, mainly the large difference of glass transition temperature T_G, we suppose that the stable cylindrical formations are formed by the component with higher T_G, *i.e.* by PBuMA chains coming both from the homopolymer and copolymer

molecules. On the contrary, the soft, surrounding POS material has not enough mechanical stability and flows down from the primary microemulsion (μE) structure.

The lateral dimension of the "teeth" at their base (ca 190 nm) correspond with the average dimensions (from tens to hundreds of nanometers) of microemulsions from TEM images published *e.g.* in [36] and [37]. We are of course aware that the surface structures are often more or less different from the arrangement in bulk matter and the continuous structure typical for bicontinuous μE probably cannot be observed in this case.

The vertical size of the formations is ca 800 nm and their surface under AFM did not exhibit any additional substructures.

Because of the described unique behavior observed in μE of ternary systems, we believe in a great potential of those blends usable in nanotechnology applications, mainly at templating of regular cylindrical shapes. Those can be subsequently used directly in *e.g.* producing of base components for nanodevices, or physically and/or chemically modified to form highly structured membranes with regular pores dimension or to fabricate various types of nanocontainers.

Interesting results were also obtained from examination of ternary systems consisting of a mixture of diblock copolymer and two mutually incompatible solvents, where we stay focused on the influence of either variable concentration of polymer or the composition of binary mixture of solvents.

In experiments with variable concentration of diblock copolymers in the solutions we found both diffusive and non-diffusive dynamic processes. Their relaxation times – and therefore corresponding R_h or ξ – were strongly dependent on the system temperature (*i.e.* if the temperature is above or below the T_c of the binary solvent) and on the concentration of diblock copolymer.

Generally we can say, that above the phase separation temperature are present both molecularly dissolved chains ($R_h \sim 4$ nm) and large-scale clusters (R_h of hundreds of nm). In concentrated solutions highly above the c* also large-scale inhomogeneities (size in μm) are present, however, because of the size, which exceeds the limits of DLS, we did not study them in details.

Below the phase separation temperature one important dynamic mode was found in all solutions, and we assigned it to micelles (R_h around 50 nm) formed in the system after phase separation of the binary solvent.

From the obtained results from both experiments with either variable concentration of polymer or binary solvent composition we can say, that the dynamic behavior of the OB / C7 / DMF system is strongly dependent on the diblock copolymer concentration while the content of DMF has only secondary function and causes only the shift of the obtained results on the temperature scale. The composition of the binary solvent has also no

influence on the number of dynamic processes in the studied system that is on the contrary influenced by the diblock copolymer concentration. The presence of diblock copolymer also stabilizes the solutions by lowering of the T_c of the used binary solvent system.

Several samples used in DLS experiments were also explored by SAXS to investigate the possible presence a highly organized self-assembled structures in the solution. We found that such organization does not occur in the studied systems and instead of this we confirmed the presence of hollow micelles in the solution.

After more a detailed study we found that the structural behavior of these samples (below the phase separation temperature of the binary solvent and at the constant content of DMF in the mixture) is not a function of applied temperature, but is only a function of diblock copolymer concentration. The obtained results are in good correspondence with the results obtained by DLS, where we also observed a decrease of micellar size with increasing OB concentration.

It was also found that after preparation of the solutions and their cooling to the measurement temperature (*i.e.* below the T_C), a distinct part of both DMF and OB is precipitated and settled at the bottom of the cuvette as predicted in ref. [79]. The micellar solution above the sediment is therefore significantly diluted and compared to the original concentration contains ca 30 to 50 % of both added diblock copolymer and DMF.

It is necessary to say that the micellar solutions based on hollow micelle structure can play an important role in the delivery systems, *e.g.* in the medicine *etc.* In the inner "capsule" of the micelle can be transported *e.g.* sensitive or vice versa aggressive solvents and/or solutes to the desired place, where the hollow structure can be (at certain conditions) "unfolded" and the content of the "mobile capsule" released for the required use.

Another possibility is to cross-link the outer shell of the hollow structure and we can obtain a stable container suitable for *e.g.* protecting a reactive center, which will however still remain attainable for low-molecular materials as solvent and gases.

At this time we of course are not able to predict a usability of the studied system *e.g.* directly in the mentioned bio-application, however it is important that we enlarge the general knowledge with another polymer / solvent combination.

Generally we can say that the POS / PBuMA combination forms a very attractive macromolecular system that can be useful in various experiments.

For example it is possible to study its behavior in solutions of simple or binary solvents and to widen the general understanding of polymer systems. Mutual incompatibility of both components is also important and it is useful in self-assembly studies or applications meant

for thin layers, and consequently it has potential usability in nanotechnology applications. It is also possible to utilize the physical and chemical properties (as T_g and/or chemical analogy) of individual homopolymers and try to combine them *e.g.* with different materials to prepare new bulk blends with tunable parameters.

It is not, of course, possible to cover all mentioned examples in this dissertation, and therefor the POS / PBuMA system potential still offers a lot of inspiration for the other experiments and projects.

List of figures

List of tables

Bibliography

[1] Kwei T.K.; Frisch H.L; Radigan W.; Vogella S. *Macromolecules* **1977**, ,

[2] Ribbe A.E.; Hashimoto T. *Macromolecules* **1997**, 30, 3999

[3] Karatasos K; Vlachos G.; Vlassopoulos D.; Fytas G. *Macromolecules* **1998**, ,

[4] Buxton G.A., Balazs A.C. *Macromolecules* **2005**, 38, 488

[5] Bates F.S.; Fredrickson G.H. *Physic today*, February **1999**, 32-38

[6] Klok H. A.; Lecommandoux S. *Adv. Mater.* **2001**, 13, 1217

[7] Alexandridis P. *Curr. Opin. Colloid Interface Sci.* **2000**, 5, 312

[8] Chen J.T.; Thomas E.L.; Zimba C.G.; Rabolt J.F. *Macromolecules* **1995**, 28, 5811

[9] Urbas A.; Fink Y.; Thomas E.L. *Macromolecules* **1999**, 32, 4748

[10] Urbas A.; Sharp R.; Fink Y.; Thomas E.L.; Xenidou M.; Fetters L.J. *Adv. Mater.* **2000**, 12, 812

[11] Bartl M.H.; Boettcher S.W.; Hu E.L.; Stucky G.D. *J. Am. Chem. Soc.* **2004**, 126, 10826

[12] Liu G.; Ding J.; Guo A.; Herfort M.; Bazett-Jones D. *Macromolecules* **1997**, 30, 1851

[13] Liu G.; Ding J. *Adv. Mater.* **1998**, 10, 69

[14] Liu G.; Ding J.; Hashimoto T.; Kimishima K.; Winnik F.M.; Nigam S. *Chem. Mater.* **1999**, 11, 2233

[15] Liu G.; Ding J.; Stewart S. *Angew. Chem. Int. Ed.* **1999**, 38, 835

[16] Hashimoto T.; Tsutsumi K.; Funaki Y. *Langmuir* **1997**, 13, 6869

[17] Hashimoto T.; Koizumi S.; Hasegawa H.; Izumitani T.; Hyde S.T. *Macromolecules* **1992**, 25, 1433

[18] Renker S.; Mahajan S.; Babski D.T.; Schnell I.; Jain A.; Gutmann J.; Zhang Y.; Gruner S.M.; Spiess H.W.; Wiesner U. *Macromol. Chem. Phys.* **2004**, 205, 1021

[19] Rabatic B.M.; Pralle M.U.; Tew G.N.; Stupp S.I. *Chem. Mater.* **2003**, 15, 1249

[20] Sidorenko A.; Tokarev I.; Minko S.; Stamm M. *J. Am. Chem. Soc.* **2003**, 125, 12211

[21] Lichterfeld F.; Schmeling T.; Strey R *J. Phys. Chem.* **1986**, 90, 5760

[22] Kahlweit M.; Strey R.; Firman P. *J. Phys. Chem.* **1986**, 90, 671

[23] Jahn W.; Strey R. *J. Phys. Chem.* **1988**, 92, 2294

[24] Lawrence M.J.; Rees G.D. *Adv. Drug Deliv. Rev.* **2000**, 45, 89

[25] Fredrickson G.H.; Bates F.S *Eur. Phys. J. B* **1998**, 1, 71

[26] Berdjane K.; Berdjane Z.; Rueda D.R.; Bénachour D.; Baltá-Calleja F.J. *J. Appl. Polym. Sci.* **2003**, 89, 2046

[27] Pluta M.; Bartczak Z.; Pawlak A.; Galeski A.; Pracella M. *J. Appl. Polym. Sci.* **2001**, 82, 1423

[28] Fortelný I.; Kruliš Z.; Michálková D.; Horák Z. *Angew. Makromol. Chem.* **1999**, 270, 28

[29] Fortelný I.; Šlouf M.; Sikora A.; Hlavatá D.; Hašová V.; Mikešová J.; Jacob C. *J. Appl. Polym. Sci.* **2006**, 100, 2803

[30] Morkved T.L.; Chapman B.R.; Bates F.S.; Lodge T.P.; Stepane P.; Almdal K. *Faraday Discuss.* **1999**, 112, 335

[31] Huh J.; Jo W.H. *J. Chem. Phys.* **2002**, 117, 9920

[32] Morkved T.L.; Stepanek P.; Krishnan K.; Bates F.S.; Lodge T.P. *J. Chem. Phys.* **2001**, 114, 7247

[33] Štěpánek P.; Morkved T.L.; Krishnan K.; Lodge T.P.; Bates F.S. *Physica A* **2002**, 314, 411

[34] Fredrickson G.H.; Bates F.S. *J. Polym. Sci., Part B* **1997**, 35, 2775

[35] Broseta D.; Fredrickson G.H. *J. Chem. Phys.* **1990**, 93, 2927
[36] Hillmyer M.A.; Maurer W.W.; Lodge T.P.; Bates F.S.; Almdal K. *J. Phys. Chem. B* **1999**, 103, 4818
[37] Corvazier L.; Messe L.; Salou C.L.O.; Young R.; Fairclough J.P.A.; Ryan A.J. *J. Mater. Chem.* **2001**, 11, 2864
[38] Akpalu Y.A.; Karim A.; Satija S.K.; Balsara N.P. *Macromolecules* **2001**, 34, 1720
[39] Wang H.; Composto R.J.; Hobbie E.K.; Han C.C. *Langmuir* **2001**, 17, 2857
[40] Sprenger M.; Walheim S.; Budkowski A.; Steiner U. *Interface Sci.* **2003**, 11, 225
[41] Holoubek J.; Baldrian J.; Lednický F.; Málková Š.; Lal J. *Macromol. Chem. Phys.* **2006**, 207, 1834
[42] Mortensen K.; Talmon Y.; Gao B.; Kops J. *Macromolecules* **1997**, 30, 6764
[43] Hanley J.K.; Lodge T.P.; Huang Ch.I. *Macromolecules* **2000**, 33, 5918
[44] Bahadur P. *Curr. Sci.* **2001**, 80, 1002
[45] Lally T.P.; Price C. *Polymer* **1974**, 15, 325
[46] Price C.; Woods D. *Polymer* **1974**, 15, 389
[47] Marie P.; Duplessix R.; Gallot Y.; Picot C. *Macromolecules* **1979**, 12, 1180
[48] Shibayama M.; Hashimoto T.; Hasegawa H.; Kawai H. *Macromolecules* **1983**, 16, 1427
[49] Shibayama M.; Hashimoto T.; Kawai H. *Macromolecules* **1983**, 16, 1432
[50] Balsara N.P.; Stepanek P.; Lodge T.P.; Tirrell M. *Macromolecules* **1991**, 24, 6227
[51] Hanley K.J.; Lodge T.P. *J. Polym. Sci., Part B* **1998**, 36, 3101
[52] Kelarakis A.; Havredaki V.; Booth C.; Nace V.M. *Macromolecules* **2002**, 35, 5591
[53] Hadjichristidis N.; Pispas S.; Floudas G., *Block Copolymers (Synthetic Strategies, Physical Properties, and Applications)*, Wiley-Interscience **2003**
[54] Gallot Y.; Franta E.; Rempp P.; Benoit H. *J. Polym. Sci., Part C* **1964**, 4, 473
[55] Talingting M.R.; Munk P.; Webber S.E.; Tuzar Z. *Macromolecules* **1999**, 32, 1593
[56] Shibayama M.; Hashimoto T.; Kawai H. *Macromolecules* **1983**, 16, 16
[57] Nose T.; Numasawa N. *Comput. Theor. Polym. Sci.* **2001**, 11, 167
[58] Ouarti N.; Viville P.; Lazzaroni R.; Minatti E.; Schappacher M.; Deffieux A.; Borsali R. *Langmuir* **2005**, 21, 1180
[59] Penfold J.; Staples E.; Tucker I. *J. Phys. Chem. B* **2002**, 106, 8891
[60] Roy S.; Dey J. *Langmuir* **2003**, 19, 9625
[61] Croce V.; Cosgrove T.; Dreiss C.A. *Langmuir* **2004**, 20, 7984
[62] Balsara N.P.; Tirrell M.; Lodge T.P. *Macromolecules* **1991**, 24, 1975
[63] Konak C.; Fleischer G.; Tuzar Z.; Bansil R. *J. Polym. Sci., Part B* **2000**, 38, 1312
[64] Nie H.; Bansil R.; Ludwig K.; Steihart M.; Koňák Č,; Bang J. *Macromolecules* **2003**, 36, 2003
[65] Koňák Č.; Fleischer G.; Tuzar Z.; Bansil R. *J. Polym. Sci., Part B* **2002**, 38, 1312
[66] Bansil R.; Nie H.; Koňák Č.; Helmstedt M.; Lal J. *J. Polym. Sci., Part B* **2002**, 40, 2807
[67] Nie H.; Li M.; Bansil R.; Koňák Č.; Helmstedt M.; Lal J. *Polymer* **2004**, 45, 8791
[68] Raspaud E.; Lairez D.; Adam M. *Macromolecules* **1994**, 27, 2956
[69] Sakurai S.; Hashimoto T.; Fetters L.J. *Macromolecules* **1996**, 29, 740
[70] Yu Y.M.; Blacher S.; Brouers F.; Homme G.L.; Jérôme R. *Macromolecules* **1997**, 30, 4619
[71] Lairez D.; Adam M.; Carton J.P.; Raspaud E. *Macromolecules* **1997**, 30, 6798
[72] Fleischer G.; Koňák Č.; Puhlmann A.; Rittig F.; Kärger J. *Macromolecules* **2000**, 33, 7066

[73] Jiang Y.; Zhu J.; Jiang W.; Liang H. *J. Phys. Chem. B* **2005**, 109, 21549

[74] Ravi P.; Wang C.; Tam K.C.; Gan L.H. *Macromolecules* **2003**, 36, 173

[75] Oupický D.; Koňák Č.; Ulbrich K; Wolfert M.A.; Seymour L.W. *J. Control. Release* **2000**, 65, 149

[76] Tuzar Z.; Bahadur P.; Kratochvíl P. *Makromol. Chem.* **1981**, 182, 1751

[77] Tuzar Z.; Stepanek P.; Konak C.; Kratochvil P. *J. Colloid Interface Sci.* **1985**, 105, 372

[78] Cogan K.A.; Gast A.P. *Macromolecules* **1990**, 23, 745

[79] Dan N.; Tirrell M. *Macromolecules* **1993**, 26, 637

[80] Štěpánek P.; Tuzar Z.; Nallet F.; Noirez L. *Macromolecules* **2005**, 38, 3426

[81] Cantor R. *Macromolecules* **1981**, 14, 1186

[82] Tuzar Z.; Kratochvíl P. *Macromolecules* **1977**, 10, 1108

[83] Ligne de lumiere SWING "SAXS/WAXS-ing" [online], **2005**, Accessible from WWW: <http://www.synchrotron-soleil.fr/francais/vie-scientifique/experiences/swing/fiche-swing.htm>

[84] Baldrian J. et al., *Základy fyziky pevných polymerů*, Edice Macro, Praha **1987**

[85] Trent J.S.; Scheinbeim J.I.; Couchman P.R. *Macromolecules* **1983**, 16, 589

[86] Ford N.C., Theory and Practice of Correlation Spectroscopy, In *Measurement of Suspended Particles by Quasi-Elastic Light Scattering*, Edited by Barton E. Dahneke, John Wiley & Sons, Inc. **1983**

[87] QELS [online], **2005**, Accessible from WWW: <http://www.wyatt.com/theory/qels/>

[88] Charles S. Johnson, Jr. and Don A. Gabriel, *Laser Light Scattering*, Dover Publications Inc., New York **1994**

[89] Štěpánek P.; Koňák Č. *Adv. Colloid Interface Sci.* **1984**, 21, 195

[90] Štěpánek Petr, Data analysis in dynamic light scattering, In *Dynamic Light Scattering; The method and some applications*, Edited by Wyn Brown, Clarendon Press, Oxford **1993**

[91] Jakes J. *Czech J. Phys. B* **1988**, 38, 1305

[92] Yasuda M.; Murakami Y.; Sowa A.; Ogino H.; Ishikawa H. *Biotechnol. Prog.* **1998**, 14, 601

[93] Bolten M.; Niermann M.; Eimer W. *Biochemistry* **1999**, 38, 12416

[94] Aggeli A.; Fytas G.; Vlassopoulos D.; McLeish T.C.B.; Mawer P.J.; Boden N. *Biomacromolecules* **2001**, 2, 378

[95] Hossain K.S.; Ochi A.; Ooyama E.; Magoshi J.; Nemoto N. *Biomacromolecules* **2003**, 4, 350

[96] Campbell J.N.; Epand R.M.; Russo P.S. *Biomacromolecules* **2004**, 5, 1728

[97] Vijayanathan V.; Lyall J.; Thomas T.; Shirahata A.; Thomas T.J. *Biomacromolecules* **2005**, 6, 1097

[98] Binning G.; Quate C.F.; Gerber Ch. *Phys. Rev. Lett.* **1986**, 56, 930

[99] Blanchard R.Ch. *The Chemical Educator* **1996**, 1, 1

[100] Vlček P.; Lochmann L. *Prog. Polym. Sci.* **1999**, 24, 793

[101] Jagur-Grodzinski J. *Reactive and Functional Polymers* **2001**, 49, 1

[102] Hadjichristidis N.; Iatrou H.; Pispas S.; Pitsikalis M. *J. Polym. Sci. A: Polym. Chem.* **2000**, 38, 3211

[103] Allen R.D.; Long T.E.; McGrath J.E. *Polymer Bulletin* **1986**, 15, 127

[104] NIMS Materials Database [online], **2006 [cit. 2006-06-10]**, Accessible from WWW: <http://mits.nims.go.jp/db_top_eng.htm>

[105] Garetz B.A.; Newstein M.C.; Dai H.J.; Jonnalagadda S.V.; Balsara N.P. *Macromolecules* **1993**, 26, 3151

[106] Stepanek P.; Almdal K.; Lodge T.P. *J. Polym. Sci., Part B* **1997**, 35, 1643

[107] Štěpánek P.; Nallet F.; Diat O.; Almdal K.; Panine P. *Macromolecules* **2002**, 35, 7287

[108] Jian T.; Semenov A.N.; Anastasiadis S.H.; Fytas G.; Yeh F.J.; Chu B.; Vogt S.; Wang F.; Roovers J.E.L. *J. Chem. Phys.* **1994**, 100, 3286

[109] Martys N.S.; Douglas J.F. *Phys. Rev. E* **2001**, 63, 031205

[110] Matsen M.W.; Bates F.S. *Macromolecules* **1996**, 29, 1091

[111] Krausch G.; Magerle R. *Adv. Mater.* **2002**, 14, 1579

[112] Minko S.; Kiriy A.; Gorodyska G.; Stamm M. *J. Am. Chem. Soc.* **2002**, 124, 10192

[113] Yang J.; Mayer M.; Kriebel J.K.; Garstecki P.; Whitesides G.M. *Angew. Chem. Int. Ed.* **2004**, 43, 1555

[114] Pyun J.; Kowalewski T.; Matyjaszewski K. *Macromol. Rapid Commun.* **2003**, 24, 1043

[115] Zhao B.; Brittain W.J. *Prog. Polym. Sci.* **2000**, 25, 677

[116] Prucker O.; Rühe J. *Langmuir* **1998**, 14, 6893

[117] Cui Y. et al. *Science* **2001**, 293, 1289

[118] Duffy D.C.; McDonald J.C.; Schueller O.J.A.; Whitesides G.M. *Anal. Chem.* **1998**, 70, 4974

[119] Rasmont A.; Leclère Ph.; Doneux C.; Lambin G.; Tong J.D.; Jérôme R.; Brédas J.L.; Lazzaroni R. *Colloids Surf. B* **2000**, 19, 381

[120] Xu T.; Zvelindovsky A.V.; Sevink G.J.; Gang O.; Ocko B.; Zhu Y.; Gido S.P.; Russel T.P. *Macromolecules* **2004**, 37, 6980

[121] Huang H.; Hu Z.; Chen Y.; Zhang F.; Gong Y.; He T. *Macromolecules* **2004**, 37, 6523

[122] Kim G.; Libera M. *Macromolecules* **1998**, 31, 2569

[123] Rhurn-Albrecht T.; Steiner R.; DeRouchey J.; Stafford C.M.; Huang E.; Bal M.; Tuominen M.; Hawker C.J.; Russell T.P. *Adv. Mater.* **2000**, 12, 787

[124] Hahm J.; Sibener S.J. *Langmuir* **2000**, 16, 4766

[125] Prucker O.; Rühe J. *Macromolecules* **1998**, 31, 602

[126] Tokarev I.; Krenek R.; Burkov Y.; Schmeisser D.; Sidorenko A.; Minko S.; Stamm M. *Macromolecules* **2005**, 38, 507

[127] Xuan Y.; Peng J.; Cui L.; Wang H.; Li B.; Han Y. *Macromolecules* **2004**, 37, 7301

[128] Budkowski A.; Bernasik A.; Cyganik P.; Raczkowska J.; Penc B.; Bergues B.; Kowalski K.; Rysz J.; Janik J. *Macromolecules* **2003**, 36, 4060

[129] Černoch P.; Štěpánek P.; Pleštil J.; Šlouf M.; Sidorenko A.; Stamm M. *Eur. Polym. J.* **2007**, 43, 1144

[130] Bittrich J.; Kilian B.; Geier K. *Z. Phys. Chem. (Leipzig)* **1979**, 260 (1), 59

[131] Lath D.; Bohdanecký M. *J. Polym. Sci. - Letters Ed.* **1977**, 15, 555

[132] Karandinos A.; Nan S.; Mays J.W.; Hadjichristidis N. *Macromolecules* **1991**, 24, 2007

[133] Huber K.; Bantle S.; Lutz P.; Burchard W. *Macromolecules* **1985**, 18, 1461

[134] Pritchard M.J.; Caroline D. *Macromolecules* **1980**, 13, 957

[135] Štěpánek P.; Koňák Č.; Sedláček B. *Macromolecules* **1982**, 15, 1214

[136] Grosberg A.Y.; Kutznetsov D.V. *Macromolecules* **1992**, 25, 1970

[137] Katime I. A.; Garay M. T.; Francois J. *Journal of the Chemical Society-FaradayTransactions Ii* **1985**, 81, 705

[138] Marek Antonín, Ph.D. thesis, Charles University in Prague, Czech Republic **2006**

[139] Zhao Y.; Chen W.; Hair D.; Xu J.; Wu C.; Han C.C. *Eur. Polym. J.* **2005**, 41, 447

[140] Pan C.; Maurer W.; Liu Z.; Lodge T.P.; Stepanek P.; Meerwall E.D.; Watanabe H. *Macromolecules* **1995**, 28, 1643

[141] Jian T.; Anastasiadis S.H.; Semenov A.N.; Fytas G.; Adachi K.; Kotaka T. *Macromolecules* **1994**, 27, 4762

[142] Liu Z.; Kobayashi K.; Lodge T.P. *J. Polym. Sci., Part B* **1998**, 36, 1831

[143] Fukumine Y.; Inomata K.; Takano A.; Nose T. *Polymer* **2000**, 41, 5367

[144] Riess G. *Prog. Polym. Sci.* **2003**, 28, 1107

[145] Radzilowski L.H.; Carvalho B.L.; Thomas E.L. *J. Polym. Sci., Part B* **1996**, 34, 3081

[146] Lyakhova K.S.; Horvat A.; Zvelindovsky A.V.; Sevink G.J.A *Langmuir* **2006**, 22, 5848